Crystal Field Effect on Quasi-particle Excitations in Heavy Fermion Systems

Hiroaki Ikeda

OSAKA UNIVERSITY
GRADUATE SCHOOL OF ENGINEERING SCIENCE
DEPARTMENT OF MATERIAL PHYSICS
TOYONAKA OSAKA

Thesis

Crystal Field Effect on Quasi-particle Excitations in Heavy Fermion Systems

Hiroaki Ikeda

OSAKA UNIVERSITY
Graduate School of Engineering Science
Department of Material Physics
Toyonaka Osaka

January 1997

Contents

Abstract

In recent years, the physics in the strongly correlated system, such as the heavy fermion system, have been actively investigated both experimentally and theoretically. From the theoretical point of view, the Anderson model and the Hubbard model have been studied. Owing to the development of the recent numerical calculation, the nature of these models has been almost clarified. The common characteristic in these models is the temperature dependence. Namely, they exhibit the behavior of collection of the localized spins at high temperatures and that of heavy quasiparticles in the Fermi liquid theory at low temperatures. However, the effect of the Crystalline Electric Field (CEF), which is important in real metals, still remains in the early stage research. It seems important to clarify now the influence of the CEF effect on the low-energy properties of quasi-particle excitations. Therefore, we investigate the CEF effect in the lattice Anderson model from the two points of view.

First, the CEF effect on the quasi-particle state is discussed with the use of the mean field theory of the slave boson technique. The Anderson model of $f^0 - f^1$ configuration well reproduces the nature of Cerium system, in which only the lowest CEF level is renormalized in the situation of heavy fermions. On the other hand, in the f^2 state, it is shown that the f^1 CEF splitting is highly renormalized leading to essentially the degenerate CEF ground state. In addition, if the f^2 singlet ground state is realized, the quasi-particle contribution to the spin susceptibility comes from that of conduction electrons and is not enhanced, while the quasi-particle density of states is highly renormalized. This new class of the heavy fermion state, in which both the charge fluctuation and the spin fluctuation of quasiparticles are suppressed in spite of the highly renormalization of the quasi-particle density of states, seems to describe the anomalous behavior of UPt_3 around the superconducting transition, which has been discovered quite recently by the Knight shift experiment.

Secondly, we discuss the effect of $\boldsymbol{k}$-dependence of the hybridization matrix elements

reflecting the symmetry of the f^1 ground CEF state. Such $\boldsymbol{k}$-dependence can give rise to an anisotropic hybridization gap of heavy fermions of Cerium compounds if the filling of electrons corresponds to that of the band insulator. The most interesting case occurs when the hybridization vanishes along some symmetry axis of the crystal reflecting a particular symmetry of the ground CEF state. The results of a model calculation are consistent with wide range of anomalous properties observed in CeNiSn and its isostructural compounds, the nature of which has been remained in puzzle since its discovery. In particular, highly sensitive effect of impurity scattering on the residual density of states for zero energy excitation and the anisotropic temperature dependence of the resistivity are well explained. It is also discussed that a weak semimetallic behavior arises through the weak $\boldsymbol{k}$-dependence of the f-electron self-energy $\Sigma_f(\boldsymbol{k}, 0)$.

Chapter 1

Introduction

1.1 Recent Topics of Heavy Fermion Systems

A kind of f-electron systems, such as Cerium or Uranium compounds, are named "Heavy Fermion Systems". One of the characteristics of these compounds is that the effective mass of electrons estimated from the specific heat is remarkably enhanced by $100 \sim 1000$ times compared to the conventional metals. Its heavy mass has been detected by the de Haas van Alphens (dHvA) effect in some materials.[1, 2] This enhancement of mass arises from the many-body effect, i.e., the correlation effect due to the strong Coulomb interaction between electrons. Nowadays, the investigation of "Heavy Fermion System" becomes one of the basic problems in the condensed matter physics, i.e., the so-called physics in "Strongly Correlated System".

In Cerium atom and Uranium atom electrons take the following configurations:

$$\begin{aligned} \text{Ce} &: [\text{Xe}]4f^1 5s^2 5p^6 5d^1 6s^2 \\ \text{U} &: [\text{Rn}]5f^3 6s^2 6p^6 6d^1 7s^2 \end{aligned}$$

The electrons in $5\text{d}^1\text{6s}^2$ and $6\text{d}^1\text{7s}^2$ state are involved in conduction electrons while f-electrons keep the locality at the atomic state. Roughly speaking, Cerium ions are in trivalent (f^1) state and Uranium ions are in tetravalent (f^2) or trivalent (f^3) state. These f-electrons control the magnetism of such compounds. In fact, many actinide compounds show the magnetic order because of the RKKY interaction between localized f-electron spins.

On the other hand, the resistivity of some kinds of actinide compounds which do not undergo such magnetic transition exhibits the behavior like Kondo effect ($\propto -\log T$) at

around the room temperature.[3] The Kondo effect is a phenomenon of single magnetic impurity in a non-magnetic metal.[4] It is a typical example arising from a local correlation effect owing to the strong Coulomb interaction. The localized spin at the impurity site is screened by many conduction electrons below the characteristic temperature ($T_{\rm K}$) and is accompanied by a "Kondo cloud" which is a screening cloud of spins of conduction electrons extending to the order of $\hbar v_{\rm F}/T_{\rm K}$. Reflecting this fact, as lowering temperature the resistivity increases like $-\log T$ and then becomes constant value of the unitarity limit at $T < T_{\rm K}$. This phenomenon is intuitively understood as follows: at $T > T_{\rm K}$ the localized spin is fluctuating quantum mechanically and it gives rise to the extra scattering process on conduction electrons while at $T < T_{\rm K}$ this localized spin makes the singlet state with the "Kondo cloud" and the scattering process is reduced.

In the heavy fermion systems the behavior of the resistivity is different from that of the impurity case since f-electron spins, corresponding to impurity spins, line up periodically. In Fig. 1.1 the temperature dependence of the resistivity (per Ce) is illustrated for $Ce_xLa_{1-x}Cu_6$, when the concentration of f-electron spins is systematically changed. While the resistivity (per Ce) keeps constant in the impurity case, in the lattice case it

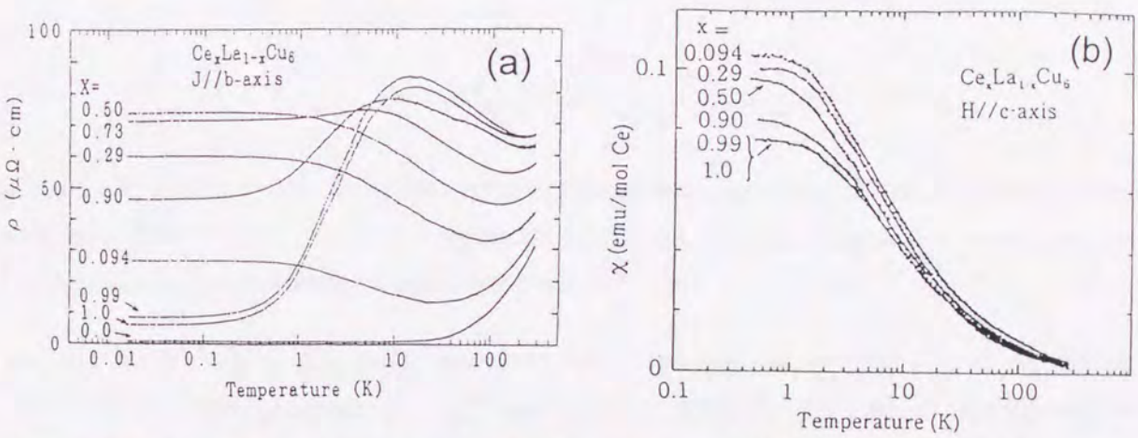

Figure 1.1: (a) The resistivity and (b) the spin susceptibility in $Ce_xLa_{1-x}Cu_6$. The resistivity shows the Kondo effect at high temperature and a constant value of the unitarity limit in the impurity case or T^2 in the lattice case. The spin susceptibility behaves obeying the Curie-Weiss law at high temperature and like the large enhanced Pauli paramagnetism at low temperature.[3]

exhibits the Kondo effect ($\propto -\log T$) at high temperatures and then metallic behavior at low temperatures. In the latter case the temperature dependence of the resistivity is proportional to T^2 as expected in the Fermi liquid theory. The experiments of the

spin susceptibility also support the above picture, i.e., the Curie-like behavior of the localized spin at high temperatures and the Pauli-like behavior of the Fermi liquid at low temperatures.[3] In Fig. 1.1(b) one can confirm that at high temperature region the spin susceptibility obeys the Curie-Weiss law with effective magnetic moment $2.5\mu_B$ of Ce^{3+} configuration and at low temperature region it becomes constant showing the enhanced Pauli paramagnetism. This crossover occures at temperature corresponding to the Kondo temperature T_K. At $T < T_K$ the apparent localized spin moment at each Cerium atom disappears and the magnetic response of this system changes into the enhanced Pauli paramagnetism.

Furthermore, the characteristic density of states (DOS) in Cerium system is directly observed by means of the photoemission spectroscopy[5] and Bremsstrahlung isochromat spectroscopy and typically shows well-known three peak structures such as shown in Fig. 1.2. These three peak structures are composed of one sharp peak near the Fermi level

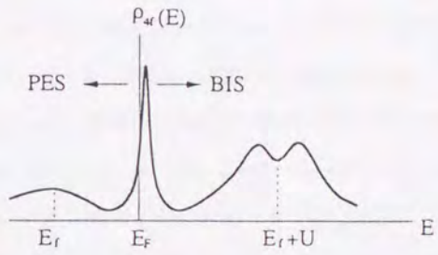

Figure 1.2: The conceptual figure of the photo emission spectra of Cerium based heavy fermions. Three peak structures represent the lower Hubbard band, the quasi-particle band, and the upper Hubbard band from the left side.

and two broad humps; one hump exists at the vicinity of the original f-level E_f, which corresponds to the transition $f^1 \rightarrow f^0$, and another hump $E_f + U$, which corresponds to the transition $f^1 \rightarrow f^2$. These two broad peaks correspond to the so-called lower Hubbard band and upper Hubbard band and hold the character of the f-electron localized spin. It is the quasi-particle bands that are the sharp peak near the Fermi level on the center and construct heavy electrons observed in the specific heat and the spin susceptibility at $T \ll T_K$. This quasi-particle peak is called "Kondo resonance" and is sensitive to the temperature.

Thus, one of the most important characters in the heavy fermion system is the difference of the behavior in each temperature region. At least in Cerium system, it has been checked out experimentally that at high temperature its behavior is that of localized spin

system and at low temperature it is described by the Fermi liquid theory in which its effective mass is extremely enhanced.

We can classify the recent topics in the heavy fermion system as follows:

(1) meta-magnetism ($CeRu_2Si_2$, etc.)

(2) low carrier system (CeP, CeAs, etc.)

(3) Kondo insulator (SmB_6, YbB_{12}, CeNiSn, $Ce_3Bi_4Pt_3$, etc.)

(4) unconventional superconductor (UPt_3, $CeCu_2Si_2$, etc.)

The meta-magnetic transition in $CeRu_2Si_2$ investigated as a main subject (1) is a typical one in heavy fermions. The Kondo temperature of this material is $T_K = 20K$ and the meta-magnetic transition is occurred at around the magnetic field of 80kOe in which the Zeeman energy $g\mu_B H$ is comparable to $k_B T_K$.[6] There may exist the critical magnetic field h_c corresponding to T_K; at $h > h_c$ the system exhibits localized-spin like behavior and at $h < h_c$ the Fermi-liquid like one, although its "transition" seems to be continuous.[7] In fact, the experiment of the dHvA effect[8] indicates that f-electrons are itinerant before the meta-magnetic transition occurs and are localized after the transition, i.e., its Fermi surface can be explained by that of $LaRu_2Si_2$, which contains no f-electrons. This problem is related to the Luttinger theorem, which states that the $\boldsymbol{k}$-space volume surrounded by the Fermi surface is not changed even if the interaction is switched on, and is actively investigated in recent years as the basic problem on the Fermi liquid theory.

A typical low carrier system investigated in the subject (2) is Cerium mono-pnictide, such as CeP and CeAs, etc. In this system there are few carrier number at low temperature and this system is very sensitive to the pressure.[9] And also this system is a compensated metal and its complex magnetic phase is wellknown as Davil's stair case.[10] While this system is similar to the Kondo insulator in the sense that the transports are sensitive to the pressure, the physics may be rather different.

Now, so far, we have introduced the metallic case in which f-electrons behave like itinerant at low temperature $T < T_K$. Next, we consider a group of materials, investigated in the subject (3), which behave like insulator or semiconductor at low temperatures. Such materials are called "Kondo insulator" or "Kondo semiconductor". In the early stage of research, YbB_{12} and SmB_6 were discovered[11] and in recently 3-element system such as $Ce_3Bi_4Pt_3$, CeNiSn, CeRhSb and CeBiAs, etc. renew an intensive interest.[12-16] These systems are similar to superconductors in the point of gap formation at low temperature although they do not show the phase transition. Furthermore, CeNiSn and CeRhSb are quite interesting systems which have V-shaped gap as revealed from the measurements

of the longitudinal NMR relaxation rate.[17-19] (this can compare with the anisotropic superconductor of heavy fermions.) Here, we should note the fact that any Kondo insulators have even number of electrons in one unit cell and have the condition as the band insulators in a form or another. It is a challenging problem to clarify the scenario of gap formation including the many-body effects and the difference from the conventional band insulators and semiconductors.

Finally, let us give a brief introduction about unconventional superconductors concerning the subject (4). In the heavy fermion system there are many materials which exhibit superconductivity at low temperature, for example, $CeCu_2Si_2$, UPt_3, UBe_{13}, URu_2Si_2, UPd_2Al_3, UNi_2Al_3, etc.[20-25] All of these belong to the unconventional superconductor, in which any physical properties obey the power law at $T \ll T_c$. Furthermore, they have intimate connection with the magnetism in the superconducting phase near the antiferromagnetic phase in $CeCu_2Si_2$, $CePd_2Si_2$, UPt_3, UBe_{13}, or, coexistence with the antiferromagnetic phase in URu_2Si_2, UPd_2Al_3, UNi_2Al_3. The existence of multi-phase superconducting transition in UPt_3 etc.[26] is a smoking gun for the unconventional superconductivity. While most of these compounds include Uranium atoms, the nature of quasi-particle states in the Uranium compounds has not yet been made clear at all so that the study of these superconducting state inevitably remains as a phenomenological level.[27-31] To get the microscopic understanding of such various superconducting states, we should shed light on the character of quasiparticles of heavy fermions which contain multi number of f-electrons as in Uranium compounds.

1.2 Theoretical Overview of Heavy Fermion System

We have introduced some recent topics in the heavy fermion system from the experimental point of view so far. One of consepts we got is that the heavy fermion system is the typical strong correlation system with the interplay between f-electrons, which are rather localized and have the strong Coulomb repulsion, and conduction electrons, which form the wide energy band-width. Next, let us consider theoretically the model Hamiltonian governing such the heavy fermion system, especially Ce compounds.

First of all, f-levels in Ce^{3+} ion has the 14-fold degeneracies without any interaction and considering the strong spin-orbit interaction, are splitting into total angular momentum $j = 7/2$ and $j = 5/2$ states. Because the levels of $j = 7/2$ states are located at higher energies than $j = 5/2$ states by a few eV, $j = 7/2$ states can be neglected usually.

In compounds such $j = 5/2$ states of Ce^{3+} ions are influenced by the crystalline electric field (CEF) corresponding to the local symmetry and are seperated into 2 or 3 levels. These localized enough levels are weakly hybridized with the wide band-width conduction electrons through the slight overlap with a f-wave function. It is the lattice Anderson model that can successfully discribe these cases and for simplicity only one CEF ground state is often taken into account. This model Hamiltonian is the extension to the lattice case of the impurity Anderson model and f-sites corresponding to many impurities exist periodically side by side and is expressed by

$$H = \sum_{\boldsymbol{k}\sigma} \xi_{\boldsymbol{k}} c^{\dagger}_{\boldsymbol{k}\sigma} c_{\boldsymbol{k}\sigma} + \sum_{i\sigma} E_f f^{\dagger}_{i\sigma} f_{i\sigma} + \frac{1}{2} U \sum_{i} f^{\dagger}_{i\uparrow} f_{i\uparrow} f^{\dagger}_{i\downarrow} f_{i\downarrow} + \frac{1}{\sqrt{N}} \sum_{\boldsymbol{k}\sigma i} (V_{\boldsymbol{k}} c^{\dagger}_{\boldsymbol{k}\sigma} f_{i\sigma} \exp(-i\boldsymbol{k}\cdot\boldsymbol{R}_i) + h.c.), \tag{1.1}$$

where the first term represents the conduction band with the wide band-width, the second term the f-site energy, the third term the strong interaction between f-electrons and the last term the hybridization matrix elements between the f-electrons and the conduction electrons. In this Hamiltonian it is characteristic that are almost non-dispersible f-level E_f, the strong Coulomb repulsion between f-electrons and the weak hybridization $V_{\boldsymbol{k}}$. In resent years, this Anderson model and its extension have been actively investigated by analytic methods, such as the perturbation theory on the basis of the Fermi liquid theory[32] and the $1/N$ expansion method with slave bosons,[33] etc., and by numerical calculations, such as the exact diagonalization,[34] the quantum Monte Carlo method with the help of the $d = \infty$[35] and the numerical renormalization group method.[36]

We can get overall features of this Hamiltonian (1.1) applying the perturbation theory. With the use of the Hartree-Fock approximation and the second perturbation,[37] the DOS shown in Fig. 1.3 is computed. In other numerical calculation the central peak at low temperature becomes more sharp. The right-and-left broad humps can be regard as the so-called lower and upper Hubbard bands and have relations to behaviors like localized spins at high temperature in the heavy fermion system. The central peak grows up as lowering the temperature and is sensitive to temperature. While we have denoted in the previous section that in the heavy fermion system the behaviors at low temperature are experimentally governed by heavy quasiparticles, this central peak indeed can be considered to represent such heavy quasi-particle bands at low temperature. Such quasi-particle structure at low temperature in the periodic Anderson model has been investigated by the several authors. For example, the $1/N$ expansion method with the slave bosons has

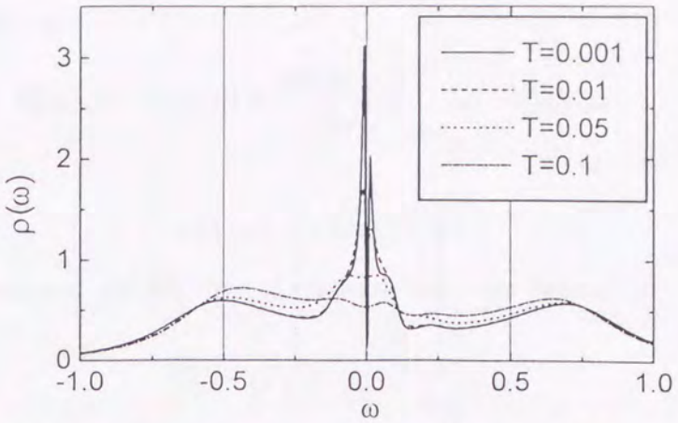

Figure 1.3: The DOS calculated with the use of the Hartree-Fock approximation and the second perturbation. The right-and-left broad humps are regard as the so-called lower and upper Hubbard bands and the central coherent peak is the quasi-particle band. This coherent peak represents the formation of the heavy fermion band at low temperature and is sensitive to the temperature.

proved that there exists the coherent temperature T_{coh} and the quasi-particle bands are formed at $T < T_{coh}$. And the details of such quasiparticles have been presented on the basis of the Fermi liquid theory and the low energy excitations at the low temperature prove to be described by the quasiparticles. Let us introduce briefly this theory on the basis of the Fermi liquid theory.[38, 39]

Without the interaction term eq.(1.1) becomes an one-body problem and it is clear that formed are hybridization bands between f-electrons and conduction electrons. In fact, due to the strong Coulomb repulsion, the problem becomes complex. Including this interaction into the f-electron self-energy $\Sigma(\boldsymbol{k}, \omega)$, the f- and conduction-electron Green's fucntions are given by

$$G_\sigma^c(\boldsymbol{k}, \omega) = \frac{1}{\omega - \xi_{\boldsymbol{k}} - \dfrac{V_{\boldsymbol{k}}^2}{\omega - E_f - \Sigma(\boldsymbol{k}, \omega)}}, \tag{1.2a}$$

$$G_\sigma^f(\boldsymbol{k}, \omega) = \frac{1}{\omega - E_f - \Sigma(\boldsymbol{k}, \omega) - \dfrac{V_{\boldsymbol{k}}^2}{\omega - \xi_{\boldsymbol{k}}}}. \tag{1.2b}$$

The low energy excitations are described by quasiparticles, eigenvalues of which are given by poles of these Green's functions. The self-energy can be expanded concerning ω at low

energy regions as follows:

$$\Sigma(\boldsymbol{k},\omega) = \Sigma(\boldsymbol{k},0) + \left.\frac{\partial\Sigma(\boldsymbol{k},\omega)}{\partial\omega}\right|_{\omega=0}\omega, -i\Delta(\boldsymbol{k},\omega), \tag{1.3}$$

where

$$\Delta(\boldsymbol{k},\omega) = -\mathrm{Im}\Sigma(\boldsymbol{k},\omega). \tag{1.4}$$

Thus, the eigenvalues and the life time of quasiparticles are defined as

$$E^*_{\boldsymbol{k}} = \left[\tilde{E}_f + \frac{\tilde{V}^2_{\boldsymbol{k}}}{E^*_{\boldsymbol{k}} - \xi_{\boldsymbol{k}}}\right], \tag{1.5a}$$

$$\tilde{E}_f = \tilde{z}_{\boldsymbol{k}}\left(E_f + \Sigma(\boldsymbol{k},0)\right), \tag{1.5b}$$

$$\tilde{V}^2_{\boldsymbol{k}} = z_{\boldsymbol{k}}V^2_{\boldsymbol{k}}, \tag{1.5c}$$

$$z^{-1}_{\boldsymbol{k}} = 1 - \left.\frac{\partial\Sigma(\boldsymbol{k},\omega)}{\partial\omega}\right|_{\omega=0}, \tag{1.5d}$$

$$\Gamma^*_{\boldsymbol{k}} = z_{\boldsymbol{k}}\Delta(\boldsymbol{k},\omega), \tag{1.5e}$$

where $z_{\boldsymbol{k}}$ is the renormalization factor and quasi-particle bands $E^*_{\boldsymbol{k}}$ are reduced by this factor and form the heavy-electron bands. In such case the quasi-particle DOS are enhanced by $z^{-1}_{\boldsymbol{k}}$ and experimentally the large electronic specific heat coefficient may be observed:

$$\gamma = \sum_{\boldsymbol{k}\sigma}\left[\rho^f_{\boldsymbol{k}}(0)/z_{\boldsymbol{k}} + \rho^c_{\boldsymbol{k}}(0)\right], \tag{1.6}$$

where $\rho^f_{\boldsymbol{k}}(0)$ and $\rho^c_{\boldsymbol{k}}(0)$ are the f- and conduction-electron DOS at the Fermi level, respectively. In Addition, the dumping rate of quasiparticles $\Gamma^*_{\boldsymbol{k}}$ is reduced and the lifetime of quasiparticles is extended and the quasi-particle bands appear clearly at low energy region. The contribution to the spin susceptibility of such quasiparticles is written down by

$$\chi = 2\mu^2_{\mathrm{B}}\sum_{\boldsymbol{k}}\left[\rho^f_{\boldsymbol{k}}(0)\chi^s_{\boldsymbol{k}} + \rho^c_{\boldsymbol{k}}(0)\right], \tag{1.7}$$

$$\chi^s_{\boldsymbol{k}} = 1 - \left.\frac{\partial\Sigma_\sigma(\boldsymbol{k},0)}{\partial H_\sigma}\right|_{H=0} + \left.\frac{\partial\Sigma_\sigma(\boldsymbol{k},0)}{\partial H_{-\sigma}}\right|_{H=0}, \tag{1.8}$$

where $H_\sigma = \sigma\mu_{\mathrm{B}}H$. Thus, the contribution of f-electrons to the spin susceptibility is also enhanced by the factor $\chi^s_{\boldsymbol{k}}$. Furthermore, in the heavy fermion system the resistivity at low temperature is obtained by

$$R = R_{imp} + AT^2, \tag{1.9}$$

which shows the existence of T^2 term characteristic of the Fermi liquid states without impurity effects. Such resistivity or conductivity is theoretically calculated by

$$\sigma_{\mu\nu} = e^2 \sum_{\boldsymbol{k}} \delta(\mu - E^*_{\boldsymbol{k}}) J^*_{\mu\boldsymbol{k}} \frac{1}{2\Gamma^*_{\boldsymbol{k}}} \frac{1}{C_{\boldsymbol{k}}} J^*_{\nu\boldsymbol{k}}, \tag{1.10}$$

where $J^*_{\mu\boldsymbol{k}}$, $\Gamma^*_{\boldsymbol{k}}$ and $C_{\boldsymbol{k}}$ are respectively the current, the inverse life-time of quasiparticles and the factor of order unity reflecting the existence of Umklapp processes. It is important that all factors due to the enhancement factor cancel out with each other and the conductivity is proportional to the life-time of quasiparticles.

Thus, the interested low-energy excitations at the low temperature have proved to be described by the quasiparticles. This theory can display a part of characters in many experiments which are discussed in the previous section. For example, however, temperature dependence of the spin susceptibility at high temperature demands the CEF splitting of f-electrons, which is often ignored for simplicity in these theories. Such CEF splitting may have some influence on the quasiparticles. The time comes when it must be discussed that what influence such the CEF effects have on the quasiparitcles. In this thesis we will discuss the CEF effect on the quasiparticles on the basis of the Fermi liquid theory in the heavy fermion system. The results give one interpretation to the experiments which are explained in the following two section.

1.3 Review of UPt_3

We shortly state some physical properties in UPt_3. The crystal structure of UPt_3 is classified to be the $MgCd_3$-type hexagonal close-packed structure and the lattice parameters are $a = 5.764$Å and $c = 4.899$Å. This crystal structure and the Brillouin zone are illustrated in Fig. 1.4. This material is well known as the heavy fermion superconductor with the multi-phase diagram.[26] The normal state is described by the Fermi liquid in the heavy fermion system. The specific heat is linearly proportional to temperature as shown in Fig. 1.5(a) and the coefficient γ is ~ 420mJ/mole K^2 corresponding to the heavy effective mass. The spin susceptibility $\chi(T)$ indicates the enhanced Pauli paramagnetism. The resistivity shows the T^2 behavior in Fig. 1.5(b) without impurity effects.[40, 41] At low temperature these heavy quasiparticles undergo the transition to the unconventional superconductor. In this state the temperature dependence of various thermodynamics follows the power law.[42-45] And it is interesting that the possibility of an odd-parity of the Cooper pairing was pointed out from NMR (Fig. 1.6) and μSR experiments.[46-48]

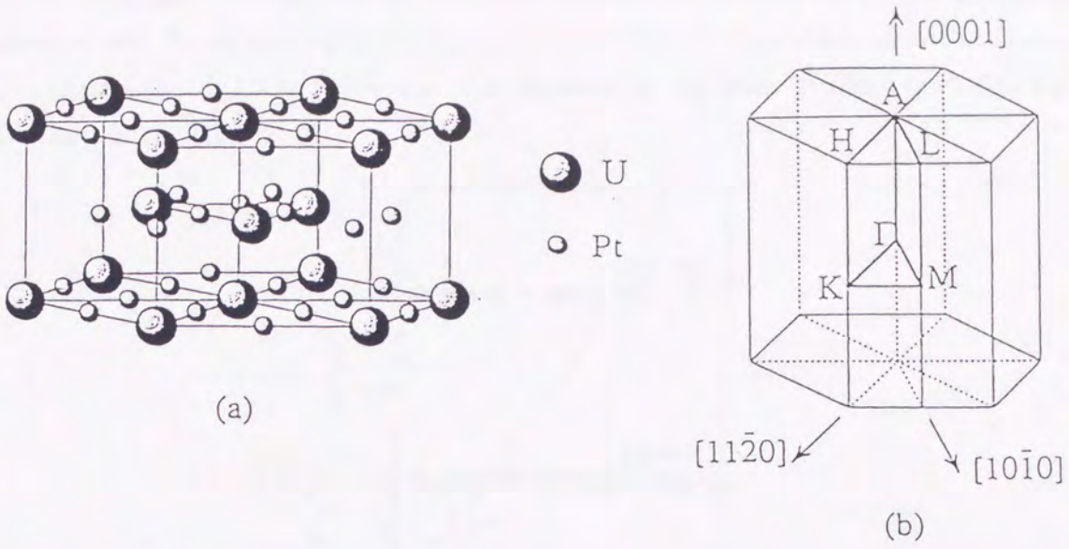

Figure 1.4: (a) The hexagonal close-packed $MnCd_3$ crystal structure and (b) the Brillouin zone in UPt_3.[49]

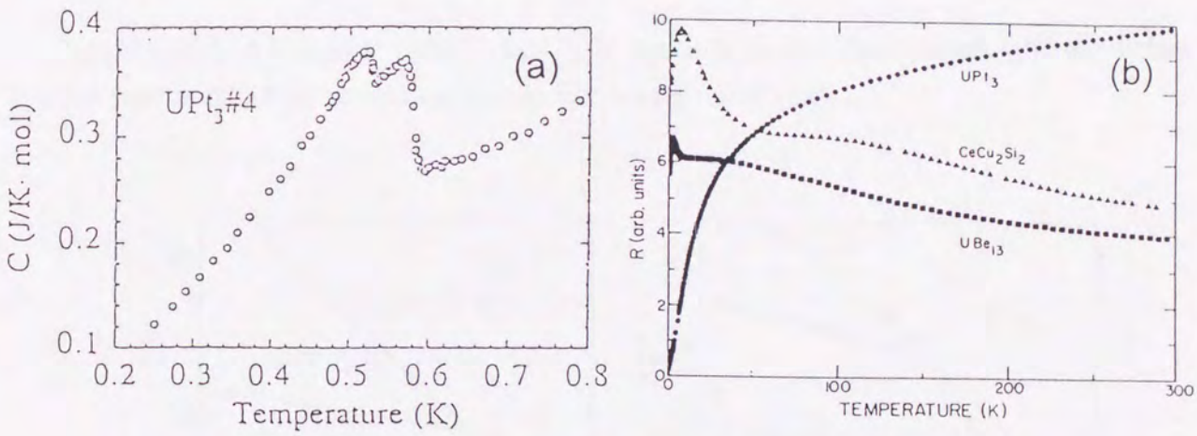

Figure 1.5: (a)The specific heat[49] and (b)the resistivity[41] of UPt_3.

It is more famous that is the double transition in the specific heat experiments[49] as shown in Fig. 1.5(a). In these days as a function of the temperature and the magnetic field the existence of three kinds of phases, "A", "B" and "C"-phases, is established as shown in Fig. 1.7. Thus, the unconventional superconducting states in UPt_3 are colorful and extensive experimental works have been carried out to clarify the mechanism. In this system only one theoretical work is phenomenological theory[27-31] on the basis of GL

theory. And one of the present problems is whether the effective spin-orbit interaction is strong or not. To solve these problems microscopically, we must make clear the characters of quasiparticles in U $(5f)^2$ system. Our theoretical approach to these problems will be discussed in the chapter 2.

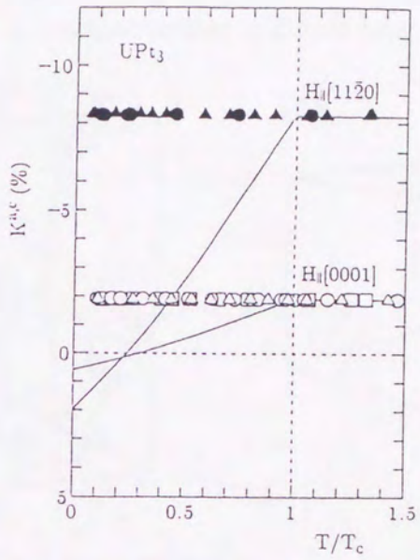

Figure 1.6: The Knight shift of UPt_3[47]. It seems to be the Pauli paramagnetism before the superconducting transition and do not change after that.

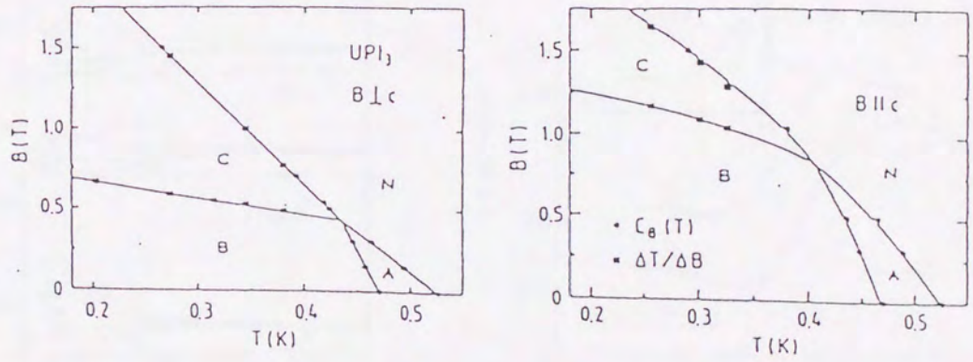

Figure 1.7: The phase diagram in UPt_3[26]. There exist three kinds of phases, "A", "B" and "C"-phases as a function of the temperature and the magnetic field.

1.4 Review of CeNiSn

CeNiSn and CeRhSb have been called "Kondo insulator" at least in the early stage since the thermodynamic behaviors[12-19] have been similar to typical "Kondo insulators", i.e., SmB_6, YbB_{12} and $Ce_3Bi_4Pt_3$, which stay in a semi-conducting state with an activation energy gap. CeNiSn have the orthorhombic ϵ-TiNiSi type structure (D_{2h}^{16} $Pnma$) with

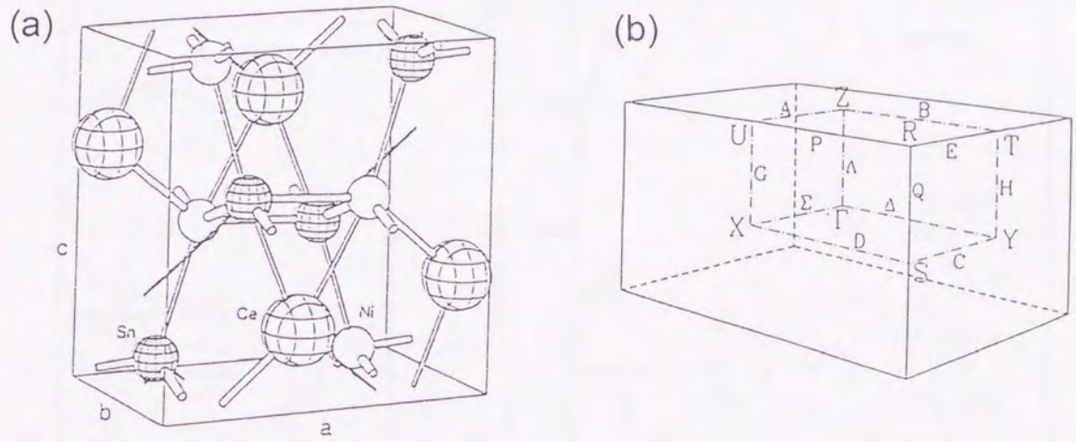

Figure 1.8: (a) The orthorhombic ϵ-TiNiSi type crystal structure and (b) the Brillouin zone in CeNiSn[50].

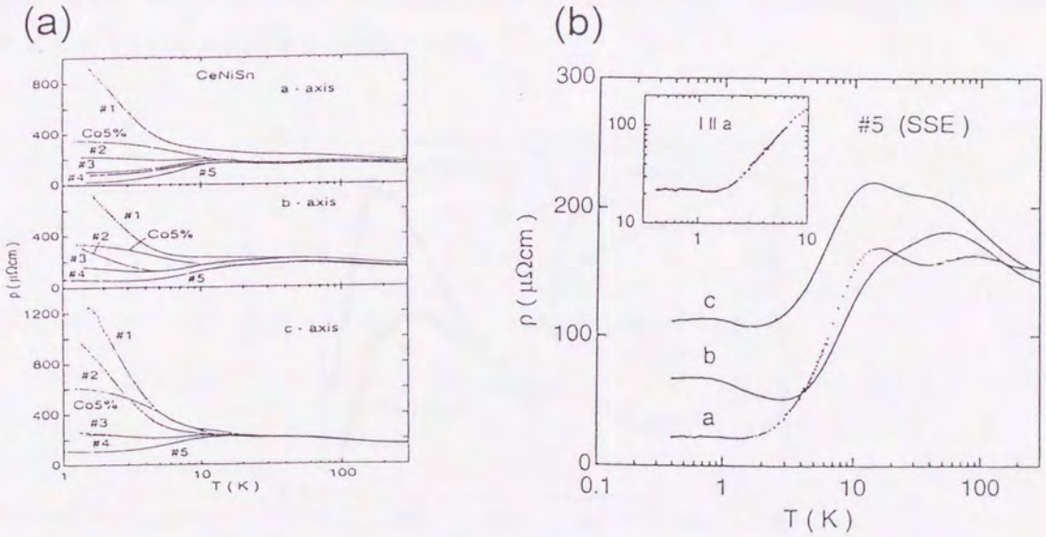

Figure 1.9: The resistivity of CeNiSn[51]. As samples are improved, the resistivity along a-axis decreases at low temperature.

lattice parameters of $a = 7.534$Å, $b = 4.598$Å and $c = 7.609$Å, as shown in Fig. 1.8 and

are different from SmB_6 and $Ce_3Bi_4Pt_3$ with the cubic structure. At high temperature a variety of experiments in "Kondo insulator" indicate the behaviors like the metallic heavy fermion system, such as $-\log T$ in the resistivity. This context is also unexceptional in CeNiSn and CeRhSb. At low temperature the resistivity (Fig. 1.9) increases except for a-axis direction and the static spin susceptibility (Fig. 1.10) along the a-axis has a peak

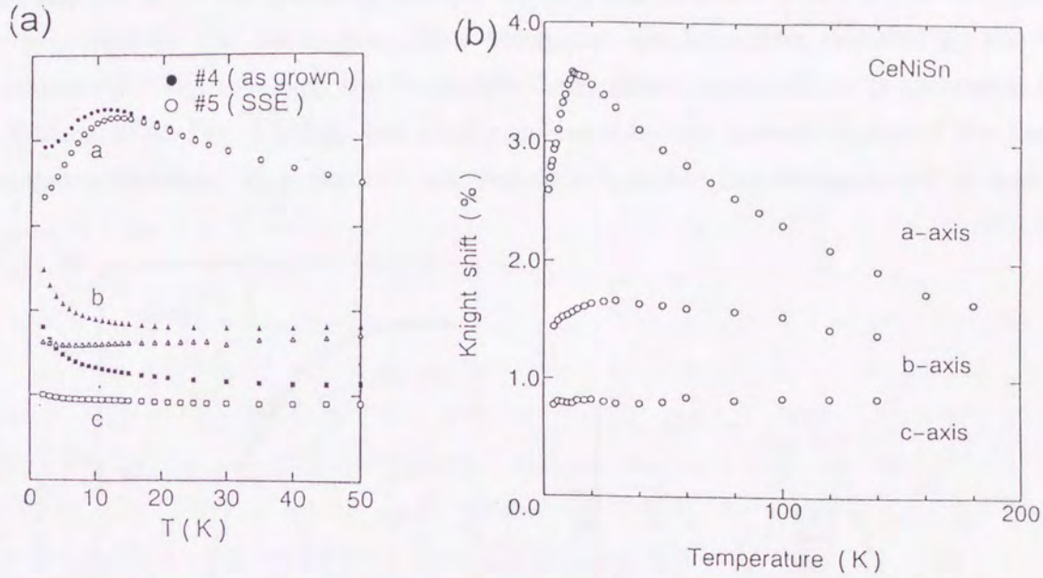

Figure 1.10: The static spin susceptibility of CeNiSn[51]. The susceptibility along the a-axis has a peak structure around 12K.

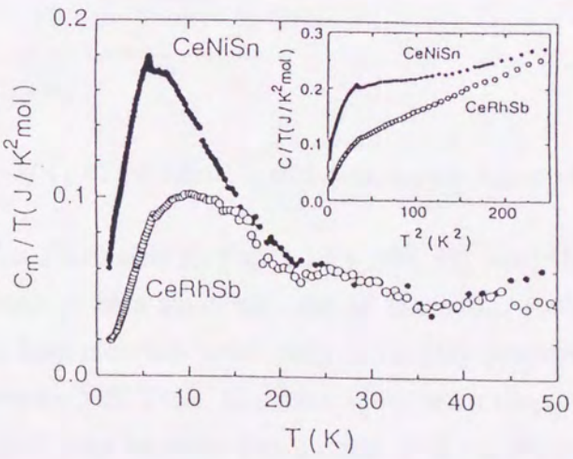

Figure 1.11: The temperature dependence of the magnetic specific heat of CeNiSn[52]. There is a peak structure around 7K.

structure around 12K and the magnetic specific heat shows a peak at about 7K and decreases proportional to T below 5K as shown in Fig. 1.11.[51-53] In addition, the inelastic neutron scatterings show the existence of anisotropic magnetic excitations in the k-space.[54-56] The attractive attention in CeNiSn has been evoked by the NMR measurement. While other "Kondo insulators" except for CeNiSn and CeRhSb show exponentially decay in the thermodynamics, the physical properties in CeNiSn and CeRhSb are governed by the power law. This viewpoint has been first revealed by the NMR experiment[17-19], in which the longitudinal relaxation rate $1/T_1$ is proportional to T^3 as illustrated in Fig. 1.12(a), and reinforced later by the measurements of the thermodynamic properties. It is pointed out that this behavior can be explained by assuming

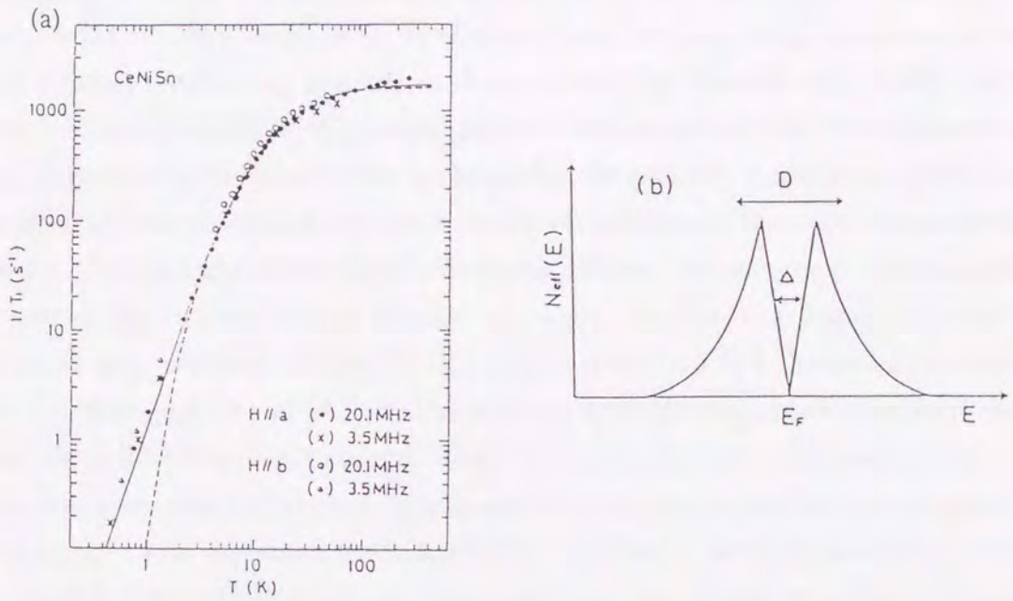

Figure 1.12: $1/T_1$ of CeNiSn[17] and conceptual figure of V-shaped DOS

the V-shaped DOS as illustrated in Fig. 1.12(b).[17, 18] And these compounds are also found to be very sensitive to a small amount of impurities such that the residual DOS at zero energy excitations increases drastically in roughly proportional to the square root of impurity concentration.[18] Thus, the relation between usual "Kondo insulators" and CeNiSn brings in mind that between the normal BCS superconductors and the "axial-type" anisotropic superconductors. Such anisotropic gap formation in CeNiSn at low temperature is an attractive problem. The mechanism of the energy-gap formation at low temperatures in the usual "Kondo insulator" has been discussed from a variety of

view points. These are classified roughly into two categories, i.e., $\boldsymbol{k}$-space and real-space approaches. In the former approach, the origin of insulating behaviors is attributed to a hybridization gap which is highly renormalized by the strong correlations among almost localized f-electrons.[57] A circumferential evidence supporting this point of view is that all the compounds called the "Kondo insulator", except for TmSe, have even number of electrons in the unit cell which is a necessary condition for the band insulator. In the latter approach, on the other hand, it is attributed to the formation of local bound state of one kind of another, such as local singlet due to the strong Kondo effect, the Wigner crystal formation, and so on.[58, 59]

A picture of the renormalized hybridization gap is based on the principle of "adiabatic continuation"[60] which was applied first by Landau in the Fermi liquid theory[61] and then has turned out very useful so far in understanding the low energy properties of wide range of strongly interacting systems as demonstrated by Yamada and Yosida for the impurity Anderson model.[32] While correctness of this picture for the "Kondo insulator" has been suggested by the Gutzwiller approach for the periodic Anderson model for this decade,[62, 63] it was recently shown more vividly on the basis of the exact diagonalization method[34], the quantum Monte Carlo calculation[35] and the numerical renormalization group method[36] with the help of the $d = \infty$ theory. On the other hand, it is reported that a charge gap is always different from a spin gap in the $d = 1$ theory on the basis of the exact diagonalization method.[64] This result is against the picture mentioned above. However, we believe that this may come from the particularity of 1-dimensionality.

There are a few papers in which anomalous properties in CeNiSn and its isostructural compounds try to be explained theoretically on the basis of such $\boldsymbol{k}$-space approach.[65] In the chapter 3 we will demonstrate more explicitly the formation of the anisotropic gap in these compounds by taking into consider the CEF effect from such point of view. We predict some physical properties at that time. Quite recently, more precise experiments have been carried out at lower temperatures, as the sample quality is better. Thus, more experiments justify our theory, while some experiments puzzle us. Let us list some recent experiments. First, T_1T=const behavior (Fig. 1.13(a)) in the longitudinal NMR relaxation rate below 1K suggests the presence of DOS at the Fermi level.[18] T_1 is also sensitive to the substitution-type impurity effects. The specific heat at low temperatures (Fig. 1.14(b)) supports the essential presence of DOS at the Fermi level.[51, 66] Futhermore, the magnetic field dependence of the specific heat has been measured[67] as shown

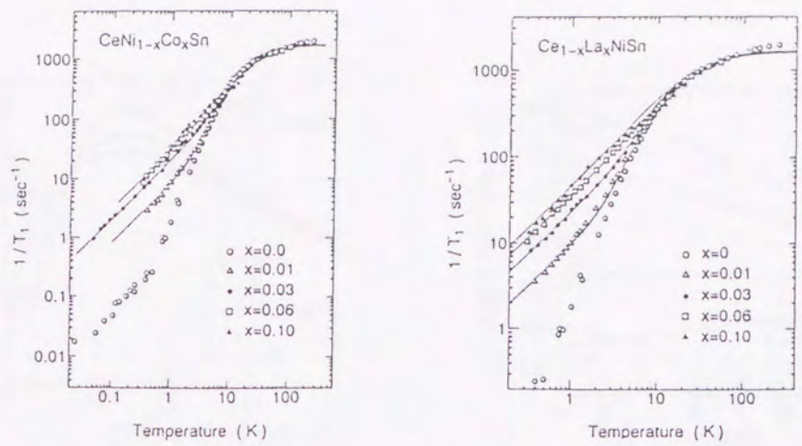

(a) (b)

Figure 1.13: T dependence of $1/T_1$ of ^{119}Sn in (a) $CeNi_{1-x}Co_xSn$ and (b) $Ce_{1-x}La_xNiSn$.

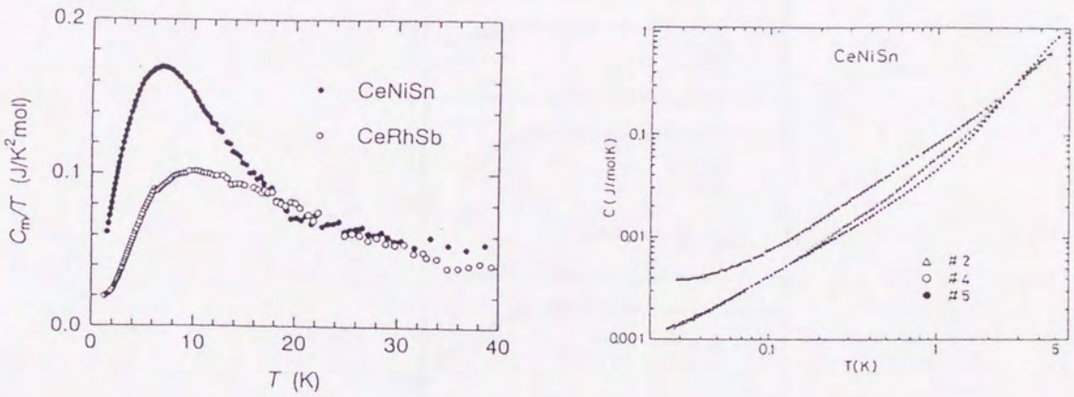

(a) (b)

Figure 1.14: (a) The magnetic specific heat divided by temperature (C_m/T)[66] and (b) the specific heat at lower temperatures in the better sample[51].

in Fig. 1.15. Second, we indicated in Fig. 1.9 that the resistivity at low temperatures decreases, as the sample quality is better.[51] Even in the best sample, however, the Hall coefficient shows the semiconductor-like behavior (Fig. 1.16).[51]

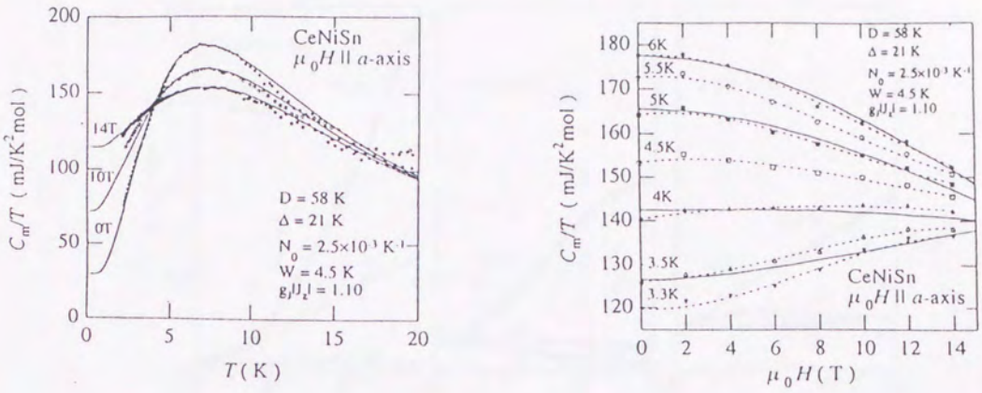

Figure 1.15: (a) The T dependence of C_m/T under the magnetic field along a-axis and (b) The magnetic field dependence of C_m/T.[67]

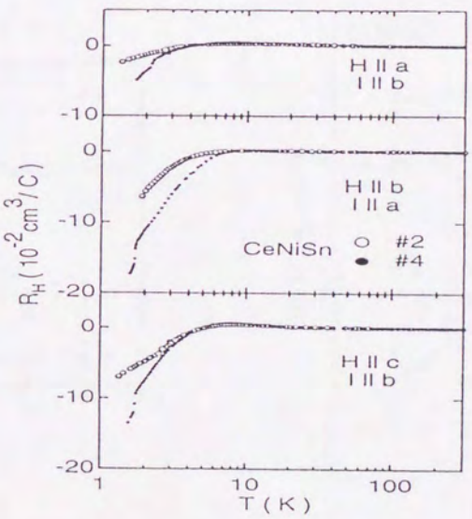

Figure 1.16: Hall coefficient for single crystals of CeNiSn #2 and #4.[51]

The magnetoresistances (MRs) illustrated in Fig. 1.17 are characterized as follows:[68]

(1) The transverse MRs are large positive and the longitudinal MRs are small.

(2) For $H \propto a$, the MRs are negative for any current direction.

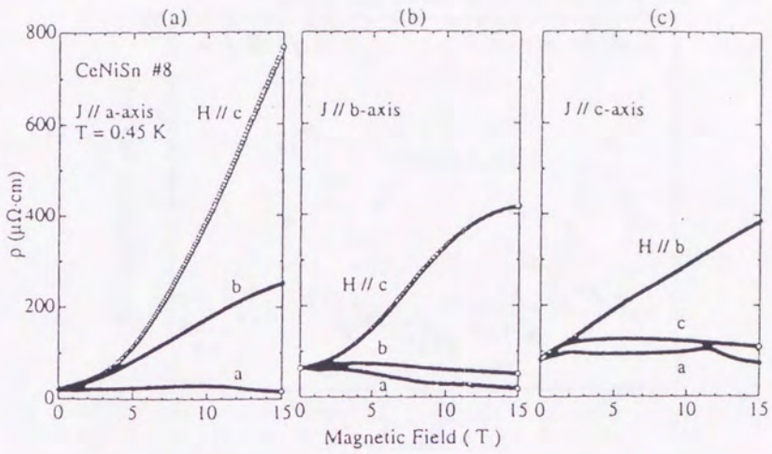

Figure 1.17: Magnetic field dependence of the MRs at 0.45K in CeNiSn.[68]

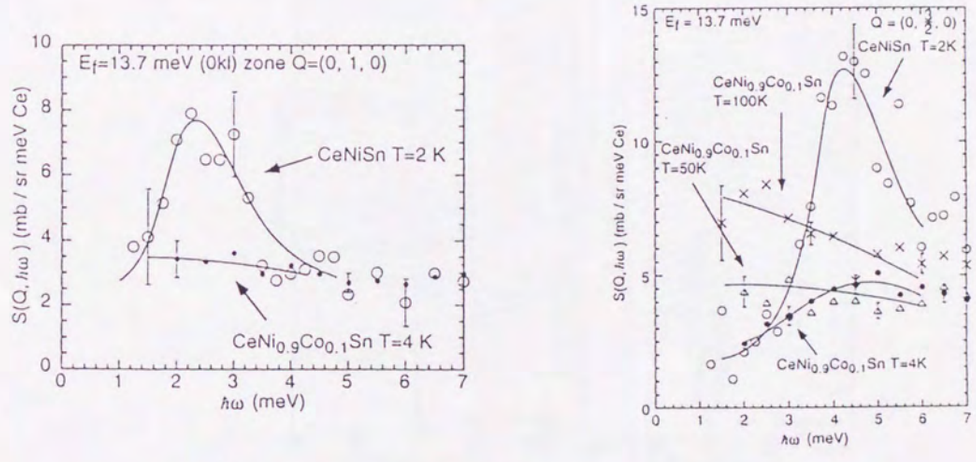

(a) (b)

Figure 1.18: Co substitution effect on (a) the peak at $\hbar\omega = 2$meV, $Q = (0, 1, 0)$ and (b) the peak at $\hbar\omega = 4$meV, $Q = (0, 3/2, 0)$.[69]

Finally, in the neutron scattering experiment it is also reported that the characteristic peak structures (Fig. 1.18, 1.19) in CeNiSn are sensitive to impurities.[69]

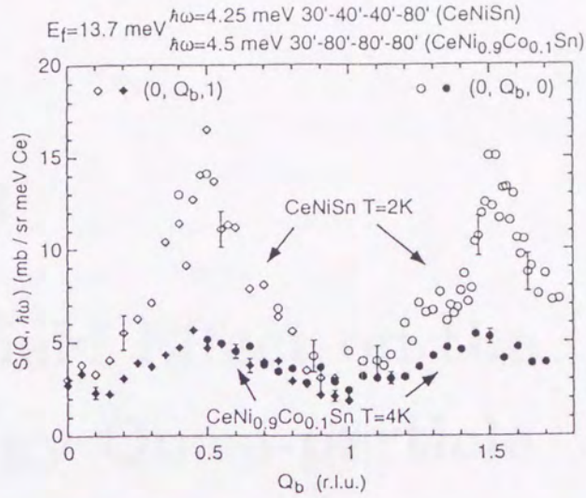

Figure 1.19: Constant-E scan along $Q = (0, Q_b, 0)$ (circle) or $Q = (0, Q_b, 1)$ (diamond).[69]

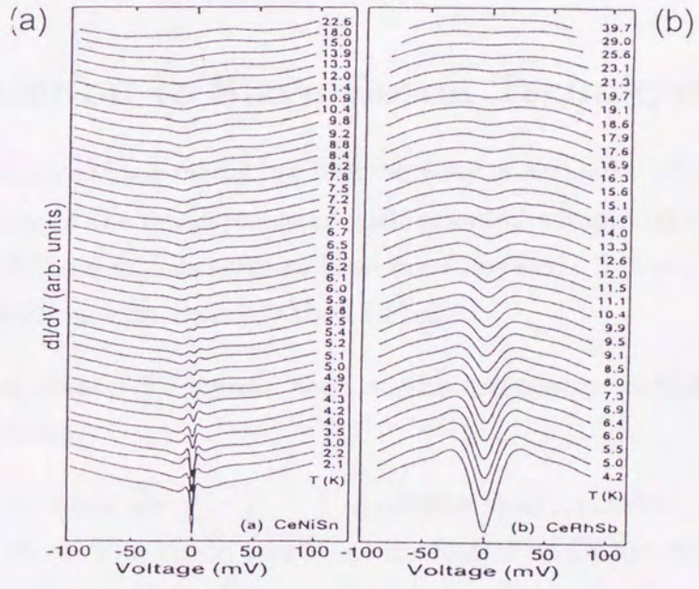

Figure 1.20: Temperature variations of the tunneling conductance for (a) CeNiSn and (b) CeRhSb.[87]

In the tunneling conductance[87] the temperature dependence of the gap formation is obtained as shown in Fig. 1.20

Chapter 2

Crystal Field Effect on the Low-Energy Quasi-particle Excitation

2.1 Introduction to Slave Boson Technique

Recently, the so-called Anderson model has been actively investigated by several theoretical methods. Because of the development of such powerful computing methods[32-36], most of characters of these models seem to have been revealed. However, there are few investigations[70] which include explicitly the CEF effect.

> *What influence these CEF effects have on the low-energy excitations, i.e. quasi-particle bands?*

In this chapter, we study the $f^0 - f^1 - f^2$ Anderson model including f^1 and f^2 multiplets by the CEF effect. This model represents the feature of Cerium compounds when the f^1-states are stabilized, and the feature of Uranium compounds when f^2-states stabilized. We are interested in the quasi-particle bands in this model. A useful tool to study quasi-particle structures in such model is the so-called Gutzwiller approximation[62] or the mean-field theory of slave bosons.[71-73] When the Hilbert space is restricted within $f^0 - f^1 - f^2$ configuration, the slave-boson technique is more convenient. If the Hilbert space includes all f-states, this mean-field theory are consistent with the Gutzwiller approximation. In fact, G. Kotliar and A. E. Ruckenstein have proved the correspondence between these two formalisms at least in the non-degenerate f-band case.[71] In addition,

this slave-boson technique is equivalent to the zeroth order of 1/N expansion method at $T = 0$, where N is the degeneracy of the f-orbitals.[74] This technique can be easily extended to the problem of calculating the quasi-particle interaction. So we discuss the multiplet effects of the system with f^1 and f^2 configuration within the mean-field approximation of slave bosons. We hope that the study in this chapter becomes a starting point of the analysis of the CEF effect on the low-energy excitations in the periodic Anderson model simulating Uranium based heavy fermions.

We formulate the slave-boson method in the $f^0 - f^1 - f^2$ Anderson model including the CEF effect in §2.2. Then, we derive the results by the mean-field approximation and discuss the difference of the CEF effect between f^1 and f^2 case in §2.3.

2.2 Formulation

First, let us consider the Hamiltonian of the $f^0 - f^1 - f^2$ Anderson model including the CEF effect. This Hamiltonian can be decomposed into three parts:

$$H = H_f + H_c + H_{\rm hyb}. \tag{2.1}$$

The first term is the f-electron part, which may be given by the ionic part on each site:

$$H_f = \sum_{i\mu} E_\mu \left|i\mu\right\rangle \left\langle i\mu\right| + \sum_{iM} E_M \left|iM\right\rangle \left\langle iM\right|, \tag{2.2}$$

where E_μ is the energy of the μ-state of f^1 multiplets as measuring from the energy of the f^0 state, E_M the M-state of f^2 multiplets and i is the f-site index. Note that $\left|i\mu\right\rangle \left\langle i\mu\right|$ and $\left|iM\right\rangle \left\langle iM\right|$ play the role of a projection operator for the state $\left|i\mu\right\rangle$ and $\left|iM\right\rangle$, respectively. Then μ and M will denote all of any quantum numbers. If we take the local crystal field environment into account, μ and M correspond to the irreducible representations of the crystal field symmetry group, and $\left|i\mu\right\rangle$ is the linear combination of the state $\left|im\right\rangle$, which is an eigen state of an azimusal component of angular momentum j_z, and $\left|iM\right\rangle$ is linear combination of the state $\left|imn\right\rangle$, which is an eigen state of an azimusal component of angular momentum J_z. In the strong spin-orbit coupling limit such as Cerium or Uranium compounds, the total angular momentum of the f^1 state is j=5/2 and that of the f^2 state is J=4.

The second term of eq.(2.1) is the conduction electron part and may be described by the usual band model:

$$H_c = \sum_{\boldsymbol{k}\sigma} \epsilon_{\boldsymbol{k}\sigma} c^\dagger_{\boldsymbol{k}\sigma} c_{\boldsymbol{k}\sigma}. \tag{2.3}$$

One can see that the conduction electrons keep exactly spin-label σ, not pseudo-spin label j_z.

The third term of eq.(2.1) is the mixing term between the f-electrons and the conduction electrons. The matrix elements connect the f^0 state $|ie\rangle$ with the f^1 states $|i\mu\rangle$, and the f^1 states $|i\mu\rangle$ with the f^2 states $|iM\rangle$ which include a component $|im\rangle$ composing $|i\mu\rangle$. This hybridization part of the Hamiltonian can be written in the form,

$$H_{\rm hyb} = \sum_{i\mu}\sum_{\boldsymbol{k}\sigma} V^{\mu e}_{\boldsymbol{k}\sigma} e^{i\boldsymbol{k}\boldsymbol{R}_i} |i\mu\rangle \langle ie| c_{\boldsymbol{k}\sigma} + \sum_{iM\mu}\sum_{\boldsymbol{k}\sigma} V^{M\mu}_{\boldsymbol{k}\sigma} e^{i\boldsymbol{k}\boldsymbol{R}_i} |iM\rangle \langle i\mu| c_{\boldsymbol{k}\sigma} + h.c. \qquad (2.4)$$

where $V^{\mu e}_{\boldsymbol{k}\sigma}$ and $V^{M\mu}_{\boldsymbol{k}\sigma}$ denote the hybridization matrix elements between f^0 and f^1 states and between f^1 and f^2 states, respectively.

This model is a generalization of the periodic Anderson model in the point that the local crystal field environment is taken into account. However, it is partially more restricted in the sense that fluctuations of f-electron number are restricted within those from f^0 to f^2 states.

2.2.1 Slave Boson Technique

It is a difficult task to treat exactly the above Hamiltonian (2.1) even numerically. So we will make use of the slave boson technique, which has successfully worked in the so-called Anderson model and Habbard model. In the present case it will be convenient to change the basis of the conduction electron states. In usual the basis of conduction electrons is classified by $\boldsymbol{k}, \sigma$ like in eq.(2.3). However, we here expand the Bloch states in terms of partial waves at each i-site f-ion as follows:[75]

$$c_{\boldsymbol{k}\sigma} = \sum_{\boldsymbol{k}' i\mu} (\boldsymbol{k}\sigma\ |\boldsymbol{R}_i; \boldsymbol{k}'\mu)\, c^i_{\boldsymbol{k}'\mu}, \qquad (2.5)$$

where $|\boldsymbol{k}\sigma)$ is the eigen state of the conduction electron band and $|\boldsymbol{R}_i; \boldsymbol{k}'\mu)$ is the eigen state with an irreducible representations μ around the site i.

Here, we may assume that in the hybridization term (2.4) the f-electron moving in/out the site i will mix only with conduction electrons in the state of the same irreducible representations. The other states of conduction electrons, which may be weakly coupled, are neglected approximately. This treatment becomes exact in the impurity Anderson model. Thus, we get the following model Hamiltonian:

$$H = \sum_{i\mu} E_\mu |i\mu\rangle \langle i\mu| + \sum_{iM} E_M |iM\rangle \langle iM| + \sum_{\boldsymbol{k}\mu} \epsilon_{\boldsymbol{k}\mu} c^\dagger_{\boldsymbol{k}\mu} c_{\boldsymbol{k}\mu}$$

$$+\left(\sum_{\boldsymbol{k}i\mu} V e^{i\boldsymbol{k}\boldsymbol{R}_i} |i\mu\rangle \langle ie| c_{\boldsymbol{k}\mu} + \sum_{\boldsymbol{k}iM\mu\nu}{}' V e^{i\boldsymbol{k}\boldsymbol{R}_i} |iM\rangle \langle i\mu| c_{\boldsymbol{k}\nu} + h.c.\right), \tag{2.6}$$

where the site index in $c_{\boldsymbol{k}\nu}$ is omitted and the prime on the summation in the last term indicates that the summation is restricted to the case where there are hybridization matrix elements between states $|iM\rangle$ and $|i\mu\rangle\,|i\nu\rangle$; $|i\nu\rangle$ is conduction-electron state with the irreducible representation ν at i-th site. Furthermore, for simplicity, $V^{\mu e}_{\boldsymbol{k}\sigma}$ and $V^{M\mu}_{\boldsymbol{k}\sigma}$ are replaced by a constant V below in this chapter and the conduction bands are taken to be structureless with a constant DOS.

To treat this Hamiltonian by the slave boson technique, we will define many slave bosons. We associate a boson e for f^0 state, $p_{i\mu}$, p_{im} for each one-body f^1 state $|i\mu\rangle$, $|im\rangle$ and bosons d_{iM}, d_{imn} for each two-body f^2 state $|iM\rangle$,$|imn\rangle$, respectively. By using these bosons, we can rewrite the Hamiltonian as the following form:

$$\begin{aligned} H' = &\sum_{i\mu} E_\mu p^\dagger_{i\mu} p_{i\mu} + \sum_{iM} E_M d^\dagger_{iM} d_{iM} + \sum_{\boldsymbol{k}\mu} \epsilon_{\boldsymbol{k}\mu} c^\dagger_{\boldsymbol{k}\mu} c_{\boldsymbol{k}\mu} \\ &+ \sum_{\boldsymbol{k}i\mu} \left(V e^{i\boldsymbol{k}\boldsymbol{R}_i} z^\dagger_{i\mu} f^\dagger_{i\mu} c_{\boldsymbol{k}\mu} + h.c. \right), \end{aligned} \tag{2.7}$$

where

$$z^\dagger_{i\mu} = (1 - Q_{i\mu})^{-1/2} \left(p^\dagger_{i\mu} e + \sum_{M\nu}{}' d^\dagger_{iM} p_{i\nu} \right) (Q_{i\mu})^{-1/2}, \tag{2.8}$$

$$Q_{i\mu} = p^\dagger_{i\mu} p_{i\mu} + \sum_{M}{}' d^\dagger_{iM} d_{iM}. \tag{2.9}$$

The factor $(1 - Q_{i\mu})^{-1/2} (Q_{i\mu})^{-1/2}$ in eq.(2.8) is necessary for Gutzwiller generalization. $p^\dagger_{i\mu}$ and $d^\dagger_{iM}$, which are used to treat the effect of multiplets properly, can be represented by the $p^\dagger_{im}$ and $d^\dagger_{imn}$ with such parameters as Clebsch-Gordon coefficients (a^μ_m, b^M_{mn}):

$$p^\dagger_{i\mu} = \sum_m a^\mu_m p^\dagger_{im}, \tag{2.10}$$

$$d^\dagger_{iM} = \sum_{mn} b^M_{mn} d^\dagger_{imn}. \tag{2.11}$$

However, the Hamiltonian H', which is defined by the enlarged Fock space, contains unphysical states. So we must impose a set of constraints to eliminate these states:

$$Q_i = e^\dagger_i e_i + \sum_\mu p^\dagger_{i\mu} p_{i\mu} + \sum_M d^\dagger_{iM} d_{iM} = 1, \tag{2.12}$$

$$Q_{i\mu} = f^\dagger_{i\mu} f_{i\mu}. \tag{2.13}$$

It is easy to check that the Hamiltonian H' under these constraints has the same matrix elements as those in the original Hilbert space. In order to investigate physical properties in this Hamiltonian H', the partition function Z will be calculated by using a functional integral over the coherent states of fermi and bose fields. Note that the commutation relations:

$$\begin{aligned} [H, Q_i] &= 0, \\ [H, Q_{i\mu}] &= 0. \end{aligned} \tag{2.14a}$$

Thus, the physical Hilbert space is preserved under the time evolution generated by this Hamiltonian H'. To enforce the constraints (2.12) at each site, it is convenient to introduce time independent Lagrange multipliers, λ_i and $\lambda_{i\mu}$. We integrate out the fermion fields to rewrite the partition function Z in terms of the effective action for the boson fields by invoking the identity:

$$\begin{aligned} \int \mathcal{D}\left(f^\dagger_{i\mu} f_{i\mu}\right) \mathcal{D}\left(c^\dagger_{\boldsymbol{k}\mu} c_{\boldsymbol{k}\mu}\right) \exp\Bigg(- \int dt \Bigg[\sum_{\boldsymbol{k}i\mu} \left(z^\dagger_{i\mu} V e^{i\boldsymbol{k}\boldsymbol{R}_i} f^\dagger_{i\mu} c_{\boldsymbol{k}\mu} + h.c. \right) \\ + \sum_{\boldsymbol{k}\mu} c^\dagger_{\boldsymbol{k}\mu} \left(\frac{\partial}{\partial\tau} + \epsilon_{\boldsymbol{k}\mu} \right) c_{\boldsymbol{k}\mu} + \sum_{\boldsymbol{i}\mu} f^\dagger_{i\mu} \left(\frac{\partial}{\partial\tau} + \lambda_{i\mu} \right) f_{i\mu} \Bigg] \Bigg) \\ = \exp\left[Tr \log\left(\frac{\partial}{\partial\tau} + E^{\pm}_{\boldsymbol{k}\mu} - \mu \right) \right], \end{aligned} \tag{2.15}$$

where μ is the chemical potential and $E^{\pm}_{\boldsymbol{k}\mu}$ represents the hybridized bands between f-electrons and conduction electrons given by

$$E^{\pm}_{\boldsymbol{k}\mu} = \frac{1}{2} \left[\epsilon_{\boldsymbol{k}\mu} + \lambda_{i\mu} \pm \sqrt{\left(\epsilon_{\boldsymbol{k}\mu} - \lambda_{i\mu} \right)^2 + 4 \left| z_{i\mu} V \right|^2} \right]. \tag{2.16}$$

The partition function can be expressed as follows:

$$Z = \int \mathcal{D}\left(e^\dagger_i e_i\right) \mathcal{D}\left(p^\dagger_{i\mu} p_{i\mu}\right) \mathcal{D}\left(d^\dagger_{iM} d_{iM}\right) d\lambda_i d\lambda_{i\mu} \exp\left[- \int d\tau \tilde{S}(\tau) \right], \tag{2.17}$$

$$\begin{aligned} \tilde{S}(\tau) = e^\dagger_i \left(\frac{\partial}{\partial\tau} + \lambda_i \right) e_i + \sum_{i\mu} p^\dagger_{i\mu} \left(\frac{\partial}{\partial\tau} + \lambda_i - \lambda_{i\mu} + E_\mu \right) p_{i\mu} \\ + \sum_{iM} d^\dagger_{iM} \left(\frac{\partial}{\partial\tau} + \lambda_i - \sum_\nu{}' \lambda_{i\nu} + E_M \right) d_{iM} - \frac{1}{\beta} Tr \log\left(\frac{\partial}{\partial\tau} + E^{\pm}_{\boldsymbol{k}\mu} - \mu \right), \end{aligned} \tag{2.18}$$

where $\beta = 1/T$ and we set $k_{\mathrm{B}} = 1$. Thus, we get the effective action $\tilde{S}(\tau)$ for the boson fields. We will approximately compute this action $\tilde{S}(\tau)$ in the next section.

2.2.2 Mean-Field Approximation

We are interested in the influences of $f^1 - f^2$ multiplets on the low-energy quasiparticle's excitations. It is well-known that at such low-energy region the saddle point approximation for the boson-field effective action in the so-called Anderson model is successful. We apply this approximation to the effective action $\tilde{S}(\tau)$, (2.18). This saddle point approximation corresponds to a mean field approximation for boson operators in the following Hamiltonian:

$$\begin{aligned} H(\lambda) = &\sum_{\boldsymbol{k}\mu} \lambda_\mu f^\dagger_{\boldsymbol{k}\mu} f_{\boldsymbol{k}\mu} + \sum_{\boldsymbol{k}\mu} \epsilon_{\boldsymbol{k}\mu} c^\dagger_{\boldsymbol{k}\mu} c_{\boldsymbol{k}\mu} + \sum_{\boldsymbol{k}\mu} \left(\tilde{V}_\mu f^\dagger_{\boldsymbol{k}\mu} c_{\boldsymbol{k}\mu} + h.c. \right) \\ &+ \sum_{i\mu} E_\mu p^2_\mu + \sum_{iM} E_M d^2_{iM} - \sum_{i\mu} \lambda_\mu Q_\mu + \sum_i \lambda \left(Q - 1 \right), \end{aligned} \tag{2.19}$$

where expectation values of boson operators are uniform and independent of sites, and $\tilde{V}_\mu = \sqrt{q_\mu} V$ ($q_\mu = \left\langle z^\dagger_{i\mu} z_{i\mu} \right\rangle$) is an renormalized hybridization. Because this Hamiltonian $H(\lambda)$ is in a quadratic form, we can diagonalize this $H(\lambda)$ and conventionally regard these eigen values as quasiparticle's bands:

$$E^\pm_{\boldsymbol{k}\mu} = E^\pm_\mu(\epsilon_{\boldsymbol{k}\mu}) = \frac{1}{2} \left[\epsilon_{\boldsymbol{k}\mu} + \lambda_\mu \pm \sqrt{\left(\epsilon_{\boldsymbol{k}\mu} - \lambda_\mu \right)^2 + 4\tilde{V}_\mu} \right]. \tag{2.20}$$

Thus, q_μ in the renormalized hybridization is the so-called renormalization factor and λ_μ is the renormalized f-levels. In this way the saddle point approximation gives us the following form for the free energy per site:

$$\begin{aligned} F = &\sum_\mu E_\mu p^2_\mu + \sum_M E_M d^2_M - \sum_\mu \lambda_\mu Q_\mu + \lambda \left(Q - 1 \right) \\ &- T \sum_\mu \int d\epsilon \rho_\mu(\epsilon) \log \left[1 + \mathrm{e}^{-\beta \left(E^\pm_\mu(\epsilon) - \mu \right)} \right], \end{aligned} \tag{2.21}$$

where $\rho_\mu(\epsilon)$ is the density of states of conduction electrons.

As the next step we must set the Lagrange multipliers to stabilize the given free energy. We obtain a set of coupled equations by differentiating the free energy F for each boson field as follows:

$$\frac{\partial F}{\partial \lambda} = Q - 1 = 0, \tag{2.22a}$$

$$\frac{\partial F}{\partial \lambda_\mu} = n^f_\mu - Q_\mu = 0, \tag{2.22b}$$

$$\frac{\partial F}{\partial e^2} = E_\mu + \lambda \tag{2.22c}$$

$$+\sum_{\nu}{}' \int_{-D}^{D} d\epsilon \rho_\nu(\epsilon) \frac{\partial}{\partial q_\nu} \left(E_\mu^{\pm}(\epsilon) f(E_\mu^{\pm}(\epsilon)) \right) \frac{\partial q_\nu}{\partial e^2} = 0, \tag{2.22d}$$

$$\frac{\partial F}{\partial p_\mu^2} = E_\mu + \lambda - \lambda_\mu \tag{2.22e}$$

$$+\sum_{\nu}{}' \int_{-D}^{D} d\epsilon \rho_\nu(\epsilon) \frac{\partial}{\partial q_\nu} \left(E_\mu^{\pm}(\epsilon) f(E_\mu^{\pm}(\epsilon)) \right) \frac{\partial q_\nu}{\partial p_\mu^2} = 0, \tag{2.22f}$$

$$\frac{\partial F}{\partial d_M^2} = E_M + \lambda - \sum_{\nu}{}' \lambda_\nu \frac{\partial n_\nu^f}{\partial d_M^2} \tag{2.22g}$$

$$+\sum_{\nu}{}' \int_{-D}^{D} d\epsilon \rho_\nu(\epsilon) \frac{\partial}{\partial q_\nu} \left(E_\mu^{\pm}(\epsilon) f(E_\mu^{\pm}(\epsilon)) \right) \frac{\partial q_\nu}{\partial d_M^2} = 0, \tag{2.22h}$$

$$q_\mu = \frac{\left| p_\mu^* e + \sum_{M\nu}{}' d_M^* p_\nu \right|^2}{(1 - Q_\mu) Q_\mu}, \tag{2.23}$$

where $n_\mu^f = \left\langle f_{i\mu}^\dagger f_{i\mu} \right\rangle$ is f-electron density of a μ state and D is half of the conduction band width. For simplicity we assume that the DOS for conduction electrons is constant ($\rho_0 = 1/2D$) and spreads over the energies ($-D \sim D$).

Thus at $T = 0$ an above-mentioned set of equations is more explicitly given by

$$e^2 + \sum_\nu p_\nu^2 + \sum_M d_M^2 = 1, \tag{2.24a}$$

$$p_\nu^2 + \sum_M{}' d_M^2 = n_\nu^f = \rho_0 V^2 q_\nu \left(\frac{1}{\lambda_\nu - \mu - \nu h} - \frac{1}{\lambda_\nu - E_\nu^-(-D)} \right), \tag{2.24b}$$

$$\lambda - \rho_0 V^2 \sum_{\nu'}{}' \log \left| \frac{\lambda_{\nu'} - \mu - \nu' h}{\lambda_{\nu'} - E_{\nu'}^-(-D)} \right| \frac{\partial q_{\nu'}}{\partial e^2} = 0, \tag{2.24c}$$

$$\lambda - \lambda_\nu + E_\nu + \rho_0 V^2 \sum_{\nu'}{}' \log \left| \frac{\lambda_{\nu'} - \mu - \nu' h}{\lambda_{\nu'} - E_{\nu'}^-(-D)} \right| \frac{\partial q_{\nu'}}{\partial p_\nu^2} = 0, \tag{2.24d}$$

$$\lambda - \sum_\nu{}' \lambda_\nu \frac{\partial n_\nu^f}{\partial d_M^2} + E_M + \rho_0 V^2 \sum_{\nu'}{}' \log \left| \frac{\lambda_{\nu'} - \mu - \nu' h}{\lambda_{\nu'} - E_{\nu'}^-(-D)} \right| \frac{\partial q_{\nu'}}{\partial d_M^2} = 0, \tag{2.24e}$$

$$\sum_\nu \left(n_\nu^f + n_\nu^c \right) = N, \tag{2.24f}$$

$$n_\nu^c = \rho_0 \left(\mu - E_\nu^-(-D) \right), \tag{2.24g}$$

where n_ν^c is a density of conduction electrons and the total electron numbers N is fixed, which is guaranteed by eq.(2.24f), so that the chemical potential μ is determined self-consistently. We also take into account the effect of magnetic field h to discuss quasi-particle contributions to the spin susceptibility. Although an upper hybridization band E_ν^+ is neglected in the above set of equations, it is necessary to include their contributions in actual calculations, depending on a position of the chemical potential.

2.3 Results

Now let us solve the above set of coupled equations in the special case. As we are interested in the CEF effect on the low-energy excitations and its variety due to f-electron number per site, we consider a simple model which includes relevant points. In this model, we assume that one-body bands have four kinds of the hybridized bands ($\mu = \pm 3/2, \pm 1/2$) and the f^2 states are composed of combination between these four f states ($M = \pm 2, \pm 1, 0$). This corresponds to the case where the spin-orbit interaction is very strong and $j - j$ coupling scheme is appropriate. Thus we pick up the $|\pm 1/2\rangle$ and $|\pm 3/2\rangle$ in the f^1 configurations and the $|\pm 2\rangle$, $|\pm 1\rangle$ and $|0\rangle$ in the f^2 configurations. For example, $|\pm 2\rangle$ is represented by $|\pm 3/2\rangle\,|\pm 1/2\rangle$ in $j - j$ coupling scheme. Futhermore, we will also consider the difference between the f^2 single and double ground state. As $|\pm 2\rangle$ can be mixed with each other in trigonal symmetry, whether the ground state is singlet or doublet can be controlled by ΔE, the energy difference in between $|\pm M\rangle = (|+2\rangle \pm |-2\rangle)/\sqrt{2}$. Referring to the information of the CEF splitting for UPd_3, which is similar to that of UPt_3, a number of parameters are determined to catch up the essence in the CEF effect on the low-energy excitations.

We have investigated basically the circumference of the following parameters:

D	V	$E_{\pm 3/2}$	$E_{\pm 1/2}$	$E_{\pm M}$	$E_{\pm 1}$
1	0.2	-0.5	-0.4	0	0.1

Here, E_s ($s = \pm 3/2, \pm 1/2, \pm M, \pm 1$) represent the energy separation between $|s\rangle$ and

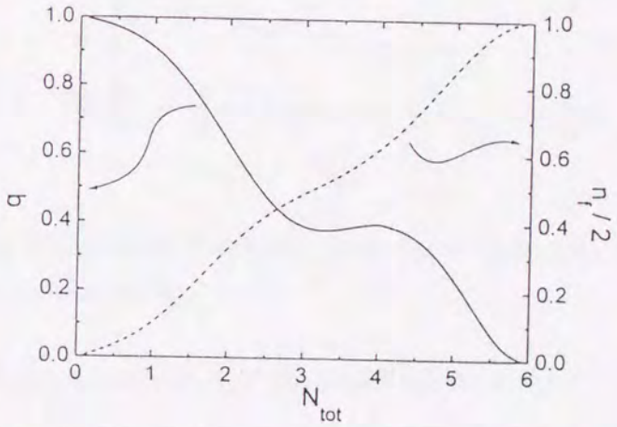

Figure 2.1: The renormalization factors q_μ and f- electron number n_f per site as a function of the total electron number per unit cell. q_μ is reduced as n_f is increasing.

the empty state $|e\rangle$.

The energy of the f^2 state $|0\rangle$ is assumed to be $E_0 = \infty$. If E_0 is near the f^2 ground state energy, the lowest quasi-particle bands are almost full-filled and the upper quasi-particle bands become empty. Thus, the quasiparticles in the lowest bands can not become heavy and the so-called heavy fermion systems are not realized. Assuming that $E_0 = \infty$, we can concentrate on the effects of the f^2 multiplets $E_{\pm M}$, $E_{\pm 1}$ in the heavy fermion systems.

Under these conditions we discuss the parameter dependence of physical properties. First of all, when the multiplet splitting is neglected, two kinds of quasi-particle bands are degenerated as shown in Fig. 2.1. One can see that the renormalization factor $q_{\pm 3/2}$ ($q_{\pm 1/2}$) becomes extremely small as $n_f = \sum_\mu n_\mu^f$ is increasing. It is noted that the quasi-particle bands are not highly renormalized even in the region $n_f \sim 1$. This is because for these parameters the empty component (e), which represents the f^0 state, still keeps a considerable weight. If the bare f^1 levels E_μ is deeper, or, $U_{\rm int} = E_{\pm M} - E_{\pm 3/2} - E_{\pm 1/2}$ is larger, then the quasi-particle bands in $n_f \sim 1$ are more renormalized, as demonstrated in Fig. 2.2.

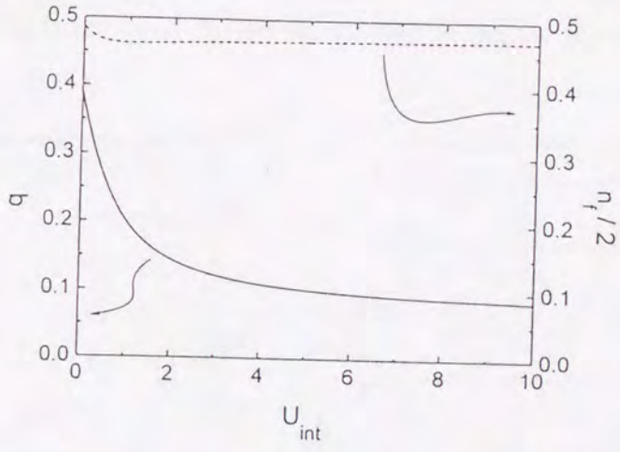

Figure 2.2: The $U_{\rm int}$ dependence of the renormalization factors q_μ in the region $n_f \sim 1$. q_μ becomes small as increasing $U_{\rm int}$.

Next, let us consider the effects of f^1 multiplet splitting. In $f^0 - f^1$ region the renormalized CEF splitting ($\Delta_{eff} = \lambda_2 - \lambda_1$) simply increases in proportional to the bare CEF splitting $\Delta = E_{\pm 1/2} - E_{\pm 3/2}$. Illustrated is the relations between Δ and the renormalization factors or Δ_{eff} in Fig. 2.3. In the region $n_f \sim 1$ the lower level is drastically renormalized and the upper one returns to be unrenormalized. In this case the renormal-

ized CEF splitting Δ_{eff} becomes larger than the bare CEF splitting Δ. In the region

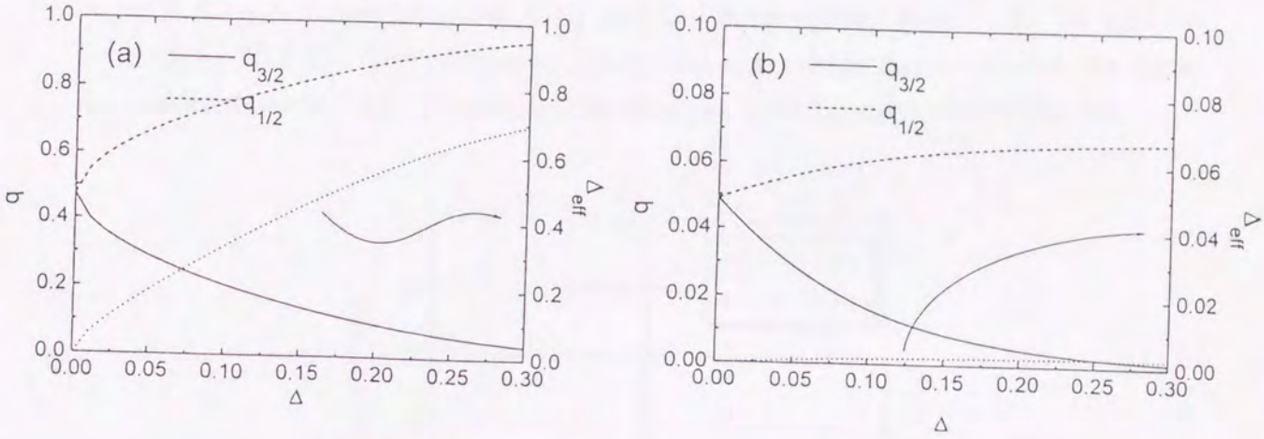

Figure 2.3: The renormalization factors q_μ and the renormalized CEF splitting $\Delta_{eff} = \lambda_{\pm 1/2} - \lambda_{\pm 3/2}$ between the renormalized bands as a function of the bare CEF splitting $\Delta = E_{\pm 1/2} - E_{\pm 3/2}$ in the region $n_f \sim 1$, (a), and in the region $n_f \sim 2$, (b). (a) As increasing Δ, $q_{\pm 3/2}$ are drastically decreasing while $q_{\pm 1/2}$ are increasing. Δ_{eff} is a monotonously increasing function of Δ. (b) All quantities remain highly renormalized.

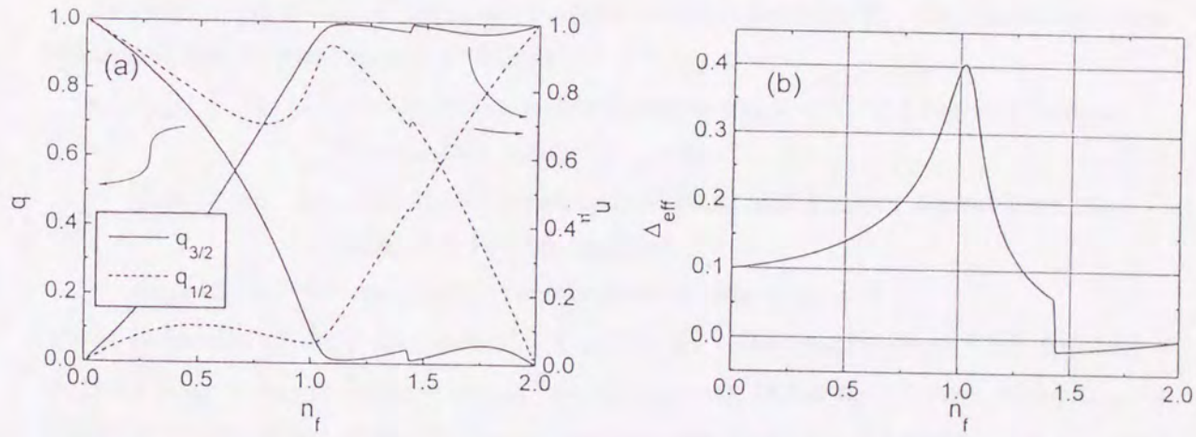

Figure 2.4: (a) q_μ and n_μ, and (b) $\Delta_{eff} = \lambda_{\pm 1/2} - \lambda_{\pm 3/2}$ as a function of total f- electron number per f-site. q_μ is reduced as n_μ increases. Δ_{eff} remains to be near Δ in the region $0 < n_f < 1$ and enhanced in $n_f \sim 1$ and renormalized in $n_f \sim 2$.

$n_f \sim 2$ both of quasi-particle bands are highly renormalized and Δ_{eff} is not almost en-

larged, i.e., "Δ_{eff} is highly renormalized," even if Δ increasing. This overall feature is demonstrated in Fig. 2.4, in which one can see that Δ_{eff} remains to be near Δ in the region $0 < n_f < 1$ and enhanced in $n_f \sim 1$ and renormalized in $n_f \sim 2$. We note the jump at $n_f \simeq 1.45$. This represents the special case where $\Delta_{eff} \sim 0$ and the highly renormalized bands ($|\pm 3/2\rangle$) exists in the wide gap ($|\pm 1/2\rangle$) as shown in Fig. 2.5.

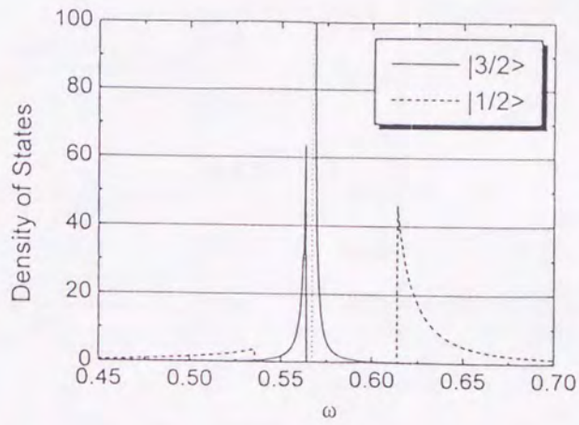

Figure 2.5: The quasi-particle DOS in $n_f \sim 1.45$. $\rho_{\pm 3/2}$ is highly renormalized and $\rho_{\pm 1/2}$ has the wide gap.

Regarding the width of the quasi-particle coherent peak as $T_{\rm K}$, the above-mentioned discussion can be summarized as follows:

- $\Delta_{eff} < T_{\rm K}$: little renormalized bands in the $0 < n_f < 1$ region (Valence Fluctuation regime).
- $\Delta_{eff} > T_{\rm K}$: one highly renormalized band and another almost bare band in $n_f \sim 1$ (Kondo regime).
- $\Delta_{eff} \ll T_{\rm K}$: two highly renormalized bands in $n_f \sim 2$.

These behaviors of Δ_{eff} are understood as follows. The renormalized CEF splitting is given by $\Delta_{eff} = \lambda_{\pm 1/2} - \lambda_{\pm 3/2} = (\lambda_{\pm 1/2} - \mu) - (\lambda_{\pm 3/2} - \mu)$. In the $n_f \sim 1$ case, while $\lambda_{\pm 3/2} - \mu$ is highly renormalized along 0, $\lambda_{\pm 1/2} - \mu$ is not renormalized. Therefore, the difference between $\lambda_{\pm 3/2} - \mu$ and $\lambda_{\pm 1/2} - \mu$ remains large. Futhermore, considering $\Delta_{eff} > \Delta$ in the $0 < n_f < 1$ region on the basis of the Fermi liquid theory,

$$\Delta_{eff} = q_{\pm 1/2}\left(E_{\pm 1/2} + \mathrm{Re}\Sigma_{\pm 1/2}(0)\right) - q_{\pm 3/2}\left(E_{\pm 3/2} + \mathrm{Re}\Sigma_{\pm 3/2}(0)\right), \quad (2.25a)$$

$$\rightarrow \left(E_{\pm 1/2} + \mathrm{Re}\Sigma_{\pm 1/2}\right), \quad (2.25b)$$

$$\sim E_{\pm 1/2} + n_{\pm 3/2} U_{\rm int}, \quad (2.25c)$$

since $q_{\pm 1/2} \sim 1$, $q_{\pm 3/2} \to 0$ as $n_f \to 1$. Because this last term is a monotonously increasing function of $n_{\pm 3/2}$, one can see that the increase of Δ_{eff} results from the increase of the Hartree term in the self-energy. On the other hand, in the $n_f \sim 2$ case Δ_{eff} is reduced, since both $q_{\pm 3/2}$ and $q_{\pm 1/2}$ are highly renormalized.

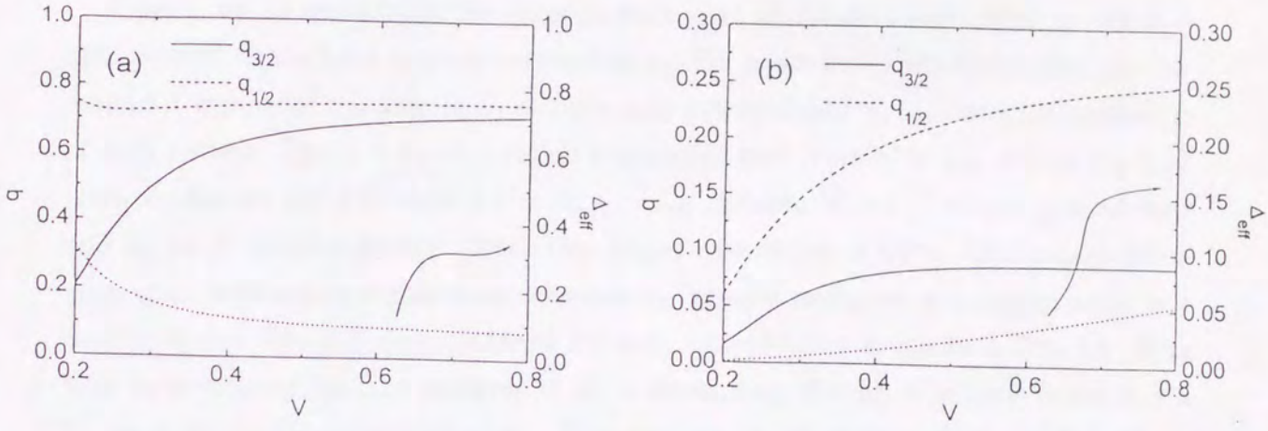

Figure 2.6: The hybridization V dependence of q_μ and Δ_{eff}. (a) in $n_f \sim 1$ only $q_{\pm 3/2}$ is largely changed and (b) in $n_f \sim 2$ all quantities make sensitive response.

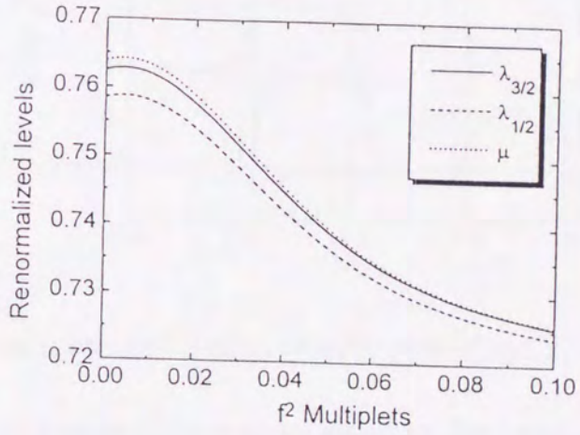

Figure 2.7: The f^2 multiplets effects on the renomalized levels $\lambda_{\pm 3/2}$ and $\lambda_{\pm 1/2}$. When the f^2 levels $E_{\pm M}$ are lower, f^1 states $\lambda_{\pm 3/2}$ and $\lambda_{\pm 1/2}$ concerning the state $|\pm M\rangle$ are pulled down.

Reflecting such fact, the hybridization dependence of Δ_{eff} is more sensitive in $n_f \sim 2$,

while only $q_{\pm 3/2}$ is largely changed in $n_f \sim 1$. (Fig. 2.6)

Furthermore, we take into consider the f^2 multiplet in addition to the f^1 multiplet. In $0 < n_f < 1$ region the effect of the f^2 multiplet can be almost neglected. In $n_f \sim 2$ small is the energy difference between the renormalized levels $\Delta_{eff} \to 0$ and two levels concerning to the f^2 multiplet trend to be pulled down.(Fig. 2.7)

Finally, let us investigate the quasi-particle part of the spin susceptibility, which is proportional to the total angular momentum j_z. For example, in the Gutzwiller approximation it is pointed out that in $n_f \sim 1$ the spin susceptibility χ_s indicates the instability of such system. The $1 < n_f < 2$ region also shows such instability ($\chi_s < 0$ in Fig 2.8). Now, we discuss the difference $\Delta E = E_{-M} - E_M$ between in the f^2 singlet ground state and in the f^2 doublet ground state. The singlet case is like in UPt_3. The energy difference, ΔE, between $|\pm M\rangle$ controls whether the ground multiplet is a singlet state or a doublet state. The ΔE dependence of the spin susceptibility is shown in Fig. 2.9. Note that as increasing ΔE the response of χ_s is decreasing, though it is hard to see it due to going across the divergence of χ_s, Nevertheless, as the quasi-particle DOS is clearly

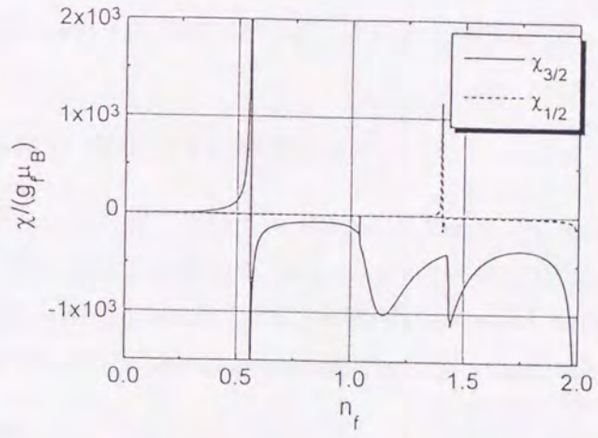

Figure 2.8: The spin susceptibility χ_s as a function of n_f. $\chi_s < 0$ in $0.5 < n_f < 2$.

enhanced, the heavy quasiparticles may be observed, for instance, in the specific heat. Therefore, there is the possibility that the f^2 singlet ground state is the new class of the heavy fermion state in which the charge susceptibility χ_c and the spin susceptibility χ_s are reduced and the electronic specific heat coefficient γ is enhanced. In such case the main part of χ_s is given by the incoherent term $\chi_{\rm inc}$, such as the so-called Van Vleck term and the quasi-particle part which is computed above is tiny. In the superconductivity

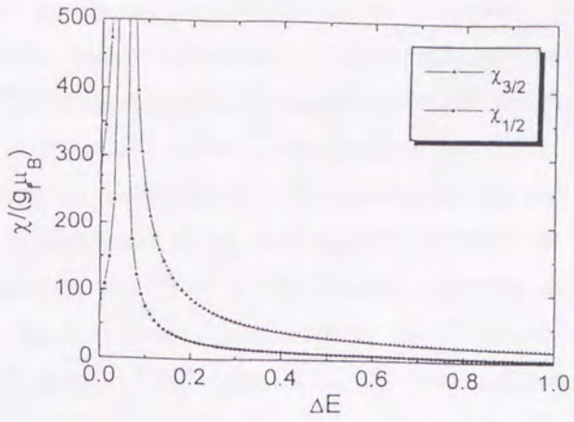

Figure 2.9: The ΔE dependence of the spin susceptibility (absolute value). As ΔE increases, χ_s is rather suppressed.

of UPt_3 it is reported that very small is the decrease of the spin susceptibility after the superconducting transition. This fact indicates that the quasiparticles which undergo the superconducting transition make few contributions to the spin susceptibility. Therefore, the above-mentioned heavy fermion state may be realized in UPt_3.

2.4 Summary and Discussions

With the use of the mean field theory in the slave boson technique it is demonstrated what influence the CEF splitting effects have on the low-energy quasi-particle exceptions in the multi-band periodic Anderson model with the constant hybridization V.

First, the results about the calculated quasi-particle bands are as follows:

	$q_{\pm 3/2}$	$q_{\pm 1/2}$	f^1 multiplet (Δ)	f^2 multiplet ($E_{-M} - E_M$)
$n_f < 1$	$\lesssim 1$	$\lesssim 1$	$\Delta_{eff} \sim \Delta < T_{\rm K}$	negligible
$n_f \sim 1$	$\ll 1$	~ 1	$\Delta_{eff} > \Delta \gg T_{\rm K}$	negligible
$n_f \sim 2$	$\ll 1$	$\ll 1$	$\Delta_{eff} < T_{\rm K} \ll \Delta$	The difference between two quasi-particle bands $\lambda_{\pm 3/2}$, $\lambda_{\pm 1/2}$ is reduced.

Here, $T_{\rm K}$ is roughly the width of the highly renormalized band, $\Delta_{eff} = \lambda_{\pm 1/2} - \lambda_{\pm 3/2}$ and q_μ are the renormalization factors.

In the region $0 < n_f < 1$ the quasi-particle bands are almost not renormalized and it corresponds to the Valence Fluctuation regime in Cerium system. In the case of $n_f \sim 1$

the quasi-particle bands are assigned to the f^1 ground CEF state since the CEF splitting is large and the upper bands are not renormalized. This case corresponds to the Kondo regime in Cerium system. In the case of $n_f \sim 2$ the quasi-particle bands are essentially degenerated since the CEF splitting is highly renormalized to vanish. This realized situation is near the f^2 states in Uranium based heavy fermion system.

Secondly, we have given qualitatively a few comments for the spin susceptibility. The spin susceptibility χ is composed of χ_{qp} and χ_{inc}. χ_{qp} represents the quasi-particle parts, which can be calculated by the effect of the Zeeman splitting and has been computed in this chapter. χ_{inc} is the incoherent part, such as the so-called Van Vleck term. In the case of $n_f \sim 1$ the f^1 ground CEF state is highly renormalized and χ_{qp} gives the most part of the spin susceptibility. In the case of $n_f \sim 2$ there are two kinds of cases. One is the case where the f^2 ground CEF state is a doublet state and another is the singlet case. In the doublet case two quasi-particle bands are highly renormalized and both bands contribute to χ_{qp}. And also χ_{inc}, which includes the Van Vleck term concerning the transition between the CEF levels, has large contributions since the quasi-particle CEF splitting is highly renormalized. Next, in the singlet case, regardless of the highly renormlization in two quasi-particle bands, χ_{qp} has few contributions to χ. Physically speaking, this contribution arises from that of the conduction electrons, which are often neglected in the heavy fermion system. In this case χ_{inc}, such as the Van Vleck term, has main contributions. Thus, the quasi-particle description in the f^2 singlet ground state may be the new class of the heavy fermion state in which the charge susceptibility χ_c and the spin susceptibility χ_s are suppressed, while the electronic specific heat coefficient γ is enhanced. Such heavy fermion state may be realized in UPt_3 around the superconducting transition.

Chapter 3

Effect of Crystalline Electric Field on Kondo Insulator

3.1 Introduction to CeNiSn

In this chapter we develop a theory of $\boldsymbol{k}$-space approach on the basis of "adiabatic continuation" to understand the anomalous properties of anisotropic semiconductor of heavy fermions, such as CeNiSn. We follow the formalism developed for the Fermi liquid theory of heavy fermions on the basis of the periodic Anderson model,[38] while we apply it to the filling corresponding to the band insulator. An essential point of our theory is that the hybridization matrix element can happen to vanish along some symmetry axis (in the $\boldsymbol{k}$-space) of the crystal for a particular symmetry of the crystal field which is expected to realize in CeNiSn. Then, the hybridization gap also vanishes along the same direction, which can explain wide range of the anomalies observed in CeNiSn.

We develop the formalism of our theory in §3.2.1 $\sim$ §3.2.5, and discuss about DOS in §3.2.6 and the effect of impurity scattering on DOS in §3.2.7. §3.3 is devoted to the discussions of physical properties and those validity: the specific heat (§3.3.1), the longitudinal NMR relaxation rate (§3.3.2), the magnetic properties (§3.3.3 and §3.3.4), the neutron scattering intensity (§3.3.5), and the anisotropic temperature dependence of the resistivity (§3.3.6) are discussed in detail on the model calculations. Furthermore, the effect of pressure (§3.3.8) and the quasi-particle lifetime (§3.3.10) are briefly discussed.

3.2 Theory

3.2.1 Hamiltonian

We start with the periodic Anderson model keeping it in mind that $(4f)^1$ configuration is realized in Ce^{3+} ion in those compounds:[39]

$$H = H_c + H_f + H_{c-f}, \tag{3.1}$$

where H_c, H_f, and H_{c-f} stands for the Hamiltonian of conduction electrons, f-electrons, and the hybridization among them, respectively. The first term in eq.(3.1), H_c, is given by

$$H_c = \sum_{\boldsymbol{k}\sigma} \xi_{\boldsymbol{k}} c^\dagger_{\boldsymbol{k}\sigma} c_{\boldsymbol{k}\sigma}, \tag{3.2}$$

where $c^\dagger_{\boldsymbol{k}\sigma}(c_{\boldsymbol{k}\sigma})$ creates (annihilates) a conduction electron in a plane wave state labeled by wave vector $\boldsymbol{k}$ and spin $\sigma(\pm)$. The plane wave state can be expanded around site i ($\boldsymbol{r}_i$) as follows:

$$|\boldsymbol{k}\sigma\rangle = \frac{1}{\sqrt{V}} e^{i\boldsymbol{k}\cdot\boldsymbol{r}} \chi_\sigma = \frac{4\pi}{\sqrt{V}} e^{i\boldsymbol{k}\cdot\boldsymbol{r}_i} \sum_{l=0}^{\infty} i^l j_l(k|\boldsymbol{r}-\boldsymbol{r}_i|) \sum_{m=-l}^{l} Y_l^{m*}(\Omega_{\boldsymbol{k}}) Y_l^m(\Omega_{\boldsymbol{r}-\boldsymbol{r}_i}) \chi_\sigma, \tag{3.3}$$

where χ_σ is the spin function, $j_l(kr)$ is the spherical Bessel function, Y_l^m is the spherical harmonics with the argument of solid angle $\Omega_{\boldsymbol{r}}$ of the position vector $\boldsymbol{r}$ or $\Omega_{\boldsymbol{k}}$ of the wave vector $\boldsymbol{k}$, and V is the volume of the crystal.

The second term in eq.(3.1), H_f, is given by

$$H_f = \sum_{\boldsymbol{k}M} E_M f^\dagger_{\boldsymbol{k}M} f_{\boldsymbol{k}M} + \frac{1}{2} U \sum_{i, M \neq M'} f^\dagger_{iM} f_{iM} f^\dagger_{iM'} f_{iM'}, \tag{3.4}$$

where $f^\dagger_{iM}(f_{iM})$ is the creation (annihilation) operator of the f-electron on the orbital M in the $4f$ shell at site i, and $f^\dagger_{\boldsymbol{k}M}(f_{\boldsymbol{k}M})$ is its Fourier transform, and E_M's denote the energy levels of the $4f$-electron which are split into j=7/2 and j=5/2 multiplets under the spin-orbit interaction and further separated by the crystal-field interaction in general. The angular part of its eigen function is expressed as

$$|M\rangle = \sum_{\mu} b_\mu^M \sum_{m\sigma} a_{lm\sigma}^\mu Y_l^m(\Omega_{\boldsymbol{r}-\boldsymbol{r}_i}) \chi_\sigma, \tag{3.5}$$

where μ is the z-component of the total angular momentum, j, and $a_{lm\sigma}^\mu$ are the Clebsch-Gordan coefficients, and b_μ^M are coefficients specifying the crystal-field level. The last

term in eq.(3.4) represents the Coulomb repulsion U between f-electrons in the states $|M\rangle$ and $|M'\rangle$. For simplicity, we neglect M- and M'- dependence of U.

The last term in eq.(3.1), H_{c-f}, describes the hybridization between f- and conduction electrons:

$$H_{c-f} = \sum_{\boldsymbol{k}M\sigma} (V_{\boldsymbol{k}M\sigma} c^{\dagger}_{\boldsymbol{k}\sigma} f_{\boldsymbol{k}M} + h.c.), \tag{3.6}$$

where $V_{\boldsymbol{k}M\sigma}$ is the mixing matrix element which can be calculated with the use of eqs.(3.3) and (3.5) as

$$V_{\boldsymbol{k}M\sigma} = \sqrt{4\pi} V_{kl} \sum_{\mu} b^{M}_{\mu} \sum_{m} a^{\mu}_{lm\sigma} Y^{m}_{l}(\Omega_{\boldsymbol{k}}). \tag{3.7}$$

Here, V_{kl} has the energy dependence of the mixing matrix, and is treated as a parameter of our model.

3.2.2 Hybridization and Green Function

Now we consider the case in which the crystal-field splitting is so large that we can neglect the effects of excited crystal-field states in the relevant low-temperature and low-energy phenomena. Then we are left with two conduction bands ($\pm\sigma$) and two f-levels($\pm M$). In this case the Green functions of conduction- and f-electrons are given by[38, 39]

$$G^{c}_{\sigma}(\boldsymbol{k},\omega) = \frac{1}{\omega - \xi_{\boldsymbol{k}} - \dfrac{V^2_f(\boldsymbol{k})}{\omega - E_f - \Sigma_f(\boldsymbol{k},\omega)}}, \tag{3.8a}$$

$$G^{f}_{M}(\boldsymbol{k},\omega) = \frac{1}{\omega - E_f - \Sigma_f(\boldsymbol{k},\omega) - \dfrac{V^2_f(\boldsymbol{k})}{\omega - \xi_{\boldsymbol{k}}}}, \tag{3.8b}$$

where E_f is the lowest crystal-field level and $\Sigma_f(\boldsymbol{k},\omega)$ is the self-energy of f-electrons due to the Coulomb repulsion U. The hybridization $V^2_f(\boldsymbol{k})$ can be regarded as independent of σ after an appropriate linear combinations of $|M\rangle$ and $|\bar{M}\rangle$ have been taken.

$$V^2_f(\boldsymbol{k}) \equiv |V_{\boldsymbol{k}M\sigma}|^2 + |V_{\boldsymbol{k}\bar{M}\sigma}|^2 = |V_{\boldsymbol{k}M\sigma}|^2 + |V_{\boldsymbol{k}M\bar{\sigma}}|^2 \tag{3.9}$$

The $\boldsymbol{k}$-dependence of $V_f(\boldsymbol{k})$ reflects the symmetry of the lowest crystal-field level in general.[39, 76] For example, in the case of CeNiSn and its isostructual compounds, in which the approximate local symmetry of the crystal field is trigonal D_{3d}[77], the energy levels split into three doublets: $|5/2, \pm 3/2\rangle$, $a\,|5/2, \pm 1/2\rangle + b\,|5/2, \mp 5/2\rangle$, and $-b\,|5/2, \pm 1/2\rangle + a\,|5/2, \mp 5/2\rangle$, with a and b being appropriate constants satisfying $a^2 + b^2 = 1$. And in the

case of $CeCu_2Si_2$, the crystal-field ground state is $a\,|5/2, \pm 5/2\rangle + b\,|5/2, \mp 3/2\rangle$ $(a > b)$, and two excited states are $|5/2, \pm 1/2\rangle$ and $-b\,|5/2, \pm 5/2\rangle + a\,|5/2, \mp 3/2\rangle$. Depending on the symmetry of the crystal-field ground state, there occurs various angular dependence of the hybridization $V_f^2(\boldsymbol{k})$. While the hybridization is finite at any direction of $\hat{k} \equiv \boldsymbol{k}/|\boldsymbol{k}|$ in the state including $|5/2, \pm 1/2\rangle$, such as $|\pm p\rangle \equiv a\,|5/2, \pm 1/2\rangle + b\,|5/2, \mp 5/2\rangle$, it vanishes along the quantization axis (z-axis) in purely $|5/2, \pm 5/2\rangle$ and $|\pm m\rangle \equiv |5/2, \pm 3/2\rangle$:[76]

$$V_{\pm m}^2(\boldsymbol{k}) = V^2(1 - \hat{k}_z^2)(1 + 15\hat{k}_z^2), \tag{3.10a}$$

$$V_{\pm p}^2(\boldsymbol{k}) = V^2\left[a^2 2(5\hat{k}_z^4 - 2\hat{k}_z^2 + 1) + b^2 5(1 - \hat{k}_z^2)^2 - 4\sqrt{10}ab(\hat{k}_x^2 - 3\hat{k}_y^2)\hat{k}_x\hat{k}_z\right], \tag{3.10b}$$

where V^2 gives $|\boldsymbol{k}|$-dependence of $V^2(\boldsymbol{k})$ and z-axis is taken as parallel to the a-axis, the symmetry axis of these crystals.

3.2.3 Effective Hamiltonian for Quasiparticles

We are interested in the low temperature region, in which the physical properties can be described by the renormalized quasiparticles near the Fermi level after the many-body effect due to the on-site repulsion U in eq.(3.4) has been taken into account. This description is justified when f-electron number is near 1 and a CEF splitting Δ is larger than a hybridization V, such as it is shown with the use of slave boson technique in the chapter 2.

These quasiparticles are described by the effective Hamiltonian

$$\tilde{H}_{eff} = \sum_{\boldsymbol{k}\sigma} \xi_{\boldsymbol{k}} c_{\boldsymbol{k}\sigma}^\dagger c_{\boldsymbol{k}\sigma} + \sum_{\boldsymbol{k}} \tilde{E}_f \tilde{f}_{\boldsymbol{k}}^\dagger \tilde{f}_{\boldsymbol{k}} + \sum_{\boldsymbol{k}\sigma} \sum_{M=\pm} (\tilde{V}_{\boldsymbol{k}M\sigma} c_{\boldsymbol{k}\sigma}^\dagger \tilde{f}_{\boldsymbol{k}} + h.c.), \tag{3.11a}$$

where

$$\tilde{E}_f = z_{\boldsymbol{k}}\left[E_f + \Sigma_f(\boldsymbol{k}, 0)\right], \tag{3.11b}$$

$$\tilde{V}_{\boldsymbol{k}M\sigma} = \sqrt{z_{\boldsymbol{k}}} V_{\boldsymbol{k}M\sigma}, \tag{3.11c}$$

where the renormalization amplitude $z_{\boldsymbol{k}}$ is defined as

$$z_{\boldsymbol{k}} = \left[1 - \frac{\partial \Sigma_f(\boldsymbol{k}, \omega)}{\partial \omega}\right]_{\omega=0}^{-1} \ll 1 \tag{3.12}$$

Here, the renormalized f-level $\tilde{E}_f$ has a $\boldsymbol{k}$-dependence through that of the self-energy $\Sigma_f(\boldsymbol{k}, 0)$ in general. However, we first investigate the case where the $\boldsymbol{k}$-dependence can be neglected, because the heavy quasiparticles themselves would not be formed if $\Sigma_f(\boldsymbol{k}, 0)$

had appreciable dispersion. The effect of its $\boldsymbol{k}$-dependence will be discussed later in relation to the resistivity (§3.3.6) and the effect of pressure (§3.3.8).

Then we can rewrite the Green functions, eqs.(3.8), as

$$G^c_\sigma(\boldsymbol{k},\omega) = \frac{1}{\omega - \xi_k - \tilde{V}_f^2(\boldsymbol{k})/(\omega - \tilde{E}_f)} = \frac{A^c_+(\boldsymbol{k})}{\omega - E^+_{\boldsymbol{k}}} + \frac{A^c_-(\boldsymbol{k})}{\omega - E^-_{\boldsymbol{k}}}, \tag{3.13a}$$

$$G^f_M(\boldsymbol{k},\omega) = \frac{z_{\boldsymbol{k}}}{\omega - \tilde{E}_f - \tilde{V}_f^2(\boldsymbol{k})/(\omega - \xi_{\boldsymbol{k}})} = z_{\boldsymbol{k}} \left(\frac{A^f_+(\boldsymbol{k})}{\omega - E^+_{\boldsymbol{k}}} + \frac{A^f_-(\boldsymbol{k})}{\omega - E^-_{\boldsymbol{k}}} \right), \tag{3.13b}$$

where $E^\pm_{\boldsymbol{k}}$ are two hybridized quasi-particle bands given by

$$E^\pm_{\boldsymbol{k}} = \frac{1}{2}\left[\xi_{\boldsymbol{k}} + \tilde{E}_f \pm \sqrt{(\xi_{\boldsymbol{k}} - \tilde{E}_f)^2 + 4\tilde{V}_f^2(\boldsymbol{k})} \right], \tag{3.14}$$

where

$$\tilde{V}_f^2(\boldsymbol{k}) = z_{\boldsymbol{k}} V_f^2(\boldsymbol{k}). \tag{3.15}$$

The residues $A^c_\pm(\boldsymbol{k})$ and $A^f_\pm(\boldsymbol{k})$ in eqs.(3.13) are

$$A^c_\pm(\boldsymbol{k}) = \left[1 + \frac{\tilde{V}_f^2(\boldsymbol{k})}{(E^\pm_{\boldsymbol{k}} - \tilde{E}_f)^2} \right]^{-1}, \tag{3.16a}$$

$$A^f_\pm(\boldsymbol{k}) = \left[1 + \frac{\tilde{V}_f^2(\boldsymbol{k})}{(E^\pm_{\boldsymbol{k}} - \xi_{\boldsymbol{k}})^2} \right]^{-1}, \tag{3.16b}$$

which give the spectral weight of conduction- and f-electrons, respectively, in the upper/lower bands.

So far we have talked about k-dependence of hybridization matrix elements on general CEF ground states. It is considered that such k-dependence will be specially important when the Fermi level is located near a hybridization gap. However we do not dispute these importance here and we will do it in detail in §3.3.10. First, we will show that how interesting properties such k-dependence of hybridization matrix elements results in, when the Fermi level is located in quasi-particle hybridization gap. In particular we will get the fact that overall features of some anomalous properties in so-called "Kondo insulator", CeNiSn and CeRhSb, which are called "Kondo semimetal" lately, can be explained in the case where the CEF ground state is $|5/2, \pm 3/2\rangle$. We will discuss this remarkable fact below. While other "Kondo insulators", such as $Ce_3Bi_4Pt_3$, SmB_6, are in future problem, those will be argued from this point of view in §3.4

3.2.4 Band Insulator of Quasiparticles

As we have mentioned above, almost all the compounds called "Kondo insulator" contain even number of electrons in the unit cell and have a right to be a band insulator. If we assume that low-energy excitations in "Kondo insulator" can be described by quasi-paritcles such as the metallic case of heavy fermion system, it can be considered that at low temperature "Kondo insulator" forms highly renormalized quasi-particle bands by strong correlation effect between f-electrons and its electron filling corresponds to the band insulator. In one word we can say that "Kondo insulator" is the quasi-particle band insulator. We will state whether the quasi-particle bands can be formed in the insulating case. Hereafter, we focus on the properties in the quasi-particle band insulator. In such case of the electron filling corresponding to the band insulator, the renormalized Fermi level is located in between $E^+_{\boldsymbol{k}}$ and $E^-_{\boldsymbol{k}}$ forming the renormalized hybridization gap and low-energy quasi-particle excitations reflect this gap structure seriously. As the gap structure is related to the hybridization matrix elements, k-dependence of this hybridization becomes very important. This k-dependence is determined by the character of the CEF ground state at f-site. We mainly investigate the case where the ground crystal-field level is $|5/2, \pm 3/2\rangle$, which turn out to be consistent with anomalous properties of CeNiSn as discussed below.[78] Then, due to eqs.(3.10a),(3.14) and (3.15), the hybridization gap $\Delta(\boldsymbol{k}_{\rm B})$ is given by

$$\Delta(\boldsymbol{k}_{\rm B}) \simeq 2\frac{\tilde{V}_f^2(\boldsymbol{k}_{\rm B})}{\xi_{\boldsymbol{k}_{\rm B}}} \simeq 2z_{\boldsymbol{k}_{\rm B}}\frac{V_f^2(\boldsymbol{k}_{\rm B})}{\xi_{\boldsymbol{k}_{\rm B}}} \equiv T_{\rm K}(1-\hat{k}^2_{{\rm B}z})(1+15\hat{k}^2_{{\rm B}z}) \tag{3.17}$$

where $\boldsymbol{k}_{\rm B}$ denotes the wavevector at the zone boundary and $T_{\rm K} \equiv 2z_{\boldsymbol{k}_B}V^2/D$. For simplicity we neglect $|\boldsymbol{k}|$-dependence of V^2 and $\boldsymbol{k}$-dependence of $z_{\boldsymbol{k}_{\rm B}}$. In deriving eq.(3.17), we have assumed that the renormalized hybridization $\sqrt{z_{\boldsymbol{k}_B}}V$ is much smaller than the bare band-width of conduction electrons $2D$. Thus the hybridization gap vanishes at points on the zone boundary where $\hat{k}_{{\rm B}z} = \pm 1$ and becomes a pseudogap. That is, the renormalized DOS have no clear gap threshold. This is to be compared to the "axial-like gap" in anisotropic superconductors, although the resultant DOS is totally different as discussed below.

3.2.5 Effect of Impurity Scattering

It can be shown, on the basis of the Ward identity arguments, that the s-wave impurity potential u is renormalized by many-body vertex correction as[79]

$$u \to \tilde{u} = u \cdot \left[1 - \frac{\partial \Sigma_f(\boldsymbol{k}, \omega)}{\partial \omega}\right]_{\omega=0} = \frac{1}{z} u \tag{3.18}$$

This renormalization is shown in Fig. 3.1 in terms of the Feynman diagram. Then,

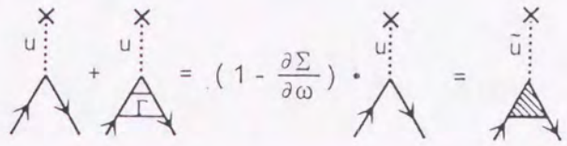

Figure 3.1: The diagram for the many-body vertex correction of impurity scattering. The broken line represents the impurity potential u of s-wave, the external solid line the Green function of the f-electrons, and internal solid line stands both f-electrons and conduction electrons. Γ is the full vertex due to the Coulomb repulsion between f-electrons. $\tilde{u}$ is a renormalized potential of impurity scattering.

for strongly correlated systems where $z^{-1} = m^*/m \gg 1$, the impurity scattering always becomes that of unitarity limit, i.e., $\tilde{u}N_{\rm F} \gg 1$, even if the bare potential u is moderate one, i.e., $uN_{\rm F} \lesssim 1$. Then the Green functions of the conduction- and f-electrons are given by

$$G_\sigma^c(\boldsymbol{k}, \omega) = \frac{1}{\omega - \xi_{\boldsymbol{k}} - \dfrac{\tilde{V}_f^2(\boldsymbol{k})}{\omega - \tilde{E}_f - \mathrm{i}z_{\boldsymbol{k}}\mathrm{Im}\Sigma_{\rm imp}(\omega)}}, \tag{3.19a}$$

$$G_M^f(\boldsymbol{k}, \omega) = \frac{z_{\boldsymbol{k}}}{\omega - \tilde{E}_f - \mathrm{i}z_{\boldsymbol{k}}\mathrm{Im}\Sigma_{\rm imp}(\omega) - \dfrac{\tilde{V}_f^2(\boldsymbol{k})}{\omega - \xi_{\boldsymbol{k}}}}, \tag{3.19b}$$

where the self-energy $\Sigma_{\rm imp}(\omega)$ due to impurity scattering is given in the t-matrix approximation by

$$\Sigma_{\rm imp}(\omega) = n_{\rm imp} \frac{\tilde{u}}{1 - \tilde{u}\sum_{\boldsymbol{k}} G_M^f(\boldsymbol{k}, \omega)}, \tag{3.20}$$

where $n_{\rm imp}$ denotes the impurity concentration. In deriving eqs.(3.19), the self-energy of conduction electrons due to impurity scattering has been neglected because the renormalization, such as eq.(3.18), does not occur. Equations (3.19) and (3.20) need to be

solved self-consistently as in the case of heavy fermion superconductors, where the impurity scattering in the unitarity limit is known to give rise to appreciable residual DOS in the V-shaped gap even for a very small impurity concentration.[80, 81]

3.2.6 Quasi-particle Density of States

The quasi-particle DOS are calculated as follows:

$$\tilde{N}(\omega) = \sum_{\boldsymbol{k}\sigma} \left[\delta(\omega - E^{+}_{\boldsymbol{k}}) + \delta(\omega - E^{-}_{\boldsymbol{k}}) \right], \tag{3.21a}$$

$$= N_{\mathrm{F}} \int_0^1 d\hat{k}_z \int_{-D}^{D} dE \left(1 + \frac{\tilde{V}_f^2(\hat{k}_z)}{E^2} \right) \delta(\omega - E)\theta(|E| - \Delta_f(\hat{k}_z)), \tag{3.21b}$$

where

$$\Delta_{\pm 1/2}(\hat{k}_z) \equiv T_{\mathrm{K}} 2(5\hat{k}_z^4 - 2\hat{k}_z^2 + 1), \tag{3.22a}$$

$$\Delta_{\pm 3/2}(\hat{k}_z) \equiv T_{\mathrm{K}}(1 - \hat{k}_z^2)(1 + 15\hat{k}_z^2), \tag{3.22b}$$

$$\Delta_{\pm 5/2}(\hat{k}_z) \equiv T_{\mathrm{K}} 5(1 - \hat{k}_z^2)^2. \tag{3.22c}$$

In deriving eq.(3.21b) from eq.(3.21a), we have assumed for simplicity that the conduction band has a linear dispersion with constant DOS, N_{F}, and extending from $-D$ to D, and $\tilde{E}_f = 0$. A result of numerical calculation of $\tilde{N}(\omega)$, eq.(3.21b), is shown in Fig. 3.2. Here, the relation between the hybridization V and renormalization factor z is determined as $zV^2/D = 0.01D$. The shapes of quasi-particle DOS shown in Fig. 3.2 have characteristic features as follows: in $|5/2, \pm 1/2\rangle$ there is a well-known constant hybridization gap; and in $|5/2, \pm 3/2\rangle$ $\tilde{N}(\omega = 0)$ is finite and it exhibits four-peak structure, i.e., there exist two energy scales ($\Delta_1 = T_{\mathrm{K}} = 0.02D, \Delta_2 \simeq 0.08D$); and in $|5/2, \pm 5/2\rangle$ $\tilde{N}(\omega = 0)$ is infinite like $1/\sqrt{\omega}$. These properties can be easily understood by investigation of the wave-vector $\boldsymbol{k}$ dependence of the each hybridization gap. Structures of hybridization gaps (3.22a) is indicated in Fig. 3.3. It is noted that there are a few points at which each Δ_f is flat and those energies correspond to peak structures at DOS. That is to say, each peak structure at DOS results from well-known Von Hove singularities. The reason why the DOS of the state $|5/2, \pm 5/2\rangle$ is infinite at zero energy is so, too. The case of the state $|5/2, \pm 3/2\rangle$, which we will investigate in detail below, is particularly interesting. In this case there exist a few states in the hybridization pseudogap Δ_1. These states result from the fact that the hybridization gap vanishes at points ($\hat{k}_z = \pm 1$). This shape of DOS

around the Fermi level $\omega = 0$ can be calculated analytically as

$$\tilde{N}(\omega) \simeq N_F \frac{D^2}{64zV^2}\left[1+2\left(1+\frac{19D^2}{12\cdot 32zV^2}\right)\frac{\omega}{D}+\cdots\right]. \tag{3.23}$$

This is in marked contrast with the case of heavy-fermion superconductors, where the

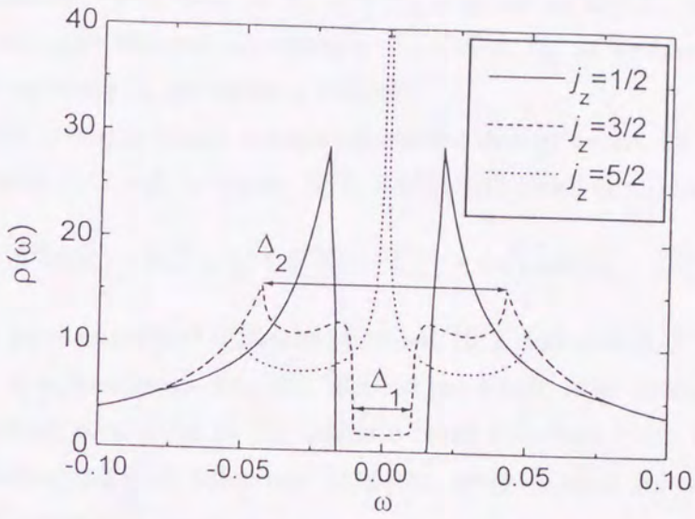

Figure 3.2: The density of states, $\tilde{N}(\omega)$, of the quasiparticles as a function of ω in the unit D, half the band-width of conduction band. The Fermi level is located at $\omega = 0$.

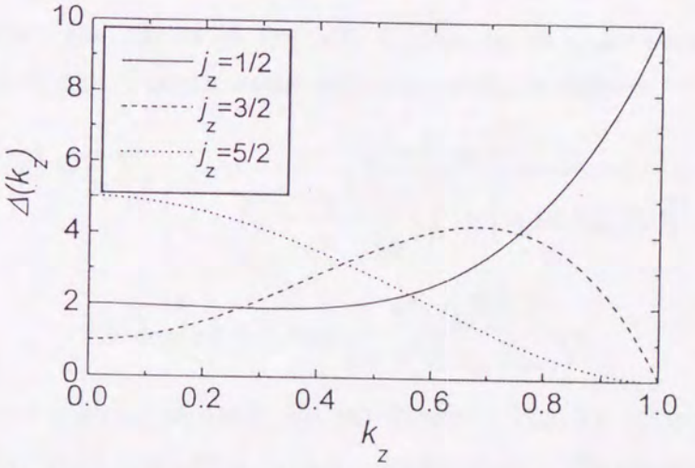

Figure 3.3: The $\hat{k}_z$ dependence of the hybridization gap Δ_f. The flat parts correspond to peak structures at DOS.

point node leads to DOS proportional to ω^2. The reason for this characteristic to hold is that there exists a singularity $\propto E^{-2}$, in the first factor of the integrand of (3.21b), which arises from the Jacobian $|\mathrm{d}\xi/\mathrm{d}E| = 1 + \tilde{V}_f^2(\hat{k}_z)/E^2$.

Furthermore, it is more interesting that there exist two energy scales, which is related to the existence of two extremum values of $\Delta_{\pm 3/2}(\hat{k}_z)$, eq.(3.22a): Δ_1 corresponds to the minimum of eq.(3.22a) at $\hat{k}_z = 0$, at which the hybridization gap is given by T_K, and Δ_2 corresponds to the maximum of eq.(3.22a) at $\hat{k}_z = \sqrt{7/15}$, in which the hybridization gap becomes maximum. The ratio of Δ_2 and Δ_1 is given as $\Delta_2/\Delta_1 = 64/15$. Most of these properties are kept without asymmetry of DOS so far as an energy dispersion of conduction electrons along k_z go across a f-level.

There is another scenario which presents these two energy scales. It is the case where the CEF ground state $|5/2, \pm p\rangle$ is mainly $|5/2, \pm 5/2\rangle$ with small admixture of $|5/2, \pm 1/2\rangle$:

$$\Delta_{\pm p}(\hat{k}) = T_{\rm K}\left[a^2 2(5\hat{k}_z^4 - 2\hat{k}_z^2 + 1) + b^2 5(1-\hat{k}_z^2)^2 - 4\sqrt{10}ab(\hat{k}_x^2 - 3\hat{k}_y^2)\hat{k}_x\hat{k}_z\right], \qquad (3.24)$$

where $a < b$. The most important difference between $|5/2, \pm p\rangle$ and $|5/2, \pm 3/2\rangle$ is whether the small gap Δ_1 is a pseudogap, i.e., the DOS at the Fermi level exists. If we quantitatively discuss physical properties in the realistic band structure, then it is questionable whether we can distinguish such difference. However, we make clear the case of $|5/2, \pm 3/2\rangle$ below on some circumstantial evidences.

3.2.7 Effect of Impurity Scattering on Density of States

Next let us consider the effects of impurity scattering on quasi-particle DOS. From eqs.(3.19b) and (3.20), DOS is calculated self-consistently as follows:

$$\tilde{N}(\omega) \approx \frac{1}{\pi}\sum_{\boldsymbol{k}} \frac{-z_{\boldsymbol{k}}{\rm Im}\Sigma_{\rm imp}(\omega)}{\left(\omega - \tilde{E}_f - \dfrac{z_{\boldsymbol{k}}V_f^2(\boldsymbol{k})}{\omega - \xi_{\boldsymbol{k}}}\right)^2 + \left[z_{\boldsymbol{k}}{\rm Im}\Sigma_{\rm imp}(\omega)\right]^2}, \qquad (3.25a)$$

$${\rm Im}\Sigma_{\rm imp}(\omega) = -n_{\rm imp}\frac{\tilde{u}^2\pi z_{\boldsymbol{k}}\tilde{N}(\omega)}{1 + \tilde{u}^2\left(\pi z_{\boldsymbol{k}}\tilde{N}(\omega)\right)^2}. \qquad (3.25b)$$

Results of numerical solution of eqs.(3.25) are shown in Fig. 3.4. One can see that the residual DOS at the Fermi level, $\tilde{N}(\omega = 0)$, is very sensitive to the impurity concentration and drastically increases with the impurity concentration $n_{\rm imp}$. In Fig. 3.5 one finds that $\tilde{N}(\omega = 0)$ is roughly proportional to $\sqrt{n_{\rm imp}}$. Precisely speaking, the residual DOS exists, even if $n_{\rm imp} = 0$. So, in the limit, $n_{\rm imp} \to 0$, its $n_{\rm imp}$-dependence is given by $N_0\sqrt{1 + c_0 n_{\rm imp}}$, where N_0 is the residual DOS without impurities, and c_0 is a proper constant of order unity. This is to be compared with the impurity effects in heavy fermion

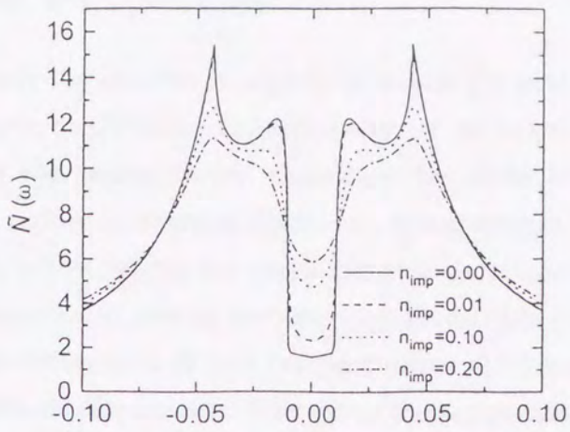

Figure 3.4: The effect of the impurity scattering on the density of states.

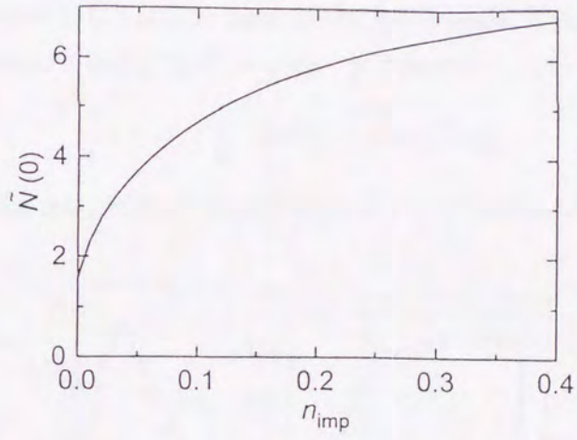

Figure 3.5: The density of states at the Fermi level as a function of the impurity concentration.

superconductors.[80, 81] The square-root dependence of the residual DOS has also been derived on the basis of a different picture, where it is understood as an impurity band similar to the doped semiconductor; namely the doping accompanied by variation of carrier number is necessary to obtain finite DOS in the true gap.[82, 83] Our theory has been developed to discuss the case where carrier number does not change, while it is easily extended to the case where carriers are doped.

3.3 Physical Properties

In this section, we study the qualitative aspects of several physical quantities and compare them with experiments in CeNiSn. For simplicity let us forget that hybridized bands have been formed by the quasiparticles which have the finite lifetime and assume that these bands respond rigidly to external fields, i.e., quasiparticles have infinite life- time. Therefore any results in this section are unreliable at high temperature or at high energy. However physical properties at present low temperature and low energy region are enough trustworthy. Some characteristics at high temperature or at high energy can be improved by considering the lifetime of quasiparticles such as the temperature dependence of quasi-particle DOS.

3.3.1 Specific Heat

The specific heat is calculated on the basis of the quasi-particle picture, and the electronic specific heat coefficient, $\gamma \equiv C(T)/T$, is given as follows:

$$\gamma = 2\int_0^\infty dx \tilde{N}(E)x^2 \mathrm{sech}^2(x), \tag{3.26}$$

where $x = E/2T$. The temperature dependence of γ is calculated with the use of eqs.(3.21)

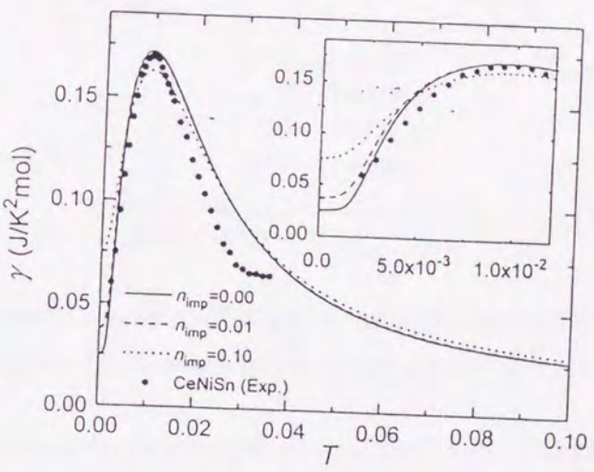

Figure 3.6: The temperature dependence of the specific heat coefficient γ. The unit of the temperature is D, half the band-width of conduction electrons. Circles are experimental data (C_m/T) of ref.52 $\Delta_1/2 = 0.01D$ corresponds to 7K.

and (3.25) and is shown in Fig. 3.6. A peak structure is found at $T \sim \Delta_1/2$. It is noted

that γ is finite at $T = 0$, which results from the existence of the residual DOS at $n_{\rm imp} = 0$. If Δ_1 is fixed as $\Delta_1/2 = 7$K, these results are in good agreement with the experimental data[51-53] at $T < \Delta_1$, where the maximum of theoretical curve for γ is adjusted so as to agree with the experiment of ref.52. We have also verified that the same quality of agreement with the data of ref.53 is obtained while its absolute value of C_m/T is about 10% larger than that of ref.52. However at $T > \Delta_1$ the agreement become poor. It is partly improved by considering temperature dependence of the quasiparticles DOS.[52]

Furthermore, assuming that the effect of the magnetic field is only inducing the Zeeman splitting, the magnetic-field dependence of γ is obtained as

$$\gamma = \int_0^\infty dx \tilde{N}(E) \left[x_+^2 \mathrm{sech}^2(x_+^2) + x_-^2 \mathrm{sech}^2(x_-^2) \right], \tag{3.27}$$

where $x_\pm = (E \pm h)/2T$, $h = g_J \mu_{\rm B} |J_z| H$, g_J being a g-factor. The results for various temperatures are shown in Fig. 3.7. The coefficient γ at low temperature exhibits two-

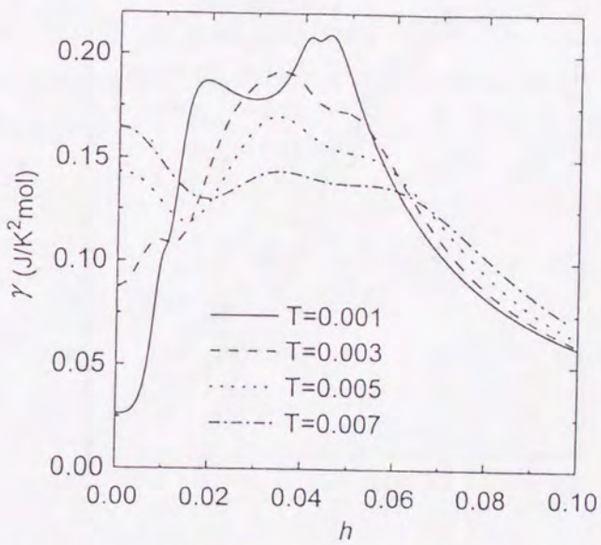

Figure 3.7: The specific heat coefficient, γ, as a function of the magnetic field, h. The unit of h is D, half the band-width of conduction electrons.

peak structure, which reflects the peak structure of DOS. This prediction has not yet been observed, partly because the strength of the magnetic field is not enough.

3.3.2 Longitudinal Relaxation Rate of NMR

The longitudinal NMR relaxation rate, $1/T_1$, is obtained as follows

$$\frac{1}{T_1 T} \propto \lim_{\omega \to 0} \sum_{q} \frac{\mathrm{Im}\chi^{-+}(q,\omega)}{\omega}, \tag{3.28a}$$

$$\propto \int_0^\infty dE \tilde{N}(E)^2 \mathrm{sech}^2(\frac{E}{2T}) \frac{1}{T}. \tag{3.28b}$$

Here we have assumed that the quasi-particle DOS directly affects $1/T_1$ at Sn site via the c-f exchange as done in the analysis of experimental data. The good reason of this assumption includes unsolved problem that what NMR observes. This is one of the future problems. The results of numerical calculations of (3.28b), together with experimental data,[18] are shown in Fig. 3.8 for the same parameters as in Fig. 3.6. For the temperature

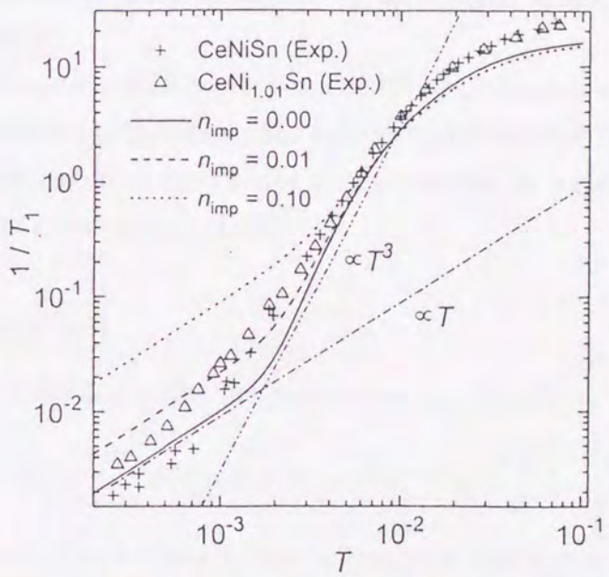

Figure 3.8: The longitudinal NMR relaxation rate, $1/T_1$ (in arbitrary unit), as a function of the temperature T in the unit D, half the band-width of conduction electrons. Triangles and crosses are experimental data of ref.18. $\Delta_1 = 0.02D$ corresponds to 14K.

region, $0.1\Delta_1 \lesssim T \lesssim \Delta_1 \simeq 0.02D$, $1/T_1$ shows the T^3-like behavior reflecting the formation of the pseudogap at $\omega \simeq \Delta_1/2$ of DOS as shown in Fig. 3.2, and for $T \lesssim 0.1\Delta_1$, it shows T-linear behavior reflecting the residual DOS at the Fermi level. These behaviors well reproduce the T-dependence of $1/T_1$ observed in the experiments,[18] if Δ_1 is fixed as $\Delta_1 = 14$K. In addition, as increasing impurity concentration n_{imp}, the residual DOS rises

up drastically and the T-linear behavior masks the T^3-like behavior. These are also in agreement with the experiments,[18] where the residual DOS shows the $n_{\rm imp}$-dependence quite similar to the theoretical curve shown in Fig. 3.5. Here one can see that impurities have very important effects.

The above results have been derived on the basis of the quasi-particle picture, so that, strictly speaking, its validity is assured only in the low temperature region $T < T_{\rm K}$. However, it may be extended to much higher temperature region as far as the qualitative aspects are concerned. Indeed, $1/T_1$ in Fig. 3.8 exhibits the localized character of f-electrons for $T > T_{\rm K} = 0.02D$, $1/T_1 \propto T^0$, and approaches asymptotically to the Korringa-like behavior at much higher temperatures, $1/T_1 \propto T$, as can be inferred from the quasi-particle DOS shown in Fig. 3.2. In the latter region, the NMR relaxation is expected to occur mainly through the coupling with the conduction electrons as in LaNiSn.[17] Recently such a behavior has been recognized by an analysis of the data of $1/T_1$ up to the room temperature.[19]

Furthermore, the magnetic field dependence of $1/T_1$ has been discussed by Nakamura et.al.. This effect masks the pseudogap state such as in the case of impurities. However, this case, which is different from the case of impurities, can be explained by the simple Zeeman splitting of the quasi-particle DOS.

3.3.3 Magnetization

The quasi-particle contribution to the magnetization is calculated as

$$M = \int_{-\infty}^{\infty} dE \, [f(E-h) - f(E+h)] \, \frac{\tilde{N}(E)}{2}. \tag{3.29}$$

The results are shown in Fig. 3.9 where one can see that the magnetization, in the unit $g_J \mu_{\rm B} |J_z|$, is proportional to h, in the unit D, at low magnetic field and the slope is given by the residual DOS. However, as increasing h the magnetization drastically increases at $h > 0.01D$ owing to the two large humps of DOS at $\omega = \pm\Delta_1/2$. These tendencies are found in the experimental data[84]. The slope of the magnetization at low field is enhanced by small amount of impurity and the whole structures of M-h curve shade off.

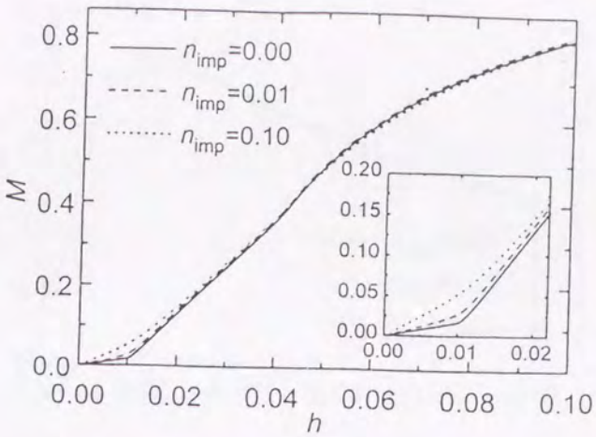

Figure 3.9: The magnetization, M (in the unit $g_J\mu_B|J_z|$), as a function of the magnetic field h (in the unit D) at $T = 0$.

3.3.4 Uniform Spin Susceptibility

The uniform susceptibility along the easy axis (a-axis), in the unit $(g_J\mu_B|J_z|)^2/D$, is given by the derivative of the magnetization as

$$\mathrm{Re}\chi(0,0) = \left.\frac{\partial M}{\partial h}\right|_{h\to 0} = \int_{-\infty}^{\infty} dE \left[-\frac{\partial f(E)}{\partial E}\right] \tilde{N}(E). \tag{3.30}$$

Its temperature dependence shown in Fig. 3.10 exhibits the peak structure like γ as discussed in §3.3.1. However, the temperature at which $\mathrm{Re}\chi(0,0)$ has the maximum ($T \simeq \Delta_1$) is different from that for γ. Increasing impurity concentration, the sharp dip at low temperature is filled up rapidly. Since the susceptibility (3.30) is given only by the contribution of the quasiparticles, the Van Vleck term is not included. If the latter is simply a constant, the observed Knight shift[18] for $H\|a$ represents the behavior of the uniform susceptibility χ^a, which is in agreement with the curves of Fig. 3.10.

Since b- and c-axis are not the easily axis, most contributions to χ^b and χ^c result from CEF excitations, such as the Van Vleck term, which require high-energy process. These may be small since most parts of the susceptibility come from the quasi-particle part in $n_f \simeq 1$ such as Cerium compounds. Thus, the anisotropy of the susceptibility reflects the CEF splitting. This is the reason why χ^b and χ^c in the experimental data are small.

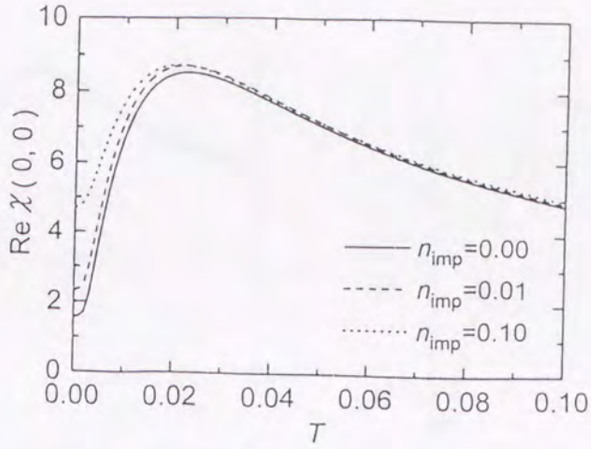

Figure 3.10: T-dependence of the uniform susceptibility, Re$\chi(0,0)$ in the unit $(g_J\mu_B|J_z|)^2/D$. The unit of T is D, half the band-width of conduction electrons.

3.3.5 Neutron Scattering

So far, the neutron scattering experiments can be characterized by three points as follows: (1) peak structure at ω =4meV and $Q = [Q_a, 1/2, Q_c]$ (Q_a, Q_c:arbitrary) (2) quasi-one dimensionarity along Q_b. (3) antiferromagnetic spin fluctuation at ω =2meV and $Q = [0,0,1]$

The spectral intensity of neutron scattering can be regarded as the imaginary part of the dynamical susceptibility, the spectral weight of f- spin fluctuations, without structural factors. One can calculate quasi-particle contributions to the imaginary part of the dynamical susceptibility without a vertex correction as

$$\mathrm{Im}\chi(\boldsymbol{Q},\omega) \simeq \pi \sum_{\boldsymbol{k}\mu\nu=\pm} \left[f(E^{\mu}_{\boldsymbol{k}}) - f(E^{\nu}_{\boldsymbol{k}+\boldsymbol{Q}}) \right] \delta\left(\omega - E^{\mu}_{\boldsymbol{k}} + Q + E^{\nu}_{\boldsymbol{k}} \right) \tag{3.31}$$

where $f(E)$ is the Fermi distribution function and $f(E^{-}_{\boldsymbol{k}}) = 1$ and $f(E^{+}_{\boldsymbol{k}}) = 0$ at $T \to 0$. The spectral weight (3.31) has been calculated numerically with the use of the quasi-particle dispersion, eq.(3.14), for specified $\boldsymbol{Q}$'s. The spectral weight at $\boldsymbol{Q} = (1/2, 0, 0)$ is shown in Fig. 3.11 (a), which shows that there exists a broad hump at around $\omega = 0.08D$. (It is noted that x-, y-, and z-axis here corresponds to the b-, c-, and a-axis, respectively of CeNiSn; so that $\boldsymbol{Q} = (1/2, 0, 0)$ implies $\boldsymbol{Q} = [0, 1/2, 0]$ in the notation of experiments of CeNiSn for instance.) This structure corresponds to the transition from one peak of DOS at $\omega = -0.04D$ to another at $\omega = 0.04D$ in DOS. For example, the former peak corresponds to the quasiparticle at $\boldsymbol{k}_1 = (-1/4, 1/2, 1/2)$, while the latter

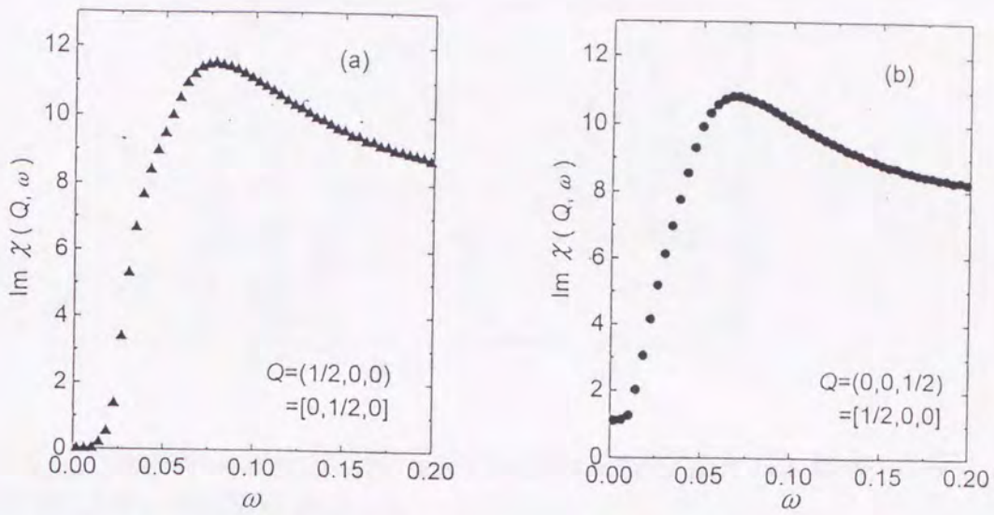

Figure 3.11: The spectral weight of spin fluctuations, $\mathrm{Im}\chi(Q,\omega)$ (in arbitrary unit), as a function of ω at $T = 0$ for (a) $Q = (1/2, 0, 0) = [0, 1/2, 0]$ and (b) $Q = (0, 0, 1/2) = [1/2, 0, 0]$. $\mathrm{Im}\chi(Q, 0)$ is finite in (b) due to a choice of non-dispersive f-level.

at $k_2 = (1/4, 1/2, 1/2)$, because $\hat{k}_{1z} = \hat{k}_{2z} \sim \sqrt{7/15}$. Thus, $Q = k_2 - k_1 = (1/2, 0, 0)$. The spectrum at $Q = (0, 0, 1/2)$ shown in Fig. 3.11 (b) has a peak at around $\omega = 0.06D$, which corresponds to the energy from an edge of the gap at $\omega = -0.02D$ to one peak at $\omega = 0.04D$ in DOS. For example, the former peak corresponds to the quasiparticle at $k_3 = (1/2, 0, 0)$, while the latter at $k_4 = (1/2, 0, 1/2)$, because $\hat{k}_{3z} = 0$ and $\hat{k}_{4z} \sim \sqrt{7/15}$. Thus, $Q = k_4 - k_3 = (0, 0, 1/2)$. It is seen that a difference between the two spectra arises from that of the possibility of energy transitions in the pseudogap. Since the hybridization gap vanishes along the $z(a)$-axis, there exist low energy excitations for the transition between two points near the $z(a)$-axis. However, these two spectra are rather similar to each other experimentally, since the spectral weights at points corresponding to transitions in the pseudogap are very small. Additionally speaking, the spectrum at $Q = (0, 0, 1/2)$ can not be observed experimentally due to the structural factor. The spectrum at $Q = (1/2, 0, 0)$ corresponds to inelastic neutron scattering spectrum at $Q = [0, 1/2, 0]$.

The spectral intensity at $\omega = 0.08D \simeq \Delta_2$ and $Q = (Q_x, 0, 0) = [0, Q_b, 0]$ is computed as a function of $Q_x(Q_b)$ and shown in Fig. 3.12. One can see the peak at $Q_x(Q_b) = 1/2$. The reason is that the peak shifts to higher energy as deviating from $Q_x(Q_b) = 1/2$. These features are consistent with Q_b-dependence of the intensity at 4.25meV in the inelastic

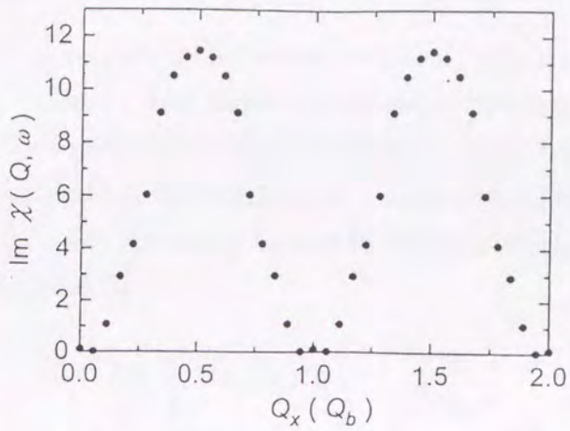

Figure 3.12: The intensity of $\mathrm{Im}\chi(Q, \omega = \Delta_2)$ in arbitrary unit as a function of Q_x (Q_b) of $Q = (Q_x, 0, 0) = [0, Q_b, 0]$ at $T = 0$.

neutron scattering.[55] The characteristic (1) can be explained by particle-hole excitations of the quasiparticles in this way.

Essentially, the details of these spectra are modified according to choices of the dispersions of conduction electrons, though characteristic structures do not change. However, when the conduction band do not cross the f-level in some direction in the k-space, the excitation energy is rather higher and the spectrum can not be observed at low energy region in general. This case may be realized in the low-energy spectrum at $Q \parallel c$-axis in the experiment.[55] If we give thought to such anisotropy of the conduction band, or, detail band structure, the characteristic (2) may be also explained.

To discuss the characteristic (3) the fact that there are two kinds of Cerium ions in one unit cell must be taken into account. It is necessary that we know the information of the hybridized band structures in detail to verify exactly the neutron scattering spectra. We can only stress that the peak structure at ω =4meV corresponds to the particle-hole excitations at the specific energy scale Δ_2 at the quasi-particle DOS and is available independent of details of the band structure without respent to its one-dimensionality.

Recently, the neutron scattering in CeNiSn is actively investigated and it has been shown that its pressure dependence and its magnetic-field dependence. By these experimental data we can confirm that the peak structure at ω =4meV is composed of the particle-hole excitations corresponding to Δ_2.

3.3.6 Anisotropy of Resistivity

It is the resistivity that is one of the measures to classify the heavy-fermion materials into "Kondo insulator" or not. The resistivity in heavy fermions exhibits the Kondo effect at high temperature region and metallic or activation-type behavior at low temperature region. We are interested in the behavior at temperatures lower than the coherent temperature $T_{\rm coh}$, in which the current is carried by the quasiparticles. In this case the conductivity can be evaluated by

$$\sigma_{\mu\nu}(T) \propto \sum_{\boldsymbol{k}} J_{\boldsymbol{k}\mu} J_{\boldsymbol{k}\nu} \tau_{\boldsymbol{k}} \left(-\frac{\partial f(E_{\boldsymbol{k}})}{\partial E_{\boldsymbol{k}}} \right), \tag{3.32}$$

where $J_{\boldsymbol{k}_\mu}$ is the velocity of the quasiparticle and $\tau_{\boldsymbol{k}}$ is its lifetime.[38] Assuming that the microscopic expression of the current is given only by the conduction electrons (neglecting the dispersion of f-electrons), the anisotropy of the conductivity is given as follows:

$$\sigma_{\parallel} \propto \sum_{\boldsymbol{k}} A^{\rm c}_{\pm}(\boldsymbol{k})^2 v_z(\boldsymbol{k})^2 \tau_{\boldsymbol{k}} \left(-\frac{\partial f(E^{\pm}_{\boldsymbol{k}})}{\partial E^{\pm}_{\boldsymbol{k}}} \right), \tag{3.33a}$$

$$\propto \int dE_{\boldsymbol{k}} \int d\Omega_{\boldsymbol{k}} \frac{E^2_{\boldsymbol{k}}}{\Lambda_{\boldsymbol{k}}} \left(-\frac{\partial f(E_{\boldsymbol{k}})}{\partial E_{\boldsymbol{k}}} \right), \tag{3.33b}$$

$$\sigma_{\perp} \propto \sum_{\boldsymbol{k}} A^{\rm c}_{\pm}(\boldsymbol{k})^2 v_x(\boldsymbol{k})^2 \tau_{\boldsymbol{k}} \left(-\frac{\partial f(E^{\pm}_{\boldsymbol{k}})}{\partial E^{\pm}_{\boldsymbol{k}}} \right), \tag{3.33c}$$

$$\propto \int dE_{\boldsymbol{k}} \int d\Omega_{\boldsymbol{k}} \frac{\sin^2\theta_{\boldsymbol{k}} E^2_{\boldsymbol{k}}}{\Lambda_{\boldsymbol{k}}} \left(-\frac{\partial f(E_{\boldsymbol{k}})}{\partial E_{\boldsymbol{k}}} \right), \tag{3.33d}$$

$$\Lambda_{\boldsymbol{k}} = \left(-z_{\boldsymbol{k}} {\rm Im}\Sigma_f(\boldsymbol{k}, E_{\boldsymbol{k}}) \right) \tilde{V}^2_f(\boldsymbol{k}) + \left(-{\rm Im}\Sigma_c(\boldsymbol{k}, E_{\boldsymbol{k}}) E^2_{\boldsymbol{k}} \right) \tag{3.34}$$

where $\sigma_{\parallel}$ and $\sigma_{\perp}$ are the conductivity along the a-axis and in the bc-plane, respectively, and

$$\frac{1}{\tau_{\boldsymbol{k}}} = \frac{\Lambda_{\boldsymbol{k}}}{E^2_{\boldsymbol{k}} + \tilde{V}^2_f(\boldsymbol{k})} \tag{3.35a}$$

$$v_z(\boldsymbol{k}) = \frac{\partial \xi_{\boldsymbol{k}}}{\partial k_z} \quad \text{and} \quad v_x(\boldsymbol{k}) = \frac{\partial \xi_{\boldsymbol{k}}}{\partial k_x}. \tag{3.35b}$$

Here we have introduced $\Sigma_c(\boldsymbol{k}, E_{\boldsymbol{k}})$, the self-energy of the conduction electrons, because $\sigma_{\parallel}$ in pure system diverges logarithmically otherwise, reflecting the fact that the conduction electrons are decoupled from f-electrons in the z-direction (a-axis) where the hybridization vanishes. We regard the renormalization factor of conduction electrons from $\Sigma_c(\boldsymbol{k}, E_{\boldsymbol{k}})$ as 1. In this model the conductivity in the bc-plane is isotropic unless the anisotropy of the

conduction band is taken into account. In deriving (3.33d) from (3.33c), we have taken into account only the low energy excitations around $\hat{k}_z = \pm 1$ so that the obtained result should be regarded as that for asymptotic behavior in the limit $T \to 0$.

In order to discuss the temperature dependence of the conductivity at low temperature region, we must calculate the energy dependence of the imaginary part of the self-energies. For simplicity we calculate these along a standard treatment of the Fermi liquid theory neglecting the momentum dependence of the full vertex:

$$\mathrm{Im}\Sigma_\mu(\boldsymbol{k}, E_{\boldsymbol{k}}^+) \propto \int dpdq A_+^\mu(\boldsymbol{k}-q) A_-^\mu(p) A_+^\mu(p+q) \\ \delta(E_{\boldsymbol{k}}^+ + E_{\boldsymbol{p}}^- - E_{\boldsymbol{k}-q}^+ - E_{\boldsymbol{p}+q}^+), \tag{3.36}$$

where $\mu = c$ or f. These integrations are computed by the Monte Carlo calculation. The numerical results are shown in Fig. 3.13. From this one can see that the energy

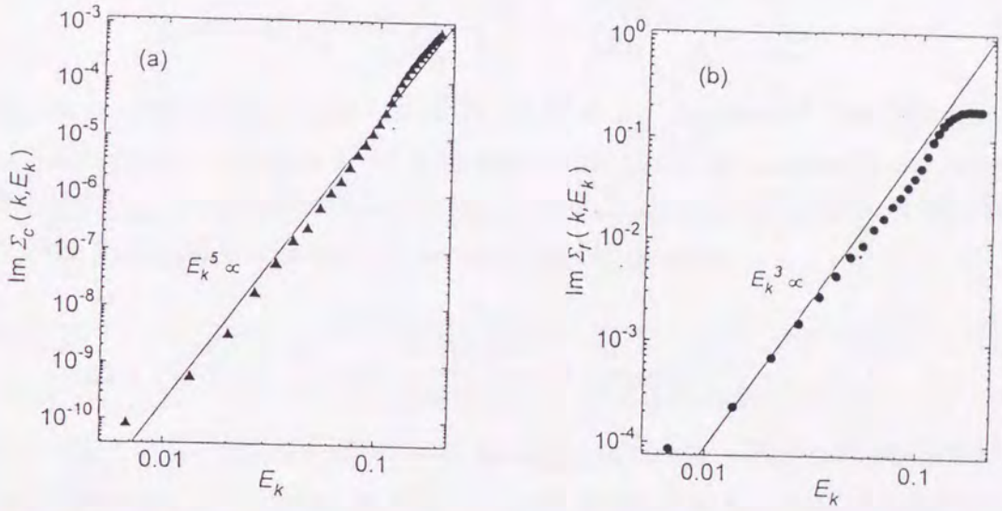

Figure 3.13: The energy dependence of the self-energies, (a) $\mathrm{Im}\Sigma_c(k, E_k)$and (b)$\mathrm{Im}\Sigma_f(k, E_k)$ at zero temperature. The straight line in (a) and (b) shows E_k^5 and E_k^3 dependence, receptively. The unit of E_k is D, half the band-width of conduction electrons.

dependence of $\mathrm{Im}\Sigma_c(\boldsymbol{k}, E_{\boldsymbol{k}})$ and $\mathrm{Im}\Sigma_f(\boldsymbol{k}, E_{\boldsymbol{k}})$ near the Fermi level at zero temperature can be approximated by $E_{\boldsymbol{k}}^5$ and $E_{\boldsymbol{k}}^3$, respectively. Furthermore, we assume that the temperature dependence of $\mathrm{Im}\Sigma_\mu(\boldsymbol{k}, E_{\boldsymbol{k}})$ is given with replacing $E_{\boldsymbol{k}}^2$ by max ($E_{\boldsymbol{k}}^2$ and $(\pi T)^2$), as can be seen from the structure of the Green functions. By using these results we can estimate the temperature dependence of the resistivity. Substituting these energy

dependence into eqs.(3.33), we obtain up to the logarithmic accuracy

$$\sigma_{\parallel} \propto T^{-1} \ , \text{ and } \ \sigma_{\perp} \propto T^{0}, \tag{3.37a}$$

i.e,

$$\rho_{\parallel} \propto T \ , \text{ and } \ \rho_{\perp} \propto T^{0}. \tag{3.37b}$$

Next we discuss the effect of impurity scattering on $\sigma_{\parallel}$. For simplicity we first assume that the self-energy $\mathrm{Im}\Sigma_c(\boldsymbol{k}, E_{\boldsymbol{k}})$ and $\mathrm{Im}\Sigma_f(\boldsymbol{k}, E_{\boldsymbol{k}})$ are independent of $E_{\boldsymbol{k}}$ and proportional to the impurity concentration n_{imp}. In this case, by using eq.(3.33b), we obtain

$$\sigma_{\parallel}^{\mathrm{imp}} \propto T^2/n_{\mathrm{imp}} \ , \text{ i.e. } \ \rho_{\parallel}^{\mathrm{imp}} \propto n_{\mathrm{imp}} T^{-2}. \tag{3.38}$$

However, if the small dispersion of f-electrons due to a possible weak $\boldsymbol{k}$-dependence of the f-electron self energy, $\Sigma_f(\boldsymbol{k}, 0)$, the current can be carried also by f-electrons, so that

$$\sigma_{\parallel} \propto \int dE_{\boldsymbol{k}} \int d\Omega_{\boldsymbol{k}} \frac{1}{E_{\boldsymbol{k}}^2} \frac{\tilde{V}_f^4(\boldsymbol{k})}{\Lambda_{\boldsymbol{k}}} \left(-\frac{\partial f(E_{\boldsymbol{k}})}{\partial E_{\boldsymbol{k}}} \right) \propto \frac{1}{n_{\mathrm{imp}}}. \tag{3.39}$$

Thus the singularity of the resistivity (3.38) at $T = 0$ is suppressed. Nevertheless, the residual resistivity in the limit $T \to 0$ increases drastically as increasing the impurity concentration n_{imp}. If we take all the contributions of the quasiparticles into consideration, including the logarithmic corrections, the resistivity is given by

$$\rho_{\parallel} = \frac{\rho_0}{\left(n_{\mathrm{imp}} + (T/T_{\mathrm{K}})^3 \right)^{-1} c_1 + \left(\dfrac{T/T_{\mathrm{K}}}{\log(c_2 T_{\mathrm{K}}/T)} + \dfrac{n_{\mathrm{imp}}}{(T/T_{\mathrm{K}})^2 \log(c_3 T_{\mathrm{K}}/T)} \right)^{-1}}, \tag{3.40}$$

where $c_1(\sim 0.1)$, $c_2(\sim 10)$ and $c_3(\sim 5)$ are fitting parameters, which are connected with the small dispersion of f-electrons, the interaction between conduction electrons and impurity scattering of conduction electrons with the Born approximation, respectively. $n_{\mathrm{imp}}\rho_0/c_1$ is the resistivity at $T \to 0$. The resistivity for proper parameters are shown in Fig. 3.14. These results are in qualitative agreement with the experimental data.[51] In particular, the temperature dependence of $\rho_{\parallel}(\rho_a)$ observed in the best sample to date is well reproduced as seen in Fig. 3.14. It is also found that the resistivity is sensitive to the concentration of impurities at low temperature in consistent with the experiments.

It should be remarked here that the weak $\boldsymbol{k}$-dependence of $\Sigma_f(\boldsymbol{k}, 0)$ inevitably gives rise to a small semimetallic Fermi surface around X-point (intersection of a-axis and the zone boundary) in general, so long as the hybridization vanishes along the a-axis as eq.(3.10a). However, such a small Fermi surface is expected to give only little effect

on the qualitative behavior of quasi-particle DOS discussed in previous sections, while it sensitively affects the low temperature behavior of the resistivity especially in the case where the impurity scattering greatly enhances the resistivity as in eq. (3.38) when there exists no $\boldsymbol{k}$-dependence of $\Sigma_f(\boldsymbol{k},0)$. In deriving (3.40), we have taken into account the dispersion of f-electron through the $\boldsymbol{k}$-dependence of $\Sigma_f(\boldsymbol{k},0)$, nevertheless we have used the same DOS as eq.(3.21). In this sense, the calculation is not self-consistent and the resistivity (3.40) should be regarded as a provisional one. However, the expression (3.40) gives a good description for $T \sim \Delta_1/2$, or a good starting point at least.

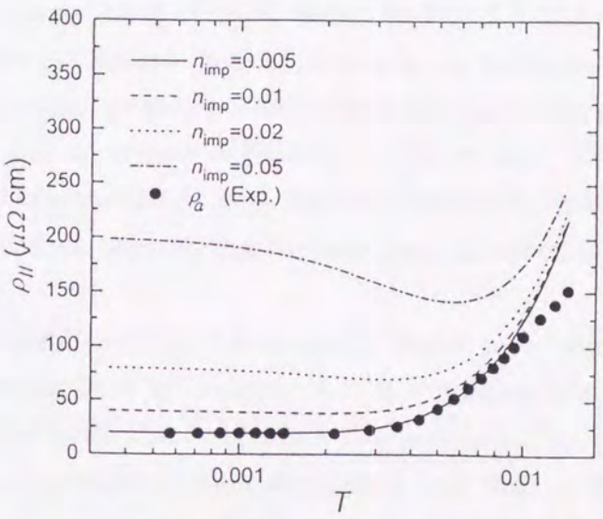

Figure 3.14: The resistivity $\rho_{\parallel}$ as a function of the temperature T, in the unit D, half the band-width of conduction electrons. The parameters in eq.(3.40) are chosen as $\rho_0 = 400$, $c_1 = 0.1$, $c_2 = 10$ and $c_3 = 5$. Closed circles show the temperature dependence of ρ_a of the best sample of CeNiSn.[51]

We should have a few words about $\rho_{\perp}$. The resistivity ρ_b and ρ_c of the same sample as shown in Fig. 3.14 exhibits a dip at $T \sim 3$K and saturate at $T \to 0$. This may be understood as follows. Since quasiparticles around $\hat{k}_z = 0$ with excitation energy ($\sim \Delta_1/2$) have large dispersion along x- or y-direction, those are expected to contribute considerably to the conduction perpendicular to $z(a)$-axis at $T \sim \Delta_1/2$, leading to the suppression of $\rho_{\perp}$ (ρ_b and ρ_c). If we use $\Delta_1/2 \simeq 7$K estimated above by means of $1/T_1$'s result, such suppression or dip is expected to occur at $T \lesssim 7$K in consistent with the above observation.

3.3.7 Magnetoresistance

Now we briefly discuss about the longitudinal magnetoresistance (MR). The change from the positive MR to the negative MR is observed with increasing magnetic field.[51] The negative MR at higher field region may be caused by the suppression of spin fluctuations by magnetic field such as in the impurity Kondo effect. However, the case of the positive MR at low field is more complicated. We have calculated magnetic-field dependence of the lifetime $\tau_{\boldsymbol{k}}$ of quasiparticles and verified that $\tau_{\boldsymbol{k}}$ is a decreasing function of the magnetic field in the low-field region. Although DOS at low energies increases with the magnetic field due to the Zeeman splitting of DOS, shown in Fig. 3.2, the weight of conduction electrons of those states decreases in general leading to the enhancement of the resistivity. Therefore, MR is determined on such a delicate balance between the effects on the lifetime of the quasiparticles and the details of DOS at the Fermi level. The experimental data can be understood as follows: MR at lower fields is positive by shortening of the lifetime and at higher fields becomes negative due to the drastic increment of quasiparticles which can carry the current.

Let us discuss the positive MR at low magnetic field in more detail. By recent careful experiment at low temperature it is shown that this positive MR has the sharp peak. There is one idea which gives this structure a interpretation. By the magnitude of the residual quasi-particle interaction magnetic excitons may exist in the hybridization gap in such system as Kondo insulators. These excitons are collective mode in the elementary excitations and composed of particle-hole excitations since particles and holes attract each other with the quasi-particle interaction. If these excitons exist, then a spin gap is different from a charge gap. From this point of view one can interpret that the difference between a spin gap and a charge gap in the $d = 1$ theory on the basis of the exact diagonalization method come from the infinity of the edge in the DOS, because the equation $1 - U_{eff}\mathrm{Re}\chi(q,\omega) = 0$ always has solutions in this case. The case in two dimension is so, too. In three dimension, however, there may exist critical interaction U_c, since the edge in the DOS is proportional to the square root of energy. Assuming that $U_{eff} > U_c$, though it is questionable whether always $U_{eff} > U_c$, poles of magnetic excitons appear in the band-like spin gap at the susceptibility. We compute the susceptibility involving vertex corrections within the random phase approximation, for example, in the isotropic case and demonstrate these in Fig. 3.15(b). Reflecting the magnetic excitons one can see the sharp structure at the positions where $\mathrm{Im}\chi(q,\omega) = 0$ before considering the RPA (Fig. 3.15(a)). Under the magnetic field these peak structures splits into three peaks,

since these magnetic excitons have spin 1. If the position of this peak is located in the

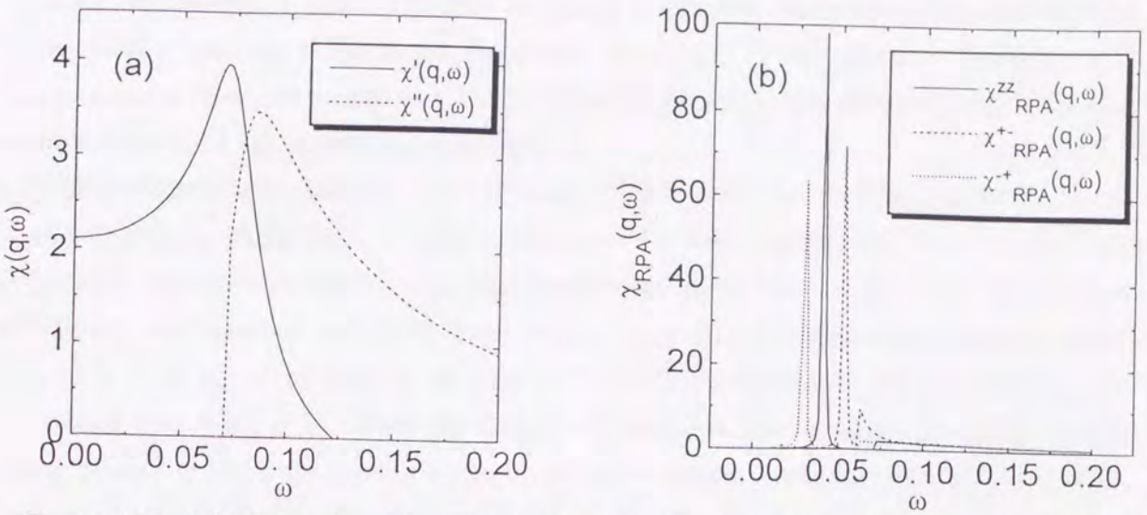

Figure 3.15: (a) The real and imaginary part of $\chi(Q,\omega)$ and (b) $\chi(Q,\omega)$ under the RPA, in which there exsists the collective mode peaks in the spin gap corresponding to the particle-hole excitations in one-body bands. These peaks are splitting into three peaks under the magnetic field.

energy E_{mag}, one of three peaks go across the zero energy under the magnetic field h_{mag} corresponding to E_{mag}. In this time the resistivity may rise up since the redundant scattering process with the collective mode becomes rather effective in the scattering process between the quasiparticles which carry the current. Estimating h_{mag} as the position of the sharp peak at the positive MR observed in CeNiSn, $U_{eff} \simeq \Delta_1$. Because assuming that the magnitude of the quasi-particle interaction is the same degree as in the impurity case, it is typically about Δ_1, the above estimation is not necessarily out of place. However, such peak structures are not observed yet. Rather, the sharp peak observed in SmB_6 may be such collective modes.

3.3.8 Pressure Dependence

Next we discuss the pressure dependence on the property of quasiparticles. As the lattice constant becomes short under the pressure, both the band-width D of conduction electrons and the hybridization V are enlarged. However, the fundamental energy scale V^2/D is expected to be an increasing function of the pressure because V is much more sensitive than D for heavy fermions where V arises through rather small overlap between f- and conduction electrons. Much more pronounced effect of pressure on the hybridization gap

(3.17) arises through enlargement of the renormalization amplitude $z_{\boldsymbol{k}}$. This is because $z_{\boldsymbol{k}}$ is an exponentially small quantity as (3.41) for heavy fermions so that its relative change under pressure is far larger than that for V and D themselves. Therefore, the energy scale of the gap is expected to increase by applying the pressure, and so is the resistivity in eq.(3.40), which is scaled by $T_{\rm K}$.

This tendency is consistent with the behavior of CeNiSn and CeRhSb where the peak of the resistivity shifts to the high temperature by the pressure.[85, 86] And also the suppression of those resistivity with the pressure in the limit $T \to 0$ can be understood as follows. As discussed in §3.3.6, there exists a very tiny semimetallic Fermi surface at around $\boldsymbol{k} = (0, 0, \pm 1)$ in general, so long as $\Sigma_f(\boldsymbol{k}, 0)$ has the dispersion along the a-axis no matter how small it is. After the Fermi surface grows further under the pressure due to the growth of the dispersion of $\Sigma_f(\boldsymbol{k}, 0)$, an apparent semimetallic behavior is expected to prevail leading to the suppression of the resistivity. That is to say, a parameter c_1, which corresponds to $\partial\Sigma_f(\boldsymbol{k}, 0)/\partial\boldsymbol{k}$, increases with the pressure in the formula (3.40), so that the resistivity in the limit $T \to 0$, $n_{\rm imp}\rho_0/c_1$, is suppressed.

3.3.9 Mass Enhancement Factor

Here, let us discuss whether quasi-particle band is renormalized, i.e., whether the renormalization factor can be small. The renormalization amplitude z for the particle-hole symmetric case has been calculated by Rice-Ueda,[62] on the basis of the Gutzwiller approximation, and by Shiba[63], on the basis of variational Monte Carlo calculations for the Gutzwiller ansatz, with the use of a model hybridization $V^2(\boldsymbol{k}) = V^2$. A similar but more extended result has recently been obtained by numerical renormalization group method[36], quantum Monte Carlo calculation[35] and the exact diagonalization method[34] in $d = \infty$ system. We have performed the calculation similar to Rice-Ueda's with anisotropic hybridization $V^2(\boldsymbol{k}) = V^2(1 - \hat{k}_z^2)$, a simplified version of (3.10a). The result for the filling corresponding to band insulator is

$$z = \frac{\mathrm{e}^{19/12} D^2}{4V^2} \exp\left(-\frac{3UD}{32V^2}\right) \tag{3.41a}$$

which is compared with that of Rice-Ueda

$$z = \frac{D^2}{V^2} \exp\left(-\frac{UD}{8V^2}\right) \tag{3.41b}$$

where the hybridization gap is constant and fully opened.

In those model calculations, the particle-hole symmetry is assumed, so that the occupation number of f-electron n_f per site is exactly unity, i.e. $n_f = 1$. However, this constraint is easily relaxed by introducing the asymmetry of conduction band on the position of the f-level. Therefore, it is possible to calculate the mass enhancement factor in the way similar to above not only in the Kondo regime, where $n_f \simeq 1$, but also in the valence-fluctuation regime.

3.3.10 Quasi-particle Lifetime

We have neglected an effect of quasi-particle damping due to inelastic scattering so far. Here we briefly discuss its effect on quasi-particle DOS and temperature dependence of physical quantities.

According to eq. (3.35a), the lifetime of quasiparticles around $\hat{k}_z = \pm 1$ is nearly proportional to $(E_{\boldsymbol{k}}^2 + \tilde{V}_f^2(\boldsymbol{k}))/\tilde{V}_f^2(\boldsymbol{k})E_{\boldsymbol{k}}^3$ at low energy region $E_{\boldsymbol{k}} < \Delta_1$. This lifetime is longer than in the case of the normal Fermi liquid theory for $E_{\boldsymbol{k}} < \Delta_1$. This is because the scattering between quasiparticles is suppressed at low energy, owing to the restriction of phase space satisfying the energy-momentum conservation law. Namely, the quasiparticles with low energy are located around (0,0,$\pm$1), so that such phase space is restricted within narrow region around (0,0,$\pm$1). These quasiparticles make the flat part near the Fermi level at DOS of Fig. 3.2.

The quasiparticle, corresponding to the peak structure at $\omega = \Delta_1/2$ in DOS of Fig. 3.2, are located along $\hat{k}_z = 0$. These quasiparticles also suffers little inelastic scatterings, again because of the restriction due to the energy-momentum conservation law. Thus these lifetime is very long, leading to $\mathrm{Im}\Sigma_f(\hat{k}_z \sim 0, E_{\boldsymbol{k}}) \sim 0$. So it is expected that the peak structure at $\omega = \Delta_1/2$ in DOS remains even if the effect of inelastic scattering is taken into account.

On the contrary, we have no reason to keep the sharp peak structure at $\omega = \Delta_2/2$ in DOS, because the restriction due to the energy-momentum conservation does not suppress the inelastic scattering of quasiparticles forming this peak. So the structure at $\omega = \Delta_2/2$ probably becomes a broad hump.

However, we believe that the two peak structure in DOS of Fig. 3.2 remains even though the effect of inelastic scattering is taken into account. Indeed, as illustrated in Fig. 3.16 the DOS calculated by the second order perturbation theory exhibits two peak structure similar to those of Fig. 3.2, although the peak at $\omega = \Delta_2/2$ is somewhat

broadened.

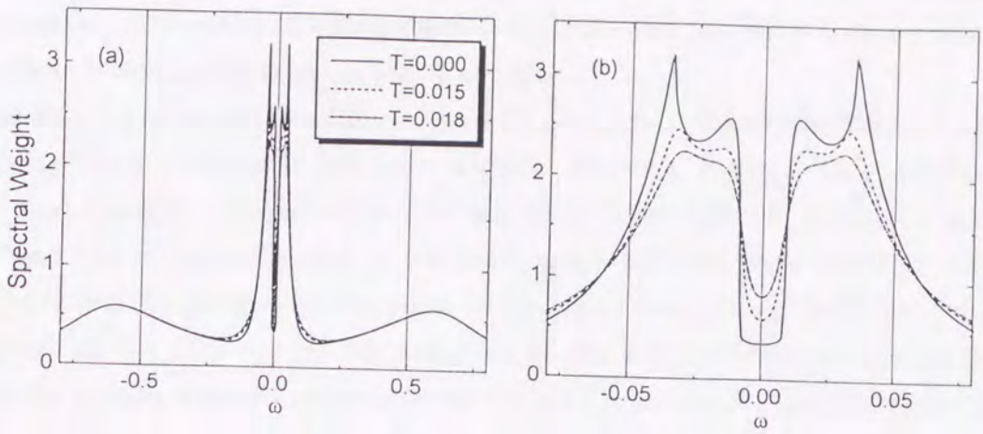

Figure 3.16: The DOS calculated by the second order perturbation theory exhibits two peak structure. The gap structure is sensitive to the temperature.

Furthermore, $T > \Delta_1$ is the temperature region where the damping effect of the quasiparticles affects temperature dependence of physical quantities. For $T > \Delta_1$, these peak structures of DOS fade out, while the physical quantities are averaged by temperature dependence of the Fermi distribution. Therefore, the neglect of the damping effect may give rise to no serious errors as far as the qualitative temperature dependence is concerned at relatively low temperature regions.

3.4 Summary and Discussions

On the basis of the idea of "adiabatic continuity", a theory of the anisotropic semiconductor of heavy fermions has been developed to explain the anomalous properties of CeNiSn and its isostructural compounds. A difference from the conventional semiconductors is that the band gap is formed by the highly renormalized quasiparticles near the Fermi level. So the gap has meaning only at low temperature region $T < \Delta_1$ (corresponding to the hybridization gap), while the coherent peak of quasiparticles fades out exhibiting the behaviors of the Kondo lattice metals.[87]

Wide range of anomalies of CeNiSn can be understood by a model of the anisotropic hybridization gap which vanishes along the a-axis. The anisotropy of the gap reflects a k-dependence of hybridization matrix elements between the conduction electrons and the

f-electron with particular symmetry of the crystal field state. The desirable $\boldsymbol{k}$-dependence occurs if the lowest crystal field state consists mainly of $|5/2, \pm 3/2\rangle$ due to its approximately trigonal symmetry and the conduction electrons near the Fermi level are described by the plane waves, as discussed in §3.2.1 and §3.2.2.

Since there is no band calculation of LaNiSn available to date, it is difficult to assess whether the latter condition is fulfilled in CeNiSn. However, it may be not unrealistic to assume that the state of conduction electrons hybridizing with the f-electron localized at Ce^{3+} ion can be approximated by the plane waves with the wave vector $|\boldsymbol{k} + \mathrm{G}| <$ several $\times (2\pi/a)$, G being some reciprocal lattice vector and a being the lattice constant. This is because the only way for the f-electron to mix with electrons on different sites is through the mixing with the plane wave states outside the muffin-tin spheres so long as the conventional LAPW calculation is performed.

Band calculations of CeNiSn shows that the bands around the Fermi level have mainly Ce $4f$ character with mixture of Ni $3d$ component.[50, 88] So, in the tight-binding picture, the hybridization is expected to arise through the overlap of Ce $4f$ wavefunction and tails of Ni $3d$ wavefunction. It is seen by a simple calculation of the tight-binding model that the hybridization between f-electron in the state $|5/2, \pm 3/2\rangle$ and d-electrons on the surrounding ions with trigonal symmetry vanishes on the k_z axis, i.e., $V(0, 0, k_z) = 0$.

In order to obtain more solid picture of the $\boldsymbol{k}$-dependence of the hybridization, we need more information of the band structure of LaNiSn. It is also interesting to discuss a difference between CeNiSn and the so-called "Kondo insulator", such as $Ce_3Bi_4Pt_3$[89] and YbB_{12}[90], with non-vanishing gap in any directions of the Brillouin zone. From the present point of view, its difference is attributed to that of the $\boldsymbol{k}$-dependence reflecting the symmetry of the lowest crystal-field level. We leave such discussions for future studies.

Chapter 4

Conclusions

We have investigated the influence of the CEF effects on the low-energy quasi-particle excitations.

First, in the chapter 2 we have discussed what influence the CEF effects have on the properties of quasi-particle excitations in the multi-band periodic Anderson model with the use of the mean field theory in the slave boson technique. The results are summarized as follows.

(1) In the case of $0 < n_f < 1$:

- The quasi-particle bands are not almost renormalized and stays near the bare bands.
- The CEF splitting of f^1 multiplets remains unchanged.

(2) In the case of $n_f \sim 1$:

- Only the quasi-particle bands corresponding to the ground CEF state are highly renormalized leading to heavy fermions.
- The CEF splitting of f^1 multiplets are enlarged by a few times.
- The main part of the spin susceptibility is described by the quasi-particle part.

(3)In the case of $n_f \sim 2$:

- The two quasi-particle bands constructing the ground f^2 multiplet are highly renormalized.
- The CEF splitting of f^1 multiplets are reduced drastically.

- For the spin susceptibility both the quasi-particle part and the incoherent part, i.e., the Van Vleck part, play an important role.
- In particular, when the ground state is a singlet, the most part of the spin susceptibility is given by the incoherent part.

Concerning the last statement in (3), we can predict the existence of a new class of the Fermi liquid state, in which both the charge fluctuation and the spin fluctuation are suppressed in spite of the highly renormalization of the density of states of the quasi-particle bands. If such quasi-particle state is realized in UPt_3 around the superconducting transition, the anomalously small decrement of the Knight shift below the transition may be well explained.

Secondly, in the chapter 3 we have considered $\boldsymbol{k}$-dependence of the hybridization matrix elements in the case of $n_f \sim 1$. As an example in which such $\boldsymbol{k}$- dependence, i.e., the anisotropy, is observed in some physical properties, we have picked up the topic of the anisotropic "Kondo insulator", such as CeNiSn and CeRhSb. Here, on the basis of the idea of "adiabatic continuity", a theory of the anisotropic semiconductor of heavy fermions has been developed to explain the anomalous properties of CeNiSn and its isostructural compounds. Wide range of anomalous properties of CeNiSn can be understood by a model of the anisotropic hybridization gap which vanishes along the a-axis. Such anisotropy of the hybridization gap can be easily demonstrated by considering $\boldsymbol{k}$- dependence of hybridization matrix elements reflecting the symmetry of the ground CEF state in f sites. The desirable $\boldsymbol{k}$-dependence occurs if the ground CEF state consists mainly of $|5/2, \pm 3/2\rangle$ due to its approximate trigonal symmetry and the conduction electrons near the Fermi level are described by the plane waves.

From the present point of view, we can explain the gap formation in the normal "Kondo insulator", such as YbB_{12}, SmB_6 and $Ce_3Bi_4Pt_3$, by the difference of $\boldsymbol{k}$- dependence of the hybridization matrix elements reflecting the symmetry of the ground CEF state. Here, we have pointed out the importance of $\boldsymbol{k}$- dependence reflecting the symmetry of the ground CEF state. In the heavy fermion system this research shed light on the importance of the $\boldsymbol{k}$-dependence of the hybridization.

Acknowledgements

I would like to express my sincere gratitude to Prof. K. Miyake for a polite guidance to the physics of the heavy fermion system and enlightening discussions throughout this work.

I would like to thank Dr. O. Narikiyo for precise indications. I also wish to acknowledge Prof. Y. Kitaoka and Dr. K. Nakamura for leading to my attention to the topics in the "Kondo insulator" and stimulating discussions. I have much benefited from informative conversations with Profs. T. Takabatake, Y. Ōnuki, M. Kasaya, H. Harima, H. Kadowaki, J. Flouquet and Drs. K. Sugiyama, T. Sato, S. Nishigori, T. Ekino and G. Nakamoto. I am grateful to Dr. H. Tou for useful discussions on NMR experiments of UPt_3. I would like to thank Dr. T. Mutou and all of the members of the mailing list "ura-mutoberi" for their comments. I thank also colleagues of Miyake Laboratory for their interesting comments. I would like to express my special thanks to Rev. Suikyoh for his warmhearted encouragements.

Finally, I thank my parents and my friends for their warmhearted helps.

Bibliography

[1] See, for example, *Valence Fluctuations in Solids,* ed. L. M. Falicov, W. Hanke and B. P. Maple (Nroth - Holland, Amsterdam, 1981)

[2] See also, *Transport and Thermal Properties of f-Electron Systems,* ed. G. Oomi, H. Fujii and T. Fujita (Plenum, New York, 1993)

[3] A. Sumiyama, Y. Oda, H. Nagano, Y. Ōnuki, K. Shibutani and T. Komatsubara: J. Phys. Soc. Jpn. **55** (1986) 1294.

[4] See, for example, *The Kondo Problem to Heavy Fermions,* ed. A. C. Hewson (Cambridge university press, 1993)

[5] F. Patthey, W.-D. Schneider, Y. Baer and B. Delley: Phys. Rev. Lett. **58** (1987) 2810.

[6] J.-M. Mignot, J. Flouquet, P. Haen, F. Lapierre, L. Puech and J. Voiron: J. Magn. Magn. Mater. **76 & 77** (1988) 97.

[7] T. Sakakibara, T. Tayama, K. Matsuhira, H. Mitamura, H. Amitsuka, K. Maezawa and Y. Ōnuki: Phys. Rev. B **51** (1995) 12030.

[8] H. Aoki, S. Uji, A. K. Albessard and Y. Ōnuki: Phys. Rev. Lett. **71** (1993) 2110.

[9] N. Môri, Y. Okayama, H. Takahashi, Y. Haga and T. Suzuki: Physica B **186 - 188** (1993) 267.

[10] T. Kasuya: Phys. Rev. B **49** (1994) 7068.

[11] M. Kasaya: J. Phys. Soc. Jpn. **61** (1992) 3841; M. Kasaya, F. Iga, M. Takigawa and T. Kasuya: J. Magn. Magn. Mater. **47 & 48** (1985) 429.

[12] T. Takabatake *et.al.*: Jpn. J. Appl. Phys. **26** Suppl. **26-3** (1987) 547; Phys. Rev. B **41** (1990) 9607; Phys. Rev. B **45** (1992) 5740.

[13] S. K. Malik and D. T. Adroja: Phys. Rev. B **43** (1991) 6277.

[14] M. F. Hundley, P. C. Canfield, J. D. Thompson, Z. Fisk and J. M. Lawrence: Phys. Rev. B **42** (1990) 6842.

[15] M. Kasaya, K. Katoh and K. Takegahara: Solid State Commun. **78** (1991) 797.

[16] Recently, CeRhAs and CeRhBi have been synthesized by S. Yoshii, M. Kasaya, H. Takahashi and N. Mori, Proc. SCES '95, to be published in Physica B.

[17] M. Kyogaku, Y. Kitaoka, H. Nakamura, K. Asayama, T. Takabatake, F. Teshima and H. Fujii: J. Phys. Soc. Jpn. **59** (1990) 1728, Physica B **171** (1991) 235.

[18] K. Nakamura, Y. Kitaoka, K. Asayama, T. Takabatake, G. Nakamoto, H. Tanaka and H. Fujii: Physica B **206-207** (1995) 829; Phys. Rev. B **53** (1996) 6385.

[19] T. Ohama, H. Yasuoka and Y. Isikawa: J. Phys. Soc. Jpn. **64** (1995) No.12.

[20] F. Steglich, J. Asrts, C. D. Bredl, W. Lieke, D. Meschede, W. Franz and H. Schäfer: Phys. Rev. Lett. **43** (1979) 1892.

[21] G. R. Stewart, Z. Fisk, J. O. Willis and J. L. Smith: Phys. Rev. Lett. **52** (1984) 679.

[22] H. R. Ott, H. Rudigier, Z. Fisk and J. L. Smith: Phys. Rev. Lett. **55** (1983) 1595.

[23] W. Schlabitz, J. Baumann, B. Pollit, U. Rauchschwalbe, H. M. Mayer, U. Ahlheim and C. D. Bredl: Z. Phys. B **62** (1986) 171.

[24] T. T. M. Palstra, A. A. Menvsky, J. van den Berg and A. J. Mydosh: Phys. Rev. Lett. **55** (1985) 2727.

[25] C. Geibel, S. Thies, D. Kaczorowski, A. Mehner, A. Grauel, B. Seidel, U. Ahlheim, R. Helfrich, K. Petersen, C. D. Bredl and F. Steglich: Z. Phys. B **83** (1991) 305; C. Geibel, C. Schank, S. Thies, H. Kitazawa, C. D. Bredl, A. Bohm, M. Rau, A. Grauel, R. Caspary, R. Helfrich, U. Ahlheim, G. Weber and F. Steglich: Z. Phys. B **84** (1991) 1.

[26] H. v. Löhneysen: Physica **197** (1994) 551.

[27] K. Machida and M. Ozaki: Phys. Rev. Lett. **71** (1993) 2146; K. Machida, T. Ohmi and M. Ozaki: J. Phys. Soc. Jpn. **62** (1993) 3216.

[28] K. Machida, M. Ozaki and T. Ohmi: J. Phys. Soc. Jpn. **64** (1995) 1064.

[29] C. H. Choi and J. A. Sauls: Phys. Rev. Lett. **66** (1991) 484.

[30] R. Joynt, V. P. Mineev, G. E. Volovik and M. E. Zitomirsky: Phys. Rev. B **42** (1990) 2014.

[31] M. E. Zitomirsky and I. A. Luk'yananchuk: Sov. Phys. JETP Lett. **58** (1993) 131.

[32] K. Yamada: Prog. Theor. Phys. **53** (1975) 970; K. Yosida and K. Yamada: Prog. Theor. Phys. **53** (1975) 1286.

[33] Y. Kuroda, Y. Ōno, K. Miura, B. Jin, H. Jichu, D. S. Hirashima and T. Matsuura: Prog. Theor. Phys. Suppl. **108** (1992) 173.

[34] T. Saso and M. Itoh: Phys. Rev. B **53** (1996) 6877.

[35] T. Mutou and D. S. Hirashima: J. Phys. Soc. Jpn. **63** (1994) 4475.

[36] O. Sakai: private communications.

[37] H. Schweitzer and G. Czycholl: Sol. Stat. Com. **74** (1990) 735.

[38] K. Yamada and K. Yosida: Prog. Theor. Phys. **76** (1986) 621.

[39] K. Yamada, K. Yosida and K. Hanzawa: Prog. Theor. Phys. **108** (1992) 141.

[40] A. de Visser, A. Menovsky and J. J. M. Franse: Physica B **147** (1987) 81; L. Taillerfer, J. Frouquet and G. G. Lonzarich: Physica B **169** (1990) 257.

[41] G. R. Stewart1: Rev. Mod. Phys. **56** (1984) 755.

[42] A. Schestrom, M-F. Xu, Y. Hong, D. Bein, M. Levy, B. K. Sarma, S. Adenwalla, Z. Zhao, T. Tokuyasu, D. W. Hess, J. B. Ketterson, J. A. Sauls and D. G. Hinks: Phys. Rev. Lett. **62** (1989) 332.

[43] Y. Kohori, T. Kohara, H. Shibai, Y. Oda, T. Kaneko, Y. Kitaoka and K. Asayama: J. Phys. Soc. Jpn. **56** (1987) 2263; ibid. Jpn. J. Appl. Phys. Suppl. **26** (1987) 1239.

[44] R. A. Fisher, S. Kim, B. F. Woodfield, N. E. Phillips, L. Taillefer, K. Hasselbach, J. Frouquet, A. L. Giorgi and J. L. Smith: Phys. Rev. Lett. **62** (1989) 1411.

[45] K. Hasselbach, L. Taillefer and J. Flouquet: Phys. Rev. Lett. **62** (1989) 1411.

[46] Y. Kohori, T. Kohara, H. Shibai, Y. Oda, Y. Kitaoka and K. Asayama: J. Phys. Soc. Jpn. **57** (1988) 395; Y. Kohori, H. Shibai, T. Kohara, Y. Oda, Y. Kitaoka and K. Asayama: J. Magn. Magn. Mater. **76 & 77** (1988) 478.

[47] H. Tou, Y. Kitaoka, K. Asayama, N. Kimura, Y. Onuki, E. Yamamoto and K. Maezawa: Phys. Rev. Lett. **77** (1996) 1374.

[48] G. M. Luke *et.al.* : Phys. Rev. Lett. **71** (1993); ibid. Physica B **186** (1993) 264.

[49] N. Kimura, R. Settai, Y. Ōnuki, H. Toshima, E. Yamamoto, K. Maezawa, H. Aoki, and H. Harima: J. Phys. Soc. Jpn. **64** (1995) 3881.

[50] A. Yanase and H. Harima: Prog. Theor. Phys. Suppl. **108** (1992) 19.

[51] T. Takabatake, G. Nakamoto, T. Yoshino, H. Fujii, K. Izawa, S. Nishigori, H. Goshima, T. Suzuki, T. Fujita, K. Maezawa, T. Hiraoka, Y. Okayama, I. Oguro, A. A. Menovsky, K. Neumaier, A. Brückl and K. Andres: Physica B**223-224** (1996) 413; G. Nakamoto, T. Takabatake, H. Fujii, A. Minami, K. Maezawa, I. Oguro and A. A. Menovsky: J. Phys. Soc. Jpn. **64** (1995) 4834.

[52] S. Nishigori, T. Suzuki, T. Fujita, H. Tanaka, T. Takabatake and H. Fujii: Physica B**199-200** (1994) 473; S. Nishigori: private communications.

[53] H. Suderow and J. Flouquet: private communications.

[54] T. E. Mason, G. Aeppli, A. P. Ramirez, K. N. Clausen, C. Broholm, N. Stücheli, E. Bucher and T. T. M. Palstra: Phys. Rev. Lett. **69** (1992) 490.

[55] H. Kadowaki, T. Sato, H. Yoshizawa, T. Ekino, T. Takabatake, H. Fujii, L. P. Regnault and Y. Isikawa: J. Phys. Soc. Jpn. **63** (1994) 2074; T. J. Sato, H. Kadowaki, H. Yoshizawa, T. Ekino, T. Takabatake, H. Fujii, L. P. Regnault and Y. Isikawa: J. Phys. C **7** (1995) 8009.

[56] S. Kambe, S. Raymond, H. Suderow, J. McDonough, B. Fak, L. P. Regnault, J. Flouquet: preprint.

[57] R. M. Martin and J. W. Allen: p. 85 in ref. 1, and references therein; P. S. Riseborough: Phys. Rev. B **45** (1992) 13984.

[58] T. Kasuya: J. Phys. Soc. Jpn. **61** (1992) 1863; J. Phys. Soc. Jpn. **63** (1994) 2037; J. Phys. C, to be published.

[59] K. Tsutsui, Y. Ohta, R. Eder, S. Maekawa, E. Dagotto and J. Riera: to appear in Proceedings of SCES96, Physica B (1996).

[60] P. W. Anderson: *Basic Notions of Condensed Matter Physics*, (Benjamin, New York, 1984) Chap. 4.

[61] L. D. Landau: Sov. Phys. JETP **3** (1957) 920; Sov. Phys. JETP **5** (1957) 101; Sov. Phys. JETP **8** (1959) 70.

[62] T. M. Rice and K. Ueda: Phys. Rev. Lett. **55** (1985) 995.

[63] H. Shiba: J. Phys. Soc. Jpn. **55** (1986) 2765.

[64] T. Nishino and K. Ueda: Phys. Rev. B **47** (1993) 12451.

[65] Y. Kagan, K. A. Kikoin and N. V. Prokof'ev: JETP Lett. **57** (1993) 600.

[66] S. Nishigori, H. Goshima, T. Suzuki, T. Fujita, G. Nakamoto, H. Tanaka, T. Takabatake and H. Fujii: J. Phys. Soc. Jpn. **65** (1996) 2614.

[67] K. Izawa, T. Suzuki, M. Kitamura, T. Fujita, T. Takabatake, G. Nakamoto, H. Fujii and K. Maezawa: J. Phys. Soc. Jpn. **65** (1996) 3119.

[68] Y. Inada, H. Azuma, R. Settai, D. Aoki, Y. Ōnuki, K. Kobayashi, T. Takabatake, G. Nakamoto, H. Fujii and K. Maezawa: J. Phys. Soc. Jpn. **65** (1996) 1158.

[69] T. J. Sato, H. Kadowaki, H. Yoshizawa, G. Nakamoto, T. Ekino, T. Takabatake, H. Fujii, L. P. Regnault, Y. Isikawa: Physica B **223-224** (1996) 432.

[70] B. R. Trees, A. J. Fedro and M. R. Norman: Phys. Rev. Lett. **51** (1995) 6167.

[71] G. Kotliar and A. E. Ruckenstein: Phys. Rev. Lett. **57** (1982) 1362.

[72] A. J. Millis and P. A. Lee: Phys. Rev. B **35** (1987) 3394.

[73] D. M. Newns and N. Read: Adv. in Phys. **36** (1987) 799.

[74] Y. Ōno, T. Matsuura and Y. Kuroda: Physica C **159** (1989) 878.

[75] P. Coleman: Phys. Rev. B **28** (1983) 5255.

[76] K. Hanzawa, K. Yamada and K. Yosida: J. Phys. Soc. Jpn. **56** (1987) 678.

[77] In $Nd_{0.3}La_{0.7}NiSn$, which is isostructural to CeNiSn, the local symmetry of Nd^{3+} was identified with D_{3d} from an analysis of the crystal field level by means of neutron scattering. See, P. A. Alekseev, E. S. Klement'ev, V. N. Lazukov, E. V. Nefedova, I. P. Sadikov, M. N. Khlopkin, A. Yu. Muzychka, I. L. Sashin, N. N. Efremova and W. Bührer: Sov. Phys. JETP **79** (1994) 665.

[78] It is suggested that the crystal-field ground state is $|5/2, \pm 3/2\rangle$ from some experimental data: The analysis of the magnetic anisotropy measured by the polarized neutron scattering shows that the ground state is $|5/2, \pm 3/2\rangle$ or mostly $|5/2, \pm 5/2\rangle$ with negligibly small admixture of $|5/2, \pm 1/2\rangle$ (ref. 55); and the ultrasonic measurement in CePtSn, which has the same crystal structure as CeNiSn, by T. Suzuki, H. Fujisaki, T. Fujita, G. Nakamoto, T. Takabatake, H. Fujii and A. Tamaki: J. Magn. Magn. Mater. **140 & 144** (1995) 1215, shows that the ground state is predominaly $|5/2, \pm 3/2\rangle$.

[79] This relation was reported without derivation by G. Kotliar, E. Abrahams, A. E. Ruckenstein, C. M. Varma, P. B. Littlewood and S. Schmitt-Rink: Europhys. Lett. **15** (1991) 655.

[80] S. Schmitt-Rink, K. Miyake and C. M. Varma: Phys. Rev. Lett. **57** (1986) 2575.

[81] P. Hirschfeld, D. Vollhardt and P. Wölfle: Solid State Commun. **59** (1986) 111.

[82] P. Schlottmann: J. Appl. Phys. **75** (1994) 7044.

[83] R. Shiina: J. Phys. Soc. Jpn. **64** (1995) 702.

[84] T. Takabatake, M. Nagasawa, H. Fujii, G. Kido, K. Sugiyama, K. Senda, K. Kindo and M. Date: Physica B **177** (1992) 177; K. Sugiyama, T. Inoue, K. Oda, T. Takabatake, H. Tanaka, H. Fujii, K. Kindo and M. Date: Physica B **211** (1995) 223; K. Sugiyama: private communications.

[85] M. Kurisu, T. Takabatake and H. Fujiwara: J. Phys. Soc. Jpn. **59** (1990) 595.

[86] Y. Uwatoko, G. Oomi, S. K. Malik, T. Takabatake and H. Fujii: Physica B 199-200 (1994) 572.

[87] T. Ekino, T. Takabatake, H. Tanaka and H. Fujii: Physica B**206-207** (1995) 837.

[88] T. J. Hammond, G. A. Gehring, and M. B. Suvasini: Phys. Rev. B **51** (1995) 2994.

[89] J. D. Thompson, W. P. Beyermann, P. C. Canfield, Z. Fisk, M. F. Hundley, G. H. Kwei, R. S. Kwok, A. Lacerda, J. M. Lawrence, and A. Severing: p. 35 in ref. 2.

[90] M. Kasaya: p. 27 in ref. 2.